OXIDATIVE ACTIVITY AND SUB-CELLULAR SORTING OF MSRB3

Claudia Chieruzzi

BSc (Hons) Molecular and Cellular Biology with Biotechnology

Submitted for the fulfilment of the requirements for the degree of Master of Science by Research in Biochemistry and Biotechnology

School of Molecular Biosciences

College of Medical, Veterinary and Life Sciences

University of Glasgow

June 2024

DECLARATION

The research presented in this thesis has not been submitted for any other academic degree. The findings reported are my own work unless otherwise stated.

Claudia Chieruzzi

ABSTRACT

MsrB3 is one of the least well characterised methionine sulfoxide reductases and has gained interest in the field of redox biology since its discovery 20 years ago due to its association with age-related diseases, cancer, and deafness. Previous evidence suggests that MsrB3 can behave both as a methionine reductase and oxidase *in vitro*. The natural substrates of this enzyme in mammalian cells are unknown. Discovering the targets of MsrB3 can be technically challenging, partly because of the background stochastic oxidation of methionine from Reactive Oxygen Species that overlaps with MsrB3-induced redox changes. In addition, there is a lack of evidence on the sub-cellular targeting of endogenous MsrB3.

It was previously postulated that MsrB3 is targeted both to the ER and the mitochondria, but this study shows that it is also a found in the cytosol of mammalian cells, isolated through fractionation. Furthermore, this investigation provides additional evidence that MsrB3 could also act as an oxidase on methionine in proteins and reports a technique for studying the enzymatic oxidation of candidate MsrB3 targets by MS analysis.

AKCNOWLEDGEMENTS

I want to express my gratitude to everyone who has supported me during the completion of my MScRes.

I would like to thank my supervisor, Dr Brian O. Smith, for his guidance in directing this project and for his encouragement in my future prospects. I would also like to express my sincere gratitude to Dr Zhenbo Cao and the rest of my supervisory team for their academic support.

I want to take this opportunity to thank all members of Professor Bulleid's lab who I had the chance to work with over the past few years. Being part of this lab has been a formative experience on many levels, and their support in my professional development was invaluable.

Likewise, I am grateful to everyone in my life who has given me advice and motivated me throughout the completion of my studies. Thank you for being so understanding.

Lastly, I would like to thank my late supervisor, Professor Neil J. Bulleid, for all the opportunities I have been afforded in his lab and for his encouragement to undertake this project. Prof Bulleid was a good mentor to me and many other people. My thoughts are and always will be with his family and friends, hoping they can find some solace in knowing the extent of the positive impact he still has on the careers of his colleagues and students.

Here is an obituary article beautifully written by his friends and peers.

Braakman, I., High, S., Kadler, K., Sitia, R., Tokatlidis, K. and Woodman, P., 2023. Neil J. Bulleid (1960–2023), a virtuoso of protein folding and redox biology.

Table of Contents

LIST OF TABLES

LIST OF FIGURES

ABBREVIATIONS

BSA	Bovine Serum Albumin
bp	Base pairs
crRNA	CRISPR RNA
ddH_2O	double-distilled water
DM	Double mutant
DMEM	Dulbecco's Modified Eagle Medium
DNA	Deoxyribonucleic acid
DOC	Sodium Deoxycholate
DPBS	Dulbecco's Phosphate-Buffered Saline
DTT	Dithiothreitol
ECM	Extracellular matrix
EDTA	Ethylenediaminetetraacetic acid
ER	Endoplasmic reticulum
FS-EC	Follistatin-like (FS) domain and an EF-hand calcium-binding (EC)
GFP	Green fluorescent protein
gRNA	guide RNA
HDR	Homologous directed repair
HEK	Human embryonic kidney cells
HeLa	Henrietta Lacks cells
HT1080	fibrosarcoma HT1080 cells
IDT	Integrated DNA Technologies
IF	Immunofluorescence
IP	Immunoprecipitation

IPTG	Isopropyl ß- d-1-thiogalactopyranoside
KI	(gene) knock-in
KO	(gene) knock-out
LC-MS-MS	Liquid Chromatography with tandem mass spectrometry
LED	Light-emitting diode
MHC1	Major Histocompatibility Complex I
MobB	Methionine oxidation by blocking
MS	Mass Spectrometry
MsrA	Methionine sulfoxide reductase A
MsrB3	Methionine sulfoxide reductase B3
MWCO	Molecular weight cut-off
ORF	Open reading frame
PAM	Protospacer-adjacent motif
PDI	Protein Disulfide Isomerase
PMSF	Phenylmethylsulfonyl fluoride
RNA	Ribonucleic acid
RNP	Ribonucleoprotein
ROS	Reactive Oxygen Species
RP-HPLC	Reverse Phase High Performance Liquid Chromatography
SDS/PAGE	Sodium dodecyl-sulfate polyacrylamide gel electrophoresis
ssODN	Single-stranded oligodeoxynucleotide
TC	Tissue culture
TCA	Trichloroacetic acid

TCL	Total cell lysate
tracrRNA	Trans-activating CRISPR
TTBST	1X Tris-Buffered Saline, 0.1% Tween® 20 Detergent
UTR	Untranslated region
WB	Western blot
WT	Wild type
X-Gal	5-bromo-4-chloro-3-indolyl-beta-D-galacto-pyranoside

1. INTRODUCTION

The work in this project concerns MsrB3, a sub-type of methionine reductase found in mammalian cells. Before discussing the important aspects of MsrB3 that were investigated, this introduction will provide background information on the research presented in this manuscript. First, Post Translational Modifications will be addressed because of their interplay with Reactive Oxygen Species. This will set the basis for introducing protein oxidation events and, more specifically, the reversible oxidation of methionine in protein. This process is crucial to the activity of MsrB3 and will be relevant for the following discussions.

1.1. Reactive Oxygen Species and Post-Translational Modifications

Post translational processes modify amino acid residues after a protein is synthesised, thus expanding the breadth of functional groups (Walsh 2006). These processes, also known as Post-Translational Modification (PTMs) include the proteolytic cleavage of peptides, or the addition of modifying groups to one or multiple residues, which can determine the fate or the function of proteins (Mann and Jensen 2003). Because of their importance in protein maturation, dysregulation of PTMs can have consequences in cellular processes and lead to disease (Ramazi and Zahiri 2021). There are over 400 reported types of PTMs, of which the most frequently recognised and studied modifications include phosphorylation, acetylation and ubiquitination (Ramazi and Zahiri 2021), whereas oxidative modifications by Reactive Oxygen Species are less encountered in the available literature.

Reactive Oxygen Species (ROS) can induce post-translational modifications by oxidising protein residues, most frequently the sulphur-containing groups of cysteine and methionine. The oxidation and reduction of cysteine has been widely characterised for its role in the functional regulation of proteins, signal transduction, and redox monitoring in cellular systems

(Janssen-Heininger, Mossman et al. 2008, Radzinski, Oppenheim et al. 2021) but methionine oxidation and reduction has been comparatively neglected.

1.2. The growing interest in the reversible oxidation of methionine and Methionine Sulfoxide Reductases

Methionine is best known as the residue used in the initiation of protein translation, but with no specific functionality otherwise. Oxidation of protein-bound methionine used to be considered a stochastic event, and according to the general dogma, the spontaneous accumulation of methionine sulfoxide over time leads to protein misfolding, due to the change in the residues physicochemical properties that can destabilise the protein 3D structure (Chao, Ma et al. 1997).

Although this picture of the effects of redox changes in methionine is limited compared to the increasing evidence that supports them having regulatory functions, it has been shown that stochastic Met oxidation can indeed alter protein structure and with the biological activity of enzymes and that these accumulate in relation to age-related diseases (Hsu, Narhi et al. 1996). For example, there is evidence that the high number of Met residues in prion protein and their susceptibility to oxidation can drive the generation of toxic prion oligomers. This was revealed by studying the outcome of mutating prion protein methionine into serine, whose polarity mimics methionine sulfoxide. The mutation of the prion protein's exposed methionine generated structures similar to the prion protein intermediates that lead to the formation of pathological aggregates (Wong, Wang et al. 1999, Younan, Nadal et al. 2012, Bettinger and Ghaemmaghami 2020).

ROS-induced methionine oxidation is also a contributing factor in the formation of α-synuclein aggregates, which damage cell homeostasis and can induce Parkinson's disease (Glaser, Yamin et al. 2005, Stefanis 2012)

Moreover, research has disclosed that a high level of methionine oxidation is found in amyloid-ß plaques of Alzheimer's disease patients, with evidence of the neurotoxic consequences of ßAP Met 35 oxidation (Varadarajan, Kanski et al. 2001, Dong, Atwood et al. 2003).

Even in the context of its traditional "passive" role in protein stability, decades of research have gathered evidence indicating that methionine in proteins could act as an antioxidant, protecting the proteome from reactive oxygen species (Levine, Mosoni et al. 1996). Research focusing on cellular prion protein (PrP^c)

has corroborated that methionine could act as an antioxidant in the proteome by "absorbing" reactive oxygen species. Although there is evidence supporting a link between oxidation of methionine in PrP^c and prion disease, several earlier studies show that neurons from PrP^c KO mice are more susceptible to oxidative damage, whereas cultured cells with high expression of PrP^c are more resistant to ROS stress (Brown, Schmidt et al. 1997, Brown, Schmidt et al. 1998).

Altogether, these findings suggest that methionine oxidation protects cells and their proteome from ROS-induced damage, but its accumulation can lead to age-related diseases. Therefore, even in cases where methionine modifications don't play a regulatory role, the oxidation of methionine protects the proteome from ROS while also representing a biological clock in cellular systems.

In recent years, a growing interest in the redox role of methionine and its oxidised form, Met Sulfoxide (MetO), has disclosed that they are involved in the regulation of cell processes, in a similar way to cysteine and its oxidised derivatives (Kim, Weiss et al. 2014). Consequently, the enzymes that catalyse the reduction of MetO, Methionine Sulfoxide Reductases (Msrs), have also been recognised as important regulators of different protein targets and crucial in the response to oxidative stress in cells. Msr genes are found in most prokaryotic and eukaryotic species, including humans and other mammals, and have generated two main families, MsrA and MsrB, which respectively reduce the chiral S-form and R-form of MetO (Kim and Gladyshev 2007). As it will be explained later into more details, some MsrAs and MsrBs were proven to also act as stereospecific methionine oxidases (see **Figure 1**).

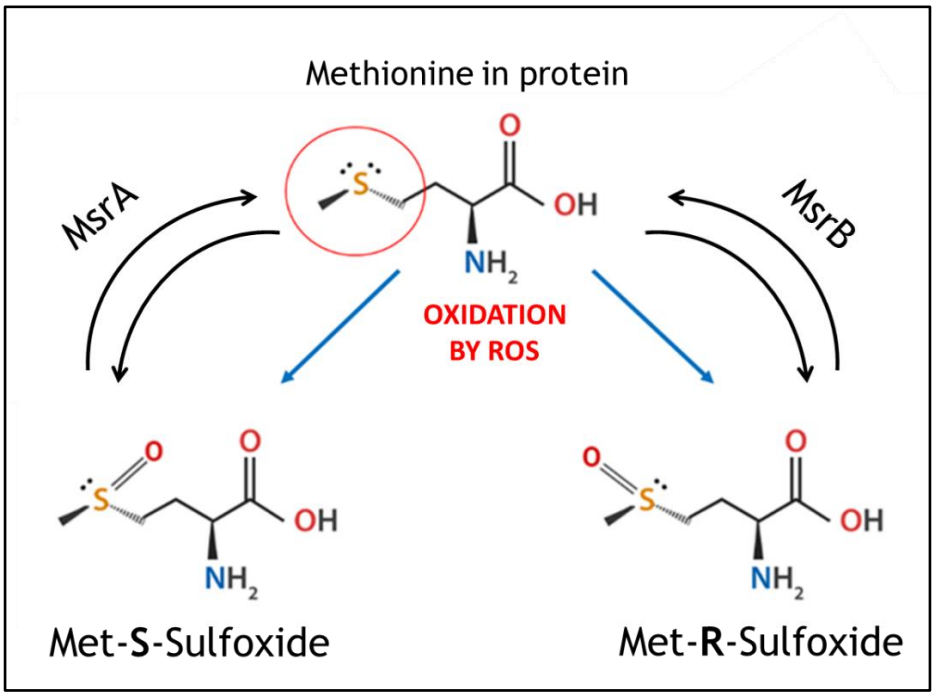

Figure 1: Stereospecificity of MsrA and MsrB. *There are two enantiomers of methionine sulfoxide that can originate from the oxidation of its sulfur group. MsrA is specific to Met-(S)-O, MsrB to Met-(R)-O.*

The first MsrA was discovered in 1981, but the first MsrB was identified only 20 years later (Tarrago, Kaya et al. 2022). Because of this timeframe, there is evidence of the in-vivo and in-vitro role of MsrA, but not for MsrB (Kim, Weiss et al. 2014).

Among the different subtypes of MsrB in mammalian cells there are MsrB1 which resides in the cytosol, MsrB2, which is specific to the mitochondria, and two splice variants of MsrB3: MsrB3B and MsrB3A, respectively targeted to the mitochondria and the endoplasmic reticulum (ER) (Kim and Gladyshev 2004). MsrB3A is also the only known Msr in the ER (see **Figure 2**) (Kim and Gladyshev 2007).

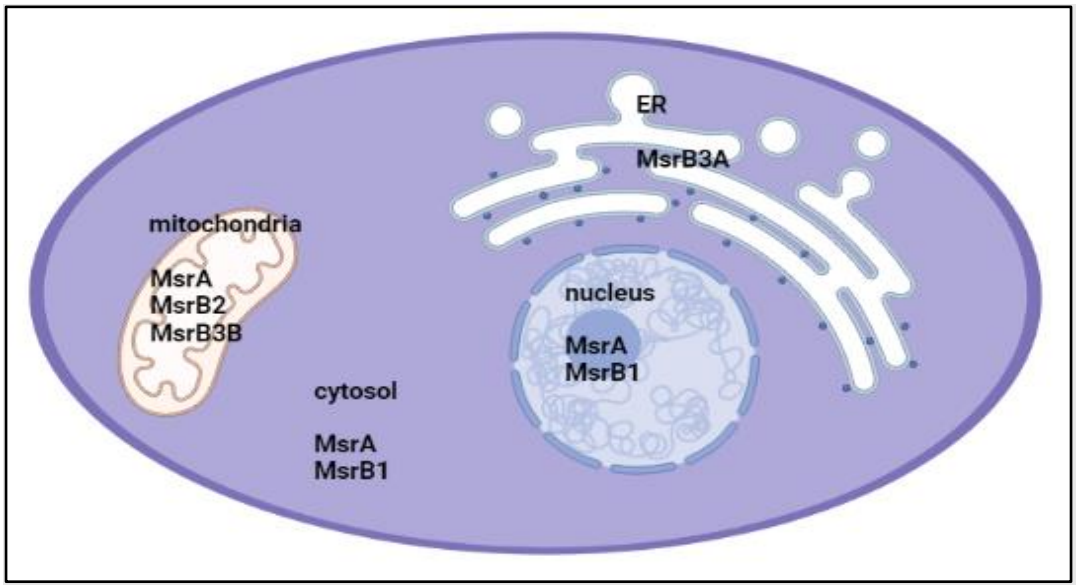

Figure 2: The distribution of the different Msrs in the mammalian cell. *There are various Msrs distributed in the mammalian cell. MsrB3A is the only known ER resident Msr. (Kim and Gladyshev 2007).*

Since their discovery, studies on Msrs and the reversible oxidation of methionine disclosed the crucial role of this class of reductases in the regulation of cellular systems, resistance to ROS and disease. For instance, loss of function of Msrs has been linked to neurodegenerative disorders and ageing (Kim and Gladyshev 2007). In this regard, mutation of Parkin Met192, which is reversibly reduced by MsrB2, is associated with the development of Parkinson's disease. Moreover, the reduced expression of MsrB2 was also linked to the same neurodegenerative disorder, hence establishing the crucial role of this reductase in the regulation of Parkin (Lee, Lee et al. 2019). Quite surprisingly, functional knockouts of all Msrs in mice result in an increased resistance to acute oxidative stress in the mutant strains. These observations strengthen the evidence that, although methionine reductases counteract the damages of ROS stress, methionine residues might act as scavengers for reactive oxygen that would otherwise alter protein function by oxidising other important residues (Levine, Mosoni et al. 1996, Lai, Sun et al. 2019) and that the accumulation of oxidised methionine, either over time or due to reduced Msr activity, links to age-related diseases.

1.3. Aberrant expression of MsrB3 leads to redox dysregulation in whole organisms and cellular systems.

MsrB3, which this investigation focuses on, is still poorly characterised to this day. Although the natural substrates of MsrB3 are unknown, its influence on redox-stress response in cells and organisms has been studied. Human MsrB3 is sometimes referred to as MsrB3A (ER version) or MsrB3B (mitochondria targeted). MsrB3A and MsrB3B only differ in their signal sequences, which arise from differential splicing

MsrB3A sequence:

MSPRRTLPRPLSLCLSLCLCLCLAAALGSAQSGSCRDKKNCKVVFSQQELRKRLTPLQYHVTQEKGTESA FEGEYTHHKDPGIYKCVVCGTPLFKSETKFDSGSGWPSFHDVINSEAITFTDDFSYGMHRVETSCSQCG AHLGHIFDDGPRPTGKRYCINSAALSFTPADSSGTAEGGSGVASPAQADKAEL

MsrB3A sequence:

MSAFNLLHLVTKSQPVALRACGLPSGSCRDKKNCKVVFSQQELRKRLTPLQYHVTQEKGTESAFEGEYT HHKDPGIYKCVVCGTPLFKSETKFDSGSGWPSFHDVINSEAITFTDDFSYGMHRVETSCSQCGAHLGHIF DDGPRPTGKRYCINSAALSFTPADSSGTAEGGSGVASPAQADKAEL

(Signal peptides) Source: UniProt Q8IXL7-1 and Q8IXL7-2.

Literature suggests that deficiency of MsrB3 causes ER stress by disrupting Ca^{2+} homeostasis and makes cells more susceptible to p53-independent apoptosis (Kwak and Kim 2017), whereas overexpression of MsrB3A was found to promote ROS resistance in A549 cells (Kwak, Lim et al. 2012). Enhanced expression of MsrB3A was also proved to extend the lifespan and resistance to heat and oxidative stress in *Drosophila* (Kwak, Lim et al. 2012, Lim, Han et al. 2012).

Because of its ROS-response activity on a cellular level, abnormal expression of the MsrB3 in tissues and organisms has been associated with cancer and age-related diseases. Experiments revealed that knocking down MsrB3 in human cell lines obtained from sub-types of breast, liver and lung cancer tissue inhibited cell proliferation, and over-expression of MsrB3 had the opposite effect (Kwak, Kim et al. 2017). Studies show that that overexpression of MsrB3 in gastric cancer tissue associates with poor prognosis (Ma, Wang et al. 2019) and that this enzyme might inhibit oncogene-induced DNA damage in malignant cells (Morel, Ginestier et al. 2017). Recently, MsrB3 was identified as a proto-oncogene in cervical cancer which might inhibit apoptosis in the malignant cells, and thus it

could be of interest as a target for miRNA therapy to induce cancer cell apoptosis (Ramezani 2023).

In mouse models, abrogation of MsrB3 results in deafness as result of degeneration of stereociliary bundles and hair cells apoptosis, which could explain why in humans' lack of MsrB3 results in hearing loss (Ahmed, Yousaf et al. 2011, Kwon, Cho et al. 2014). Similarly to other Msrs, altered expression of MsrB3 is associated with neurodegenerative disorders like Alzheimer's and neurovascular diseases (Adams, Benayoun et al. 2017). However, it is currently unknown how changes in MsrA and MsrBs expression affect the risk of Alzheimer's disease in the ageing brain, and more studies on MsrBs are needed to elucidate their role in Alzheimer's disease pathology (Chandran and Binninger 2023).

1.4. The proposed oxidoreductase mechanism of MsrB3.

Because of their earlier discovery, studies on MsrA have paved the way for the later research performed on MsrBs and have offered valuable insights into MsrB3 oxidoreductase activity. Therefore, it is most appropriate to first summarise what we know about MsrA reductase/oxidase mechanisms, to understand better their relevance in regard to MsrB3.

Mouse and bacteria MsrAs were shown to act as a stereospecific reductase for the S-epimer of MetO (Lim, You et al. 2011). Both MsrAs were proposed to have the following catalytic cycle for substrate reduction: the MsrA active site thiol becomes sulfenylated upon Met S-sulfox reduction, and it is then reduced through the formation of a disulphide bond in the resolving domain of the enzyme, thus recycling the enzyme for a subsequent substrate reduction (Antoine, Gand et al. 2006, Boschi-Muller, Gand et al. 2008).

Remarkably, stoichiometry analysis on mouse MsrA revealed that one molecule of this reductase, in the absence of a reducing agent, can reduce three molecules of MetO. MS analysis disclosed that the sulfenic acid on the catalytic C72 of MsrA can further reduce itself by autoxidising MsrA Met229 to methionine sulfoxide, when the resolving cysteines have already been oxidised (Lim, You et al. 2011). Thus, the active site C72 can be recycled first by the resolving cysteine, and then through autoxidation, allowing the MsrA-mediated reduction of three MetO substrates. Additionally, the characterisation of the oxidised MsrA species revealed that their autoxidation is derived by oxygen from water, not the sulfoxide substrate. This observation was made through MS analysis of MsrA incubated with Met^{16}O in either $H_2{}^{18}O$ or $H_2{}^{16}O$. When MsrA was incubated in heavy water, its mass increase due to the autoxidation of Met229 was 2 Da greater than the resulting mass from the incubation carried out in ^{16}O water. In the same conditions, the increase in mass of MsrA featuring oxidised Met229 and Cys72 was of 4 Da higher in the reaction with O^{18} water (Lim, You et al. 2011). This, together with other results reported by Lim and colleagues, proved that when the catalytic cysteine of MsrA becomes sulfenylated the oxygen is derived from water rather than MetO; that the active site cysteine can reduce itself by oxidising Met229; and that the oxidation process is alike and opposed to the reductase reactions, whereby water also serves as an oxygen donor to convert Met229 into Met229-S-O.

How can water participate in the reductase activity of MsrA in the first place? Structural analysis of MsrA complexed with its substrate indicates that the sulfoxide oxygen of MetO points away from the catalytic MsrA thiol, but it is equidistant from the carboxylate oxygen of Glu115 and the hydroxyl of Tyr103. This initial spatial arrangement of the atoms at play partly explains why C72 can't become directly oxidised by the oxygen from Met-S-O. To combine this observation with the MS results summarised above, the following mechanism depicted in **Figure 3** was advanced. It was proposed that MsrA Glu115 forms a hydroxyl sulfonium intermediate with MetO, stabilised by the hydroxyl group of MsrA Tyr103 (Ranaivoson, Antoine et al. 2008, Lim, You et al. 2011). The MsrA active site Cys72 forms a sulfurane intermediate with the MetO hydroxyl sulfonium. The conformation of this complex should allow a water molecule to access the active site thiol, thus forming a sulfenic acid on Cys72 and releasing reduced methionine (Lim, You et al. 2011).

Since mouse MsrA displayed auto-oxidase activity, the same study that unveiled this investigated whether MsrA can also act as a Met Oxidase. Indeed, it was found that MsrA can also act as stereospecific oxidases, thus converting Met into Met-S-O within certain proteins (Lim, You et al. 2011). It is worth noting that this observation made on bacteria and mouse MsrA wasn't mirrored in a later study on *Drosophila* MsrA, which was shown to only act as a reductase for Met-S-O (Tarafdar, Kim et al. 2019).

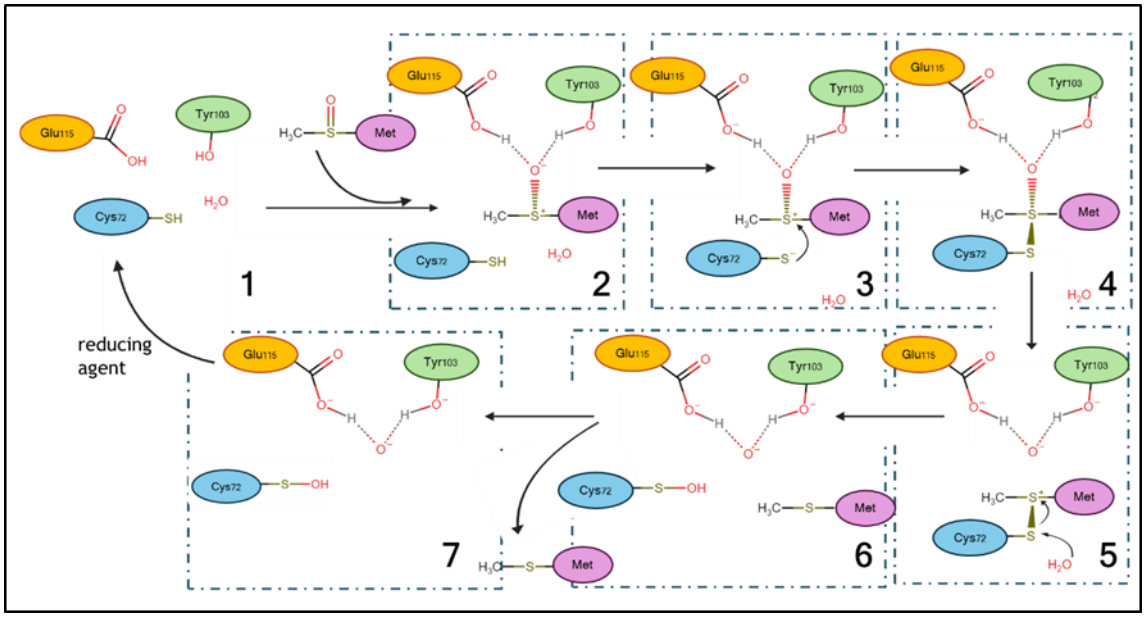

Figure 3: Proposed MsrA reductase mechanism (Lim et al., 2011). *At the beginning of the redox reaction, MsrA Glu115 protonates the sulfoxide of MetO generating sulfonium intermediate, stabilised by MsrA Tyr103 (2). The protonated sulfur atom of the MetO sulfonium intermediate is subject to nucleophilic attack from MsrA thiolate Cys72, the MsrA active site cysteine (3). This interaction will induce a sulfrane intermediate (4) which becomes protonated (likely by Tyr103) into another sulfonium intermediate. This re-arrangement allows water to act as an oxygen donor by oxidising MsrA C72 (5). This interaction will release the reduced methionine and the MsrA oxidised active site thiol (6). Reducing agents or the resolving cysteine can reduce the C72 sulfenic acid (1).*

Although MsrA and MsrB3 evolved separately, they share many similarities. Bulleid's lab helped characterise the mechanism of action and the recycling of MsrB3 after MetO reduction through a three-step process that resembles MsrA's self-recycling mechanism, except there is no indication that MsrB3 can recycle its active site through auto-oxidation like mouse MsrA. According to the proposed model (**Figure 4**), the MsrB3 active site cysteine, C126, becomes sulfenylated upon substrate reduction. C126 is then reduced through a transient disulfide with either resolving cysteines C3 and C9. Following that, C3 and C9 form an internal disulfide bond, thus recycling C126 for a successive MetO reduction (Cao, Mitchell et al. 2018). Therefore, each fully reduced MsrB3 molecule can reduce two molecules of Met R-sulfoxide. The internal disulfide

bond between C3 and C9 and the oxidation of C126 can be reversed by thioredoxin allowing the catalytic cycle to proceed (Cao, Mitchell et al. 2018). Because there is no thioredoxin in the ER, this cannot be the natural reductant of MsrB3A, but it is possible that ER-resident thioredoxin-domain containing proteins could catalyse the reduction of MsrB3A (Cao, Mitchell et al. 2018).

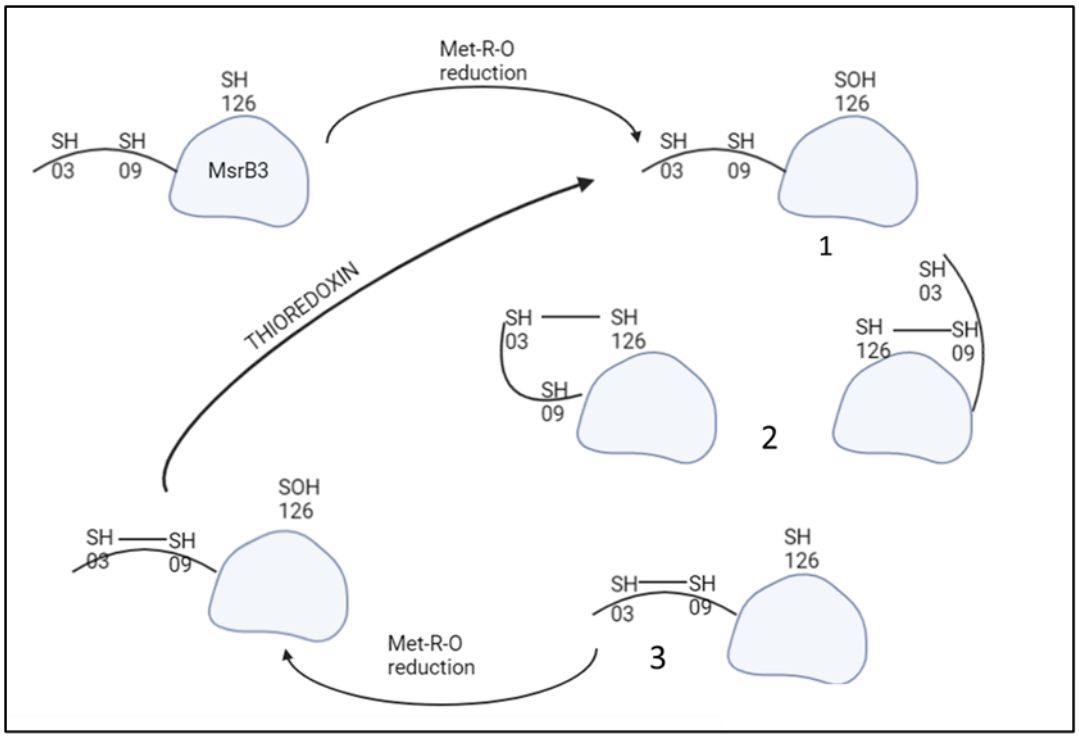

Figure 4: The three-step process of the recycling of MsrB3 C126 in vitro. *MsrB3 C126 reduces Met-R-O and becomes sulfenylated (1); either resolving cysteines forms a transient disulfide bond with C126 (2); C03 and C09 then form an internal disulfide bond (3). This internal disulfide can be reduced by thioredoxin and the reduction cycle of C126 can take place again (Cao, Mitchell et al. 2018).*

Interestingly, our studies showed that MsrB3 with a sulfenylated active C126 can act as an oxidase for methionine *in vitro*, converting it to methionine R-sulfoxide without requiring the resolving C3 and C9 (Cao, Mitchell et al. 2018). Therefore, it is possible that MsrB3 could act both as an oxidase and a reductase in cells.

Because of its shared features with MsrA, it is likely that MsrB3 too becomes oxidised by water-derived oxygen upon MetO reduction, and that the stereospecific conversion of Met to Met-R-O by MsrB3 is also mediated by water as an oxygen donor. Although this would be a reasonable assumption, it requires empirical proof.

1.5. Current challenges and solutions in redox biology.

As mentioned earlier, ROS-induced modifications of cysteine residues have historically received more attention in the regulation of cellular biosystems compared to methionine. The events affecting cysteine redox changes are often accompanied by the formation of disulphide bonds and protein structural changes, which can be easily monitored with different molecular biology techniques. For instance, a disulphide bond formation will affect the apparent hydromobility of a protein in its native state which can be revealed through WB analysis, a relatively inexpensive and straightforward technique. By contrast, redox changes of methionine residues in proteins aren't followed by structural changes that can be as easily assessed, requiring indirect measurements. The hurdles in assaying methionine redox changes are partly linked to the knowledge gap in understanding the biochemical functions of cysteine oxidation compared to methionine oxidation at present.

In addition, it's unclear what proportion of methionine sulfoxide observed in vivo is the result of Msr's enzymatic activity, or stochastic events, making the identification of Msr's substrates in the cell proteome hard to study. Identifying candidate targets of Methionine reductases in the cell can be challenging because methionine can become readily oxidised during sample preparation, leading to variability in the results.

For this reason, new approaches have been designed to distinguish methionine redox changes enzymatically regulated from those arising stochastically. As an example of these new methodologies, ^{18}O hydrogen peroxide was used recently to label reduced methionine in the proteome of human cell lines and mouse tissue (Bettinger, Welle et al. 2019, Bettinger, Simon et al. 2022). This approach allows to distinguish in MS analysis what proportion of methionine was oxidised *in vivo* before sample processing and analysis, as it will be oxidised with the most abundant oxygen isotope ^{16}O, from the originally reduced methionine which will become oxidised with ^{18}O derived from hydrogen peroxide.

This experimental procedure led Bettinger and colleagues (2022) to discover conserved patterns in the oxidation of specific methionine residues belonging to functionally related proteins in brain tissue from mice with age differences, thus

strengthening the evidence that the oxidation of methionine could be a tightly regulated modification (Bettinger, Simon et al. 2022) coordinated by the enzymatic activity of Msrs. As mentioned in section 1.4, MsrA and MsrB3 were found not only to act as reductases but also as stereospecific oxidases. In this context, it would be interesting to investigate how MsrB3 regulates the oxidation of methionine in the proteome by shifting the focus from its canonical reductase behaviour and identifying its candidate oxidation targets.

1.6. Could the collagen-binding protein SPARC be an MsrB3 target?

Water is likely the oxygen donor that oxidises MsrB3 active site thiol upon substrate reduction as seen in MsrA. If this hypothesis is correct, then oxidation of MsrB3 active site C126 generated from its enzymatic activity could be separated from its stochastic oxidation, which will generate ^{16}O sulfenic acid, by providing MsrB3 $H_2{}^{18}O$. Consequently, when MsrB3 performs its reverse reaction by oxidising methionine targets, the ^{18}O provided in solution will be found on the oxidised potential candidates. A schematic representation of the rationale behind the devised mechanism, which is inspired by the investigation on MsrA reported by Lim and colleagues (2011), can be found in **Figure 5**. In short, as the use of heavy water became useful in identifying the autoxidation of Met229 in MsrA, the same principle can be transferred to the identification of methionine in protein subject to the oxidative activity of MsrB3.

This method was applied in Bulleid's lab to identify candidate targets for MsrB3 in the proteome of microsomes extracted from WT and MsrB3 KO mammalian cells (unpublished data). The ^{18}O labelling of MsrB3 oxidation candidates in the microsomes lysate led to the identification of possible methionine targets that were oxidised with heavy oxygen exclusively in the samples generated from cells expressing MsrB3.

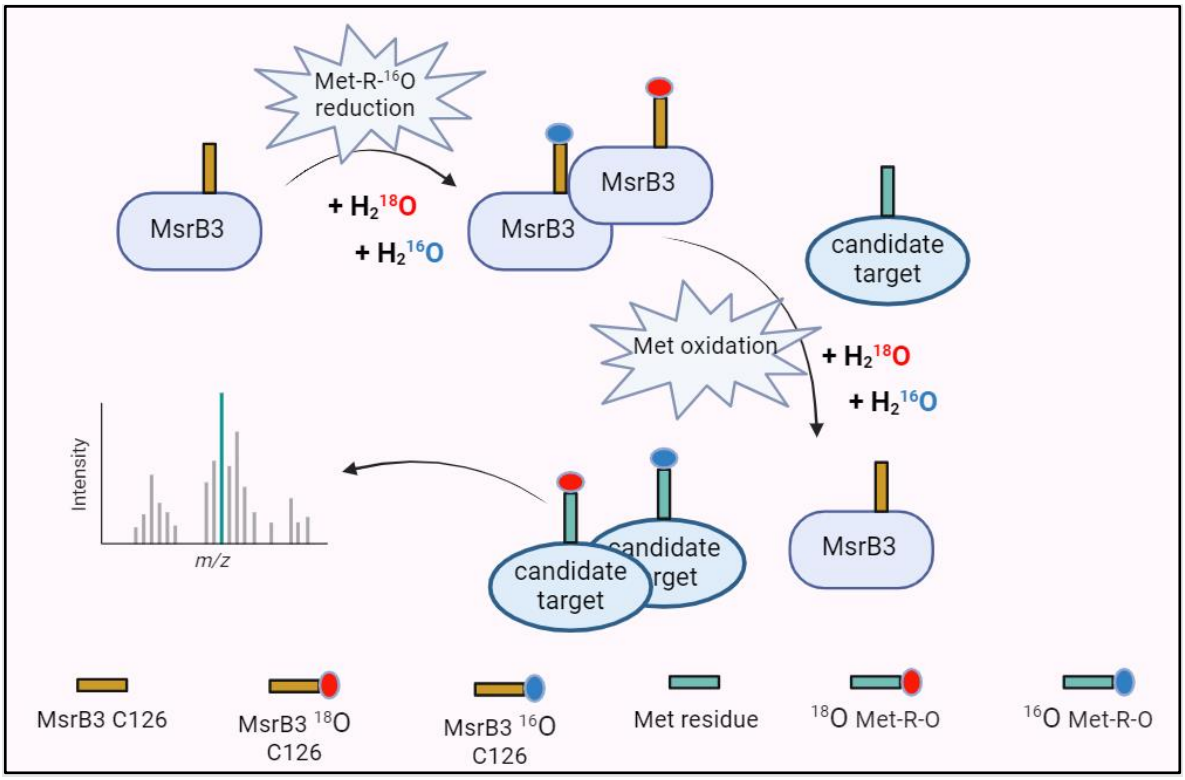

Figure 5: General overview of the ^{18}O labelling of MsrB3 oxidation substrates. *In oxidising conditions, the MsrB3 catalytic C126 becomes oxidised, and the heavy water provided will act as an oxygen (^{18}O) donor. Water will also provide the oxygen for the reverse reaction, in which the sulfenic acid on MsrB3 active site thiol catalyses the stereospecific conversion of the candidate target methionine into Met-R-^{18}O. LC-MS/MS analysis of the reactions will determine what proportion of the oxidised MsrB3 and candidate targets are ^{18}O labelled. Candidate targets and active sites thiol will become oxidised with heavy/light oxygen in proportion to the $^{18}O/^{16}O$ water present in the sample.*

One of these candidate targets is Met245 of SPARC, also known as BM-40 or Osteonectin, a matricellular protein known to bind to collagen types I-V and which regulates the correct assembly of the extracellular matrix (ECM)(Trombetta, Bradshaw et al. 2010, Rosset and Bradshaw 2016).

Secreted Protein Acidic and Rich in Cysteine (SPARC) is a highly conserved protein ubiquitous to various animal species. First identified in mammalian tissue over 40 years ago (Termine, Kleinman et al. 1981), SPARC has since been studied in mammals as well as invertebrates and model organisms (Purcell, Gruia-Gray et al. 1993, Fitzgerald and Schwarzbauer 1998, Strandjord, Madtes et al. 1999, Martinek, Zou et al. 2002, Rotllant, Liu et al. 2008).

Studies on *Zebrafish*, *Xenopus*, *Drosophila* and *C. Elegans* show that SPARC is required for normal embryonic development and survival in these species (Purcell, Gruia-Gray et al. 1993, Schwarzbauer and Spencer 1993, Martinek, Zou et al. 2002, Ceinos, Torres-Nuñez et al. 2013), whereas SPARC-null mice develop normally until their early life stages, in spite of SPARC being expressed at high levels in WT mouse embryos and adults (Mason, Murphy et al. 1986, Gilmour, Lyon et al. 1998).

In adults, SPARC is expressed in different cell types to regulate remodelling and would healing in healthy tissue (Reed and Sage 1996) and its over-expression was shown to inhibit spreading and promote partial detachment of cultured cells (Sage, Vernon et al. 1989).

While the de-adhesion and cell proliferation inhibitory features of SPARC are implicated in its role in tissue healing in healthy cells, the abnormal expression of this ECM protein bears intricate consequences in the prognosis of pathologies like cancer (Brekken and Sage 2000). In fact, the over-expression of SPARC has been associated with enhanced recurrence or proliferation of some breast, cervical and liver tumours (Chen, Shi et al. 2012, Azim Jr, Singhal et al. 2013, Shi, Jiang et al. 2016, Zhu, Yuan et al. 2016, Gao, Liu et al. 2021).

Conversely, SPARC was also found to be downregulated in ovarian tumours, and it's been studied as a cancer therapeutic because of its cell-spreading inhibitory properties (Tai and Tang 2008, Feng and Tang 2014, Zhu, Yuan et al. 2016).

SPARC is a Ca^{2+}-binding glycoprotein that mediates ECM interactions composed of three modular domains. As shown in **Figure 6**, the first SPARC module is an N-

terminal acidic segment; the second is a Follistatin-like (FS) domain, which itself consists of a cysteine-rich module and a Kazal domain (Lane and Sage 1994, Brekken and Sage 2000). The third module is the extracellular Ca^{2+} -binding (EC) domain equipped with two EF-hands (Hohenester, Maurer et al. 1996)

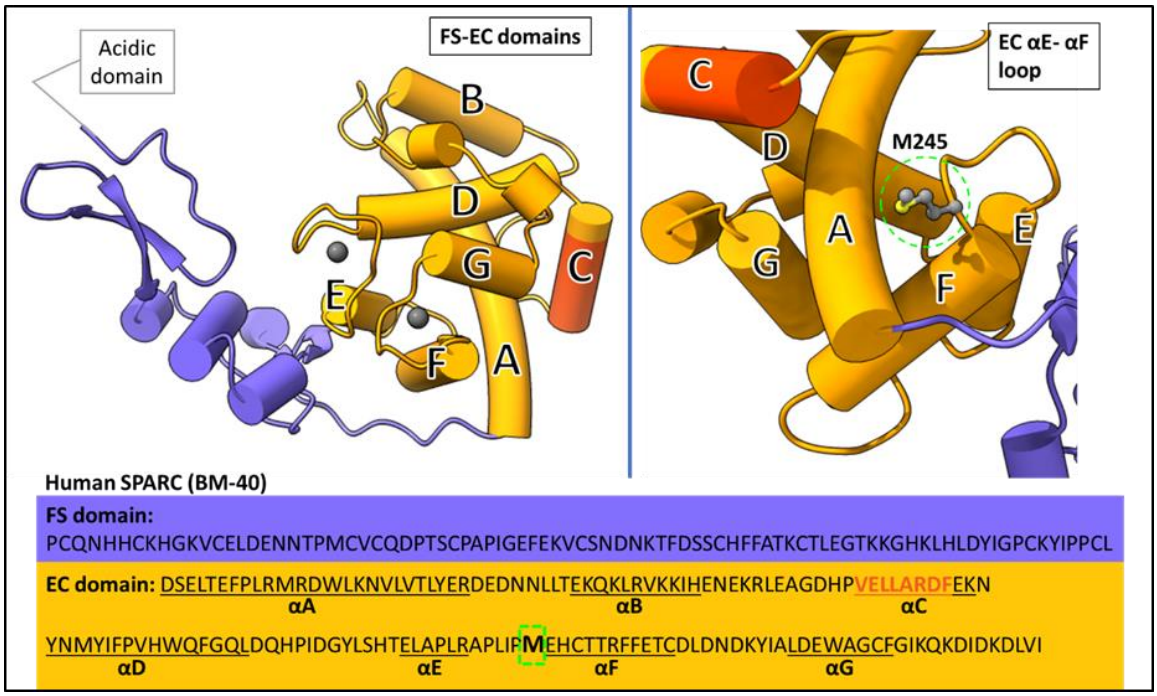

Figure 6: Sequence and cartoon structure of human SPARC based on the crystallography data found in the Brookhaven Protein Database, accession number 1BMO*. The SPARC acidic domain at the N terminal (grey box) precedes the FS domain, coloured in purple. The EC domain αA to αG helices are labelled and coloured in yellow. The EC αD, αE and αF, αG constitute, respectively, the EC domain EF-motifs 1 and 2 bound to Ca^{2+} ions (dark grey spheres). The VELLARDF sequence of the EC domain αC, which will be discussed later, is in orange (Hohenester, Maurer et al. 1996, Brekken and Sage 2000). Met 245 in the EC αE- αF loop is marked by a dashed green line. Created with ChimeraX.*

The EC portion of SPARC is its collagen binding domain. The crystal structure of humans SPARC bound to a triple-helical collagen peptide, containing the binding hotspot GVMGFO motif of collagens I-III (Xu, Raynal et al. 2011), disclosed that the collagen binding site resides between the SPARC EC αE- αF loop and the proximal αA. This structure creates a "Phe" pocket that accommodates F23 of the collagen trailing chain (Hohenester, Sasaki et al. 2008).

One of the key residues identified for the calcium-dependent binding of SPARC to collagen (Maurer, Hohenadl et al. 1995) is the BM-40 EC domain M245, highlighted in the EC αE- αF loop depicted in **Figure 6**. Alanine mutation of this EC residue (EC M245A) results in a reduced affinity to collagen I and IV marked by a disassociation constant nearly 100-fold greater than in the non-mutated EC domain (Sasaki, Hohenester et al. 1998).

The Phe pocket is formed when SPARC binds to collagen upon major remodelling of the αE- αF loop, which also involves M245 (Hohenester, Sasaki et al. 2008).

Collectively, these findings support the evidence that M245 is crucial for the interactions of SPARC to collagens I, II, III and IV and that mutating this methionine residue to alanine, which is also a nonpolar amino acid, greatly reduces BM-40 binding affinity.

Therefore, oxidation of M245 could likely affect SPARC binding affinity, as this redox change would induce a shift in the residue polarity, altering the collagen-binding site.

Considering the background information on SPARC, it was reputed that if MsrB3 indeed oxidises the EC domain Met245 as shown by the preliminary analysis, then the reductase could also regulate the SPARC activity by altering its collagen binding site. Moreover, SPARC being a secreted protein, its maturation is also mediated inside the ER, where MsrB3A is localised. This evidence encouraged Bulleid's lab to further investigate the interaction between MsrB3 and SPARC, by first confirming that the reductase can modify Met245 of the candidate substrate.

2. AIMS

There is a lack of knowledge on the natural substrates of MsrB3. Prof Bulleid's lab has identified a potential target of MsrB3 oxidising activity, hSPARC Met245, whose enzymatic oxidation can affect its affinity to collagen. We aim to over-express this potential substrate by transiently transfecting HEK cells with plasmid DNA encoding the protein of interest. Using this mammalian cells-based expression system, the protein will be purified, and mass spectrometry analysis will reveal whether this client target is oxidised by MsrB3 in the presence of MetO.

Furthermore, this project aims to establish cell lines selectively over-expressing the ER and mitochondrial MsrB3 (respectively, MsrB3A and MsrB3B). These cell lines will be used in future research to help identifying chemical substrates for MsrB3 that could be used in kinetic assays and live-cell monitoring of the reductase activity. A chemical probe whose fluorescent properties change ratiometrically in response to its reduction by MsrA has been identified (Makukhin et al., 2016). The future goals would focus on developing a similar organic molecule suitable for MsrB3 through an ongoing collaboration with Professor Hartley's lab in the School of Chemistry, University of Glasgow.

The investigation will also focus on studying the cell localisation of MsrB3 and the suitable antibodies for its immunodetection. Because the available antibodies against MsrB3 are not suitable for immunofluorescence analysis, the distribution of MsrB3 will be studied through both fractionation experiments and by knocking-in epitope tags at the C-terminus of the MSRB3 gene in primary cell lines, to make the detection of the endogenous protein easier. The gene knockout and knock-in procedures will be performed using the CRISPR-Cas9 technology.

Hopefully, this investigation will be of significance in understanding the important role of MsrB3, and direct future research regarding methionine sulfoxide reductases.

3. MATHERIALS AND METHODS

3.1. Mammalian cell culture

The HT1080 WT (CCL-121) and HEK 293 T (CRL-3216) were purchased from American Type Culture Collection (ATCC), HeLa WT cells were obtained from a stock belonging to a former lab member. Cells were cultured at 37 °C and 5% CO_2 in DMEM (Invitrogen 21969-035) enriched with 2 mM glutamine (Invitrogen 25030024), 100 U/ml penicillin, 100 µg/ml streptomycin (Sigma P0781) and 10% v/v foetal calf serum (Sigma F9665 or Invitrogen 10500064). For passaging, adherent cells were washed with DPBS (Invitrogen 14190094) before being treated with Trypsin-EDTA 1X (Invitrogen 25300054). Cells were kept in 5% CO_2 and 37 °C conditions.

3.2. Cell lysis and Western blotting

For the analysis of TCL, cells were lysed in lysis buffer (150mM NaCl, 50mM TrisHCl pH 8.0, 5mM EDTA, 1% v/v Triton X-100, cOmplete™, Mini, EDTA-free Protease Inhibitor Cocktail (11836170001) from Sigma, 1 tablet/10ml of lysis buffer. The TCL was spun at 14'800 rpm to pellet the cell debris. Proteins were separated through 15% w/v Acrylamide/Bisacrylamide 37.5:1 SDS/PAGE gel, unless otherwise stated, at 300V and 20mA. The protein was transferred into Cytiva Amersham™ Protran™ NC Nitrocellulose membrane (Catalog 15209804) at 300V and 210mA for 1h. The membrane was blocked in 3% w/v non-fat milk/TTBST (150mM NaCl, 10mM TrisHCl pH 8.0, 0.05% v/vTween-20) for 45' and incubated with the primary antibodies overnight at 4 °C. The membranes were washed x3 times with TTBST and then incubated with the secondary antibodies for 30'. The blots were imaged with an Odyssey CLx Imager and the Image Studio™ Software by LI-COR, unless otherwise stated. The protein marker used was Blue Protein Standard, Broad Range - NEB P7718S.

3.3. Cell fractionation

Subcellular fractionation by sequential centrifugation consists in separating cellular compartments with different densities, by progressively increasing the centrifugal force to pellet the cellular fractions obtained from homogenised cells. This biomolecular approach was used in the research presented in this manuscript to attempt the separation of ER, mitochondria and cytosol of cultured cells to study the proportion of MsrB3 found in each of these cell fractions. The homogenization step in the fractionaton precedures breaks down the cell membrane, releasing the cell organelles and cytosolic content into the solution. Because of that, after pelleting the other cell fractions by centrifugation, the cytosolic fraction and other proteins in solution were obtained by precipitating the protein in the supernatant (Supn.).

HT1080 WT cells were grown into three T75 flasks until confluency reached 80-90%. The cells were trypsinised, washed twice with DPBS and pelleted at 1400g for 4' at room temperature. The cell pellet was re-suspended in 3ml of homogenising buffer and a cell count was performed at this stage using a Countess II FL (Life Technologies) to check how many cells were intact before the homogenisation.

Homogenising buffer:

Tris-HCl pH 7.4 1M	25ml (50mM)
KCl 1M	25ml (50mM)
$MgCl_2$ 0.5M	5ml (5mM)
Sucrose	42g (250mM)
EDTA pH 8 0.5M	1ml (1mM)
DTT	77mg
PMSF	87mg
ddH_2O	up to 500ml

The cell suspension was homogenised by performing 10 strokes using an isobiotec 12 micron ball-bearing homogeniser. After the step, another cell count was performed to ascertain whether the homogenisation worked, and that the percentage of broken cells reached 80%. This percentage is just an empirical value observed in previous fractionation experiments in Prof Bulleid's lab

following this protocol. This percentage is used to indicate that the homogenisation worked and that the cells were not over-homogenised. Over-homogenising cells leads to the disruption of sub-cellular compartments, which must be avoided to aid the separation of different cell fractions.

For the separation of HT1080 WT cellular compartments, a low-speed centrifugation at 1000 g followed by a faster centrifugation at 16000 g were performed to attempt the separation of mitochondria and ER, before precipitating the remaining protein in solution found in the supernatant.

To do that, the cell homogenate was spun at 1000g for 10 minutes at 4 °C to obtain the '1K' pellet. The supernatant was collected and the 1K pellet was washed with 1ml of homogenising buffer and pelleted again.

The supernatant from the previous step was spun at 16000g for 80 minutes at 4°C to collect the '16K' pellet. The 16K pellet was washed in 3ml of homogenising buffer and the protein in the supernatant 'Supn.' was precipitated by adding a 100% w/v TCA and 4% w/v DOC solution (110ul/ml of supernatant). The sample was vortexed and kept on ice for 10 minutes, spun at max speed (21000g) for 15 minutes at 4°C. The pellet from the precipitation step was washed with 80% acetone and let dry. The 1K, 16K and precipitation pellets were all re-suspended in the same volume of lysis buffer for WB analysis.

The fractionation of cells over-expressing Myc-FLAG tagged MsrB3B aimed to separate the cytosolic protein from the cell organelles found in the cell homogenate. The homogenisation and the “1K” pellet were processed as above, then the supernatant was spun at 21’000g to obtain the “21K” pellet and the remaining protein in the supernatant ‘Supn.’ was precipitated using the TCA/DOC method just descried.

Here is a schematic representation of the fractionation steps for both experiments:

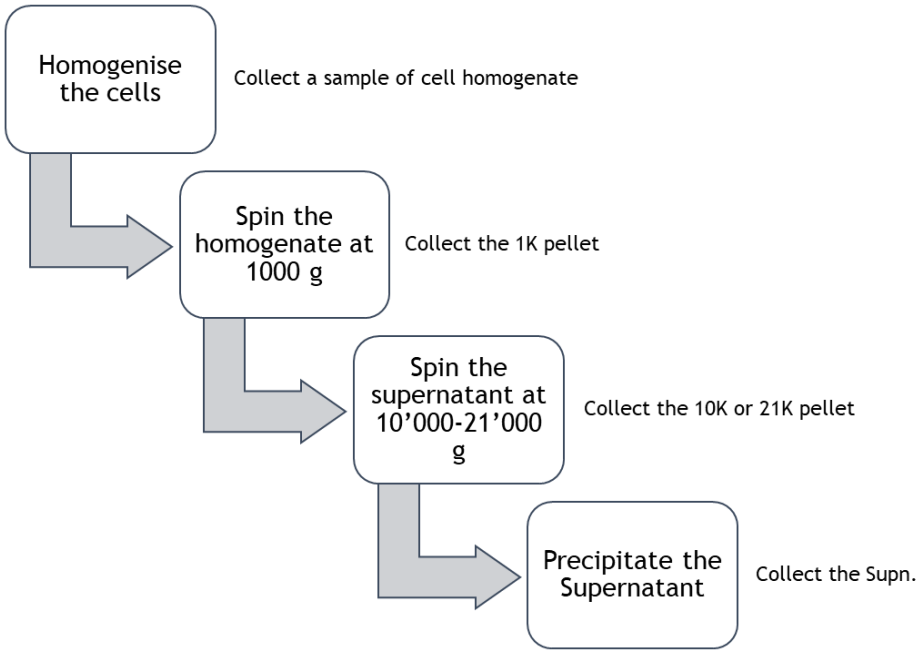

3.4. Knockout and Knock-in procedures

MsrB3 knockouts and MsrB3 x3FLAG-KAEL knock-in cells were obtained using the Invitrogen™ Neon™ Transfection System (MPK5000). crRNAs, tracrRNAs (Catalog 1072532), ssODNs for HDR, Alt-R™ S.p. Cas9 Nuclease V3 (Catalog 1081058), and Alt-R™ HDR Enhancer V2 (Catalog 10007910) were all purchased from IDT.

gRNAs and RNP complexes were re-suspended and prepared following the manufacturer's instructions.

On the day of the experiment, HT1080 and Hela cells were 80-90% confluent. Cells were trypsinised and counted to obtain 5 x10^5 cells/ electroporation. Cells were pelleted at 150g for 10m, washed with DPBS and spun again. The electroporation mix and the cells for the gene knockout (KO) and knock-in (KI) experiments re-suspended in resuspension buffer R (Invitrogen) were prepared as follows:

Gene Knock-in:

RNP complex - 10uM Cas9 and gRNA-	3ul
HDR donor (ssODN) at 50uM	1.2ul (4uM)
Cell suspension in buffer R (5x10^5 cells / electroporation tube)	10.8ul
Total volume	15ul

Gene Knockout:

RNP complex – 10uM Cas9 and gRNA-	3ul
Cell suspension in buffer R (5x10^5 cells / electroporation tube)	12ul
Total volume	15ul

Electroporation settings for both the KO and KI experiments using a 10µl Neon pipette:

Voltage	1050 V
width	35 ms
#pulses	2

After the electroporation, the cells were immediately re-suspended in complete DMEM and split into two wells of a 24 well plate. The KI cells were seeded into wells containing 2uM of HDR enhancer. Only HT1080 cells were chosen for the KO experiment, and both Hela and HT1080 cells were used for the KI experiment.

Single cells were isolated from the KO and KI cell pools by limiting dilution and individual clones were allowed to grow in 15cm tissue culture plates to allow adequate separation of the cell clones from one another.

The RNP complexes and gRNA were generated following the manufacturer's instructions. The crRNA, which were complexed with tracrRNA purchased from IDT to generate the gRNAs, for the KO and KI experiments are described below.

crRNA for the KO experiment

Sequence - Hs.Cas9.MSRB3.1.AB Alt-R® CRISPR-Cas9 crRNA, 2 nmol, 36 bases

5'- /AltR1 /rCrUrG rArGrU rGrArC rArUrG rGrUrA rCrUrG rCrArG rUrUrU rUrArG rArGrC rUrArU rGrCrU /AltR2/ -3'

Position	*Strand*	*Sequence*
65326897	Negative strand	CTGAGTGACATGGTACTGCAGGG

The PAM sequence is highlighted in yellow.

crRNA for the KI experiment

Sequence -Hs.HC9.DDYH0416.AA Alt-R® CRISPR-Cas9 crRNA, 2 nmol, 36 bases

5'-/ AltR1 /rGrArG rCrUrC rCrGrC rUrUrU rGrUrC rUrGrC rCrUrG rUrUrU rUrArG rArGrC rUrArU rGrCrU / AltR2/ -3'

Position	*Strand*	*Sequence*
65463300	Negative strand	GAGCTCCGCTTTGTCTGCCTGGG

The PAM sequence is highlighted in yellow.

HDR donor for the KI experiment

The HDR donor described was required to induce the desired mutation for the KI experiment:

Sequence - CD.HC9.SBKJ8645+ Alt-R™ HDR Donor Oligo, 2 nmol, 163 bases, Alt-R modified

5"- /Alt-R-HDR1/A*C*C GCC GAG GGA GGC AGT GGG GTC GCC AGC CCG GCC CAG GCA GAC GGC GGA GGC GGC GAC TAC AAG GAC CAC GAC GGC GAT TAC AAA GAT CAC GAT ATC GAC TAC AAG GAC GAC GAC GAT AAG AAA GCG GAG CTC TAG AGT AAT GGA GAG TGA TGG AAA CA*A* A/Alt-R-HDR2/ -3'

The UTR is highlighted in yellow.

Translation:

TAEGGSGVASPAQAD**GGGG**DYKDHDGDYKDHDIDYKDDDDKKAEL- UTR

Legend:

MsrB3 sequence preceding the KI site **/ Linker sequence /** X3 FLAG epitope tag/KAEL retention sequence

3.5. Nested PCR of gDNA and sequencing

Genomic DNA (gDNA) from WT cells and putative MsrB3 KO and MsrB3-x3FLAG-KAEL KI clones was extracted using the QuickExtract™ DNA Extraction Solution from Lucigen (Cat QE0905T) following the manufacturer's instructions.

To avoid non-specific amplification of gDNA sequences, two successive PCR reactions were performed to sequence the regions around the MsrB3 KO site and MsrB3 KI site noted below using the Herculase II Fusion DNA polymerases kit (part nº 600677). The first thermocycle reaction was carried out using a set of "outer" primers, flanking the KO and KI site, and ~150ng of gDNA as template. Three µl of the first reaction were then used as the template for a successive PCR reaction with primers designed to amplify a region contained in the desired amplified sequence, at either side of the CRISPR-Cas9 PAM recognition sites employed. The primers, purchased from Sigma Aldrich, were designed following the information on Transcript ENST00000308259.10 MSRB3-201 of Human GRCh38.p14 available on the Ensembl genome browser.

A SimpliAmp™ thermal cycler (Cat A24811) was employed to perform the PCR reactions. The thermocycle conditions are shown in **Table 1**.

Initial Denaturation	Denaturation	Annealing	Extension	Cycle length	Final Extension
5 min 95 °C	20 sec 95 °C	20 sec 60 °C	1 min 72 °C	X 25 (unless otherwise stated)	10 min 72 °C

Table 1: Thermocycle conditions elected to perform nested PCR on gDNA samples.

DNA and PCR samples were sent to Eurofins for sequencing.

The crRNA employed for the KO of the MSRB3 gene in HT1080 cells was designed to drive the CRISPR-Cas9 excision of the 1st exon following the signal sequence of MsrB3. The nuclease PAM sequence recognition site is reported below and, accordingly, the primers for the nested PCR were designed as follows:

Intron preceding the KO site

AAAAAAGGGTTTCAGGATACTGGGAGTTATAAAGCATGTACCTTGTGAATGATCAGTGAATTTTT
Outer primer forward

AGTATCACATGCTAGAGACTGGCTGTAGCATATTGTCACTGCTCCAGTGGAATCATCTGAATCTT
Inner primer forward

AAGAAACATTCATTTTAAACGTAGAGAAATAATCAGCTGCAGTTCAGGTAAGCATTTCCAGTGCA
TTAGAGACTGGTCTGGTCATTGACAAGTGACTGCAGAAGCT
GTGCTGTGGCGGTCAGCCAAAGCAATTATTTAGGATTCAAGCTAAAAAGGCTTCTTCTCCCATAT
CCTCTCTCTTTTCAG

Exon 3 (1st MsrB3 exon following the signal sequence) ENSE00001243871

GGTCGTGTAGGGATAAAAAGAACTGTAAGGTGGTCTTTTCCCAGCAGGAACTGAGGAAGCGGC
TAACACCCCTGCAGTACCATGTCACTCAGGAGAAAGGGACCGAAAG
PAM sequence

Intron following the KO site

GTAAGGTGAGCTTTAATAAAAAGTCATTAAGAGCTAGATTTCTTCTCCCCCTGCCCTCTGCAGTG
CTTTTCCTTGCCAATTAATTTAAAGCATTCTATACTTACTTGCTAAAGTCTATGAATTAGTATCCTT
GAAAAGGTTAAAATGGTGTTGTTTAGGTTAAGACTAAGTTTTATTTGTTCTTTTCTCCATTTAAT
GAATACTGCATATCTGATATAAAGTCACAAAGCTTTTGTTAAGGGCCTGTTTTTAGTTTACTACAA
AATGTGTGGAAGTAACAGCGATTTAGGTACATTTTTTGGGAAGACATCACAGTAAGCAAAACCA
Inner primer reverse

TGAGGGACTTGGCACTATGCCAGGATGCTGAAATTTTGAAGG
Outer primer reverse

The primers used for the MsrB3 KO site nested PCR are shown in **Table 2**.

Outer Forward	5' GGGTTTCAGGATACTGGGAG 3'
Outer Reverse	5' CAGCATCCTGGCATAGTGC 3'
Inner Forward	5' GTATCACATGCTAGAGACTGG 3'
Inner Reverse	5' GCTTACTGTGATGTCTTCCC 3'

Table 2: Primers designed for the amplification of the gDNA sequence flanking the MSRB3 KO site in exon 3.

As for the KI experiment, the crRNA utilised was designed to induce homologous directed repair of the MSRB3 gene with the HDR donor encoding the triple-FLAG tags by cutting the last exon of MSRB3 just before the KAEL retention sequence. The CRISPR-Cas9 RNP PAM recognition site and the primers elected for the nested PCR are reported below:

Intron preceding the KI site

CCCATCCAAAGCCAAAAGTAATGCCGGGGGAAAGATTTTATGCTGCCATGTTTCTTACAAGGGA
Outer primer forward

AGATCAAGGGTCAACTTGATTCATAAAATTACTGCAGTCATTTTTCAGCTGGCTGAGAGACTTCA
CAGATCAAAAAATACGTGGCTCCTAAATGATTTCTGATATGCACAATTCTAGTGTTTTTTGTTCTC
AGCATGTGGCGCAAAGCCTGCCAGAAACCATCTTTGCGGCTATTGACAGGCGGATTAGAAATCA
Inner primer forward

TCCACGATGGTTTCCTTCATTTCTCTACAGGCTGGTCATCCATTTAAACTGCTTAATGTGAATTC
CTCTCAAAGCCTGCTTTGTACATGCTTTTCCCTGACGTTTTGTTCTTCTCTTTCAG

Exon 7 (last MsrB3 exon) ENSE00003902807

TGTGGTGCTCACCTTGGGCACATTTTTGATGATGGGCCTCGTCCAACTGGGAAAAGATACTGC
ATAAATTCGGCTGCCTTGTCTTTTACACCTGCGGATAGCAGTGGCACCGCCGAGGGAGGCAGT
GGGGTCGCCAGCCCGGCCCAGGCAGACAAAGCGGAGCTCTAG -UTR starts-
PAM sequence

AGTAATGGAGAGTGATGGAA
ACAAAGTGTACTTAATGCACAGCTTATTAAAAAAATCAAAATTGTTATCTTAATAGATATATTTTTT
CAAAAACTATAAGGGCAGTTTTGTGCTATTGATATTTTTTCTTCTTTTGCTTAAACAGAAGCCCT
GGCCATCCATGTATTTTGCAATTGACTAGATCAAGAACTGTTTATAGCTTTAGCAAATGGAGACA
GCTTTGTGAAACTTCTTCACAAGCCACTTATACCCTTTGGCATTCTTTTCTTTGAGCACATGGCT
TCTTTTGCAGTTTTTCCCCCTTTGATTCAGAAGCAGAGGGTTCATGGTCTTCAAACATGAAAAT
AGAGATCTCCTCTGCAGTGTAGAGACCAGAGCTGGGCAGTGCAGGGCATGGAGACCTGCAAG
Inner primer reverse

ACACATGGCCTTGAGGCCTTTGCACAGACCCACCTAAGATAAGGTTGGAG
Outer primer reverse

The primers employed for the amplification of the MsrB3-x3 FLAG-KAEL KI site through nested PCR are shown in **Table 3**.

Outer Forward	5’ CCAAAGCCAAAAGTAATGCC 3’
Outer Reverse	5’ CCTTATCTTAGGTGGGTCTG 3’
Inner Forward	5’ TGCCAGAAACCATCTTTGCG 3’
Inner Reverse	5’ CATGTGTCTTGCAGGTCTCC 3’

Table 3: Primers designed for the amplification of the gDNA sequence flanking the MSRB3 KI site in exon 7.

3.6. Cloning procedures

3.6.1. Blunt-end ligation for single alleles sequencing

Whereby the nested PCR amplicons of gDNA regions of interest produced sequencing chromatograms with overlapping peaks, it was assumed that variations between either allele coding the same regions originated the mixed results. This technique was used to amplify the PCR products of the single alleles separately, to better characterise the mutations created by the gene-editing procedures described in section 3.4.

Bulleid's lab provided the pGEM3Z vector (2743bp) linearised with SmaI for this experiment. The size of the nested PCR amplicon, which was the insert in this cloning experiment, was calculated with reference to the WT DNA sequence. The ligation was performed by adding 100ng of linearised vector and PCR insert at a 1:4 ratio to the ligation mix (20ul) containing 1U of T4 Ligase and 1x T4 DNA Ligase Buffer (Catalog number: 46300018) and 20U of SmaI Restriction Enzyme (NEB R0141S). The mix was left at room temperature overnight and then stored at -20 °C.

3.6.2. Cloning of Myc-FLAG MsrB3B into pTetOne vector for inducible expression

pTetOne plasmid DNA and MSRB3B cloned into pCMV6 (OriGene RC208187) were digested with EcoRI and AgeI (New England Biolabs R3101S and R3552S) in 50ul reactions prepared as follows:

Plasmid DNA	1.5ug pTetOne / 5ug pCMV6 MSRB3B
EcoRI	1ul
AgeI	1ul
CutSMart Buffer 10X (NEB B6004S)	5ul
ddH_2O	Up to 50ul

The reactions were incubated at 37 °C for 2h, followed by a 10' incubation at 72°C to inactivate the restriction enzymes. The digested products were separated through a 1% agarose gel and visualised under low UV light (470nm) using BluPAD (BIO-HELIX - BP001CU). The gel portions corresponding to the digested pTetOne vector and Myc-FLAG MsrB3B insert were excised and purified using using the QIAquick Gel extraction kit (Qiagen 28706). One-hundred ng of

pTetOne digested with EcorI/ AgeI were combined with the My-FLAG MSRB3B insert at 1:3 and 1:5 ratios in the ligation mix (10ul) containing 1U of T4 Ligase and 1x T4 DNA Ligase Buffer (Catalog number: 46300018). The ligations mix was left at room temperature for 2h and then stored at -20 °C.

3.7. Transformation of competent cells and plasmid DNA isolation

Five ul of the ligation reactions were added to 50ul of XL-1 Blue cells and let on ice for 10'. Cells were transformed by inducing heat shock at 42 °C for 45'' and immediately placed back on ice for 10'. The transformation reactions were added 500ul of *Luria-Bertani* (LB) broth, prepared combining 10 g NaCl, 5 g of yeast extract and 10 g of tryptone in 1 L of ddH_2O, and incubated in a 37 °C shaker for 45'. Varying dilutions of competent cells transformed with the pTetOne plasmid DNA ligation mix were plated on *Agar plates* (made from the LB broth with the addition of 15 g of agar / L) prepared with 100ug/ml Ampicillin and they were incubated at 37 °C overnight. Five colonies were picked for the isolation of plasmid DNA.

The transformation mixes obtained from the pGEM3Z ligations were plated onto *Agar plates* prepared with 100ug/ml Ampicillin, 40ug/ml X-Gal and 48ug/ml IPTG. After incubating the plates at 37 °C overnight, the resulting white colonies were selected over the blue colonies for the purification of plasmid DNA.

Plasmid DNA isolation was performed following a standard alkaline lysis method:

Selected clones expressing plasmid DNA were grown overnight in 3ml of LB broth containing 100ug/ml Ampicillin. Half of the bacterial culture was pelleted in 1.5 microfuge tubes and re-suspended in 100ul of buffer P1 (QUIAGEN) and placed on ice, then 200ul of 0.2M NaOH 1% (w/v) SDS were added to lyse the cells and degrade chromosomal DNA. Then potassium acetate (5M, 150ul) was added to neutralise the reaction and to precipitate the protein. The tubes were spun and the supernatant was transferred into new tubes containing 450ul of phenol chloroform isoamyl alcohol to separate the DNA from the RNA and other organic molecules into different phases. The tubes were vortexed and spun to collect the upper phase, which was mixed with 450ul of chloroform to purify the plasmid DNA further. The tubes were spun and the upper phase was added to 800µl of pure ethanol to precipitate the plasmid DNA. The DNA pellet was washed with 70% ethanol and re-suspended in elution buffer (QUIAGEN). Larger plasmid DNA purifications were performed on 100ml cultures using the plasmid midi-kit by QIAGEN.

3.8. Agarose gel electrophoresis

The products of restriction enzymes digestions and PCR reactions were separated and visualised through gel electrophoresis with 1% w/v agarose gels in TAE buffer containing 40 mM Tris, 20 mM acetic, 1 mM EDTA and 1x SYBR™Safe DNA gel stain.

The DNA samples analysed were added NEB DNA Purple loading dye (B7024) to a 1x concentration.

Agarose gels were run at 80V and 100mA for 45-50 minutes. Gels were imaged using Azure c600 (Azure Biosystems) or visualised using low UV light.

3.9. Transfections, constructs, and reagents for recombinant protein expression

Cells growing in 6cm TC plates were transfected using MegaTran 2.0 (OriGene TT210003) and the chosen plasmid DNA at a 3:1 ratio. For the expression of His-myc-hSPARC FS-EC, HEK 293 cells were maintained under 10ug/ml Puromycin selection (Invivogen ant-pr-1) and subsequently expanded into T75 or T175 TC flasks.

Human SPARC FS-EC in His-Myc-pCEP-Pu vector

This construct for the expression of SPARC or BM40 FS-EC domains in mammalian cells was kindly provided by the Department of Life Science at the Imperial College London. The construct had previously been cloned into the pCEP-Pu vector.

Nucleotide sequence:

ATGAGGGCCTGGATCTTCTTTCTCCTTTGCCTGGCCGGGAGGGCTCTGGCAGCCCCGCT
AGTTCATCATCATCATCATCATGGTCCGCTAGTTGACGTCGCCAGCAATGAACAAAAACT
CATCTCAGAAGAGGATCTGGCTAGTATGACTGGTGGACAGCAAATGGGTCGGGATCTGT
ACGACGATGACGATAAGCTAGCCAATCCCTGCCAGAACCACCACTGCAAACACGGCAAG
GTGTGCGAGCTGGATGAGAACAACACCCCCATGTGCGTGTGCCAGGACCCCACCAGCTG
CCCAGCCCCCATTGGCGAGTTTGAGAAGGTGTGCAGCAATGACAACAAGACCTTCGACT
CTTCCTGCCACTTCTTTGCCACAAAGTGCACCCTGGAGGGCACCAAGAAGGGCCACAAG
CTCCACCTGGACTACATCGGGCCTTGCAAATACATCCCCCCTTGCCTGGACTCTGAGCTG
ACCGAATTCCCCCTGCGCATGCGGGACTGGCTCAAGAACGTCCTGGTCACCCTGTATGA
GAGGGATGAGGACAACAACCTTCTGACTGAGAAGCAGAAGCTGCGGGTGAAGAAGATCC
ATGAGAATGAGAAGCGCCTGGAGGCAGGAGACCACCCCGTGGAGCTGCTGGCCCGGGA
CTTCGAGAAGAACTATAACATGTACATCTTCCCTGTACACTGGCAGTTCGGCCAGCTGGA
CCAGCACCCCATTGACGGGTACCTCTCCCACACCGAGCTGGCTCCACTGCGTGCTCCCCT
CATCCCCATGGAGCATTGCACCACCCGCTTTTTCGAGACCTGTGACCTGGACAATGACAA
GTACATCGCCCTGGATGAGTGGGCCGGCTGCTTCGGCATCAAGCAGAAGGATATCGACA
AGGATCTTGTGATCTAA

Translation:

MRAWIFFLLCLAGRALAAPLVHHHHHHGPLVDVASNEQKLISEEDLASMTGGQQMGRDLYDD
DDKLANPCQNHHCKHGKVCELDENNTPMCVCQDPTSCPAPIGEFEKVCSNDNKTFDSSCHFF
ATKCTLEGTKKGHKLHLDYIGPCKYIPPCLDSELTEFPLRMRDWLKNVLVTLYERDEDNNLLTE
KQKLRVKKIHENEKRLEAGDHPVELLARDFEKNYNMYIFPVHWQFGQLDQHPIDGYLSHTELA
PLRAPLIPMEHCTTRFFETCDLDNDKYIALDEWAGCFGIKQKDIDKDLVI

Signal sequence His tag Myc tag Enterokinase cleavage site

FS domain EC domain

MsrB3 V5 ER version – MsrB3A V5

This construct was produced by GenScript and it was originally cloned into pcDNA3.1/Hygro(+) using the cloning sites BamHI/XbaI. The plasmid was designed for the over-expression for MsrB3 in the ER and it features a V5 tag at its C terminus, before the KAEL retention sequence. The construct was then modified to include a NotI site at the 5' and AgeI at the 3' ends that were used to clone it into pTetOne, creating an inducible expression system.

Nucleotide sequence:

ATGAGCCCGCGGCGGACCCTCCCGCGCCCCCTCTCGCTCTGCCTCTCCCTCTGCCTCTG
CCTCTGCCTGGCCGCGGCTCTGGGAAGTGCGCAGTCCGGGTCGTGTAGGGATAAAAAG
AACTGTAAGGTGGTCTTTTCCCAGCAGGAACTGAGGAAGCGGCTAACACCCCTGCAGTA
CCATGTCACTCAGGAGAAAGGGACCGAAAGTGCCTTTGAAGGAGAATACACACATCACA
AAGATCCTGGAATATATAAATGTGTTGTTTGTGGAACTCCATTGTTTAAGTCAGAAACCA
AATTTGACTCCGGTTCAGGTTGGCCTTCATTCCACGATGTGATCAATTCTGAGGCAATCA
CATTCACAGATGACTTTTCCTATGGGATGCACAGGGTGGAAACAAGCTGCTCTCAGTGT
GGTGCTCACCTTGGGCACATTTTTGATGATGGGCCTCGTCCAACTGGGAAAAGATACTG
CATAAATTCGGCTGCCTTGTCTTTTACACCTGCGGATAGCAGTGGCACCGCCGAGGGAG
GCAGTGGGGTCGCCAGCCCGGCCCAGGCAGAC***GGTAAGCCTATCCCTAACCCTCTCC***
TCGGTCTCGATTCTACGAAAGCGGAGCTCTAG

ER signal sequence ***V5 tag***

Translation:

MSPRRTLPRPLSLCLSLCLCLCLAAALGSAQSGSCRDKKNCKVVFSQQELRKRLTPLQYHVTQE
KGTESAFEGEYTHHKDPGIYKCVVCGTPLFKSETKFDSGSGWPSFHDVINSEAITFTDDFSYGM
HRVETSCSQCGAHLGHIFDDGPRPTGKRYCINSAALSFTPADSSGTAEGGSGVASPAQAD***GKP***
IPNPLLGLDSTKAEL*-

ER signal sequence ***V5 tag*** KAEL* ER retention tetrapeptide.

MsrB3 Myc-DDK(FLAG) mitochondria version

The construct for the over-expression of MsrB3 variant 2 (mitochondria version) was purchased from OriGene (Catalog RC208187). The ORF is cloned into pCMV6-Entry vector through the cloning sites SgfI/ MluI. The construct features a Myc-FLAG tag following the KAEL retention sequence at its C terminus.

Nucleotide sequence:

ATGTCTGCATTCAACCTGCTGCATTTGGTGACAAAGAGCCAGCCAGTAGCCCTTCGAGC
CTGTGGGCTTCCCTCAGGGTCGTGTAGGGATAAAAAGAACTGTAAGGTGGTCTTTTCCC
AGCAGGAACTGAGGAAGCGGCTAACACCCCTGCAGTACCATGTCACTCAGGAGAAAGGG
ACCGAAAGTGCCTTTGAAGGAGAATACACACATCACAAAGATCCTGGAATATATAAATGT
GTTGTTTGTGGAACTCCATTGTTTAAGTCAGAAACCAAATTTGACTCCGGTTCAGGTTGG
CCTv

Translation:

MSAFNLLHLVTKSQPVALRACGLPSGSCRDKKNCKVVFSQQELRKRLTPLQYHVTQEKGTESA
FEGEYTH
HKDPGIYKCVVCGTPLFKSETKFDSGSGWPSFHDVINSEAITFTDDFSYGMHRVETSCSQCGAH
LGHIFD
DGPRPTGKRYCINSAALSFTPADSSGTAEGGSGVASPAQADKAELTRTRPLEQKLISEEDLAAN
DILDYKDDDDKV

Mitochondria signal sequence myc tag DDK/FLAG tag

3.10. Purification of His-Myc tagged SPARC FS-EC

Cell media from HEK 293 T cells expressing the recombinant His-Myc SPARC FS-EC was spun to rid cell debris and it was stored at -20 °C.

A Bio-rad Econo-Pac® Chromatography Columns (Part 7321010) was packed with 2ml of Ni-NTA Agarose beads from Quiagen (Cat No: 30210). Before applying the cell media, the column was washed twice by filling it with a 5mM imidazole buffer A (300mM NaCl, 50mM TrisHCl pH 7.5, 5mM imidazole) to limit the non-specific binding of contaminants to the column.

The cell media sample from cell passage 4, sample volume: 13ml, was thawed and filtered through the column x3 times.

The column was washed x3.5 times with buffer A (x3.5 sample volume) to rid contaminants with low affinity to the agarose beads. The His-myc tagged SPARC FS-EC protein was eluted by subsequently adding x1/2 sample size volumes of buffers with increasing concentration of imidazole. The flow-through and the elution samples were separated through a 10% Acrylamide/Bisacrylamide 37.5:1 SDS/PAGE gel. The protein was either stained by incubating the gel in Quick Coomassie Stain (Generon, NB-45-00078) or characterised through WB analysis.

The samples found to contain the most purified protein were filtered using a Vivaspin™ 20 Centrifugal Concentrator with a 10000 MWCO (Sartorius VS2001) at 3500g. To remove the imidazole, the sample was re-diluted into a 150mM NaCl 50mM TrisHCl pH 7.5 buffer and concentrated using the same spin column.

3.11. Assay for MsrB3 reductase/oxidase activity

In the introduction (**Figure 4**) it was mentioned that MsrB3 active site thiol -C126- becomes sulfenylated upon reduction of methionine-R sulfoxide, and that it can be reduced by the resolving cysteines C03 and C09 which will form a disulphide bond, thus recycling C126 for one more substrate reduction. In the presence of thioredoxin, the disulphide bond between C03 and C09 can be reduced, and the active site C126 can be recycled indefinitely. When MsrB3 is fully oxidised, the sulfenylated active site C126 can reduce itself by oxidising methionine into methionine-R-sulfoxide (Cao, Mitchell et al. 2018). Since the oxidase activity of the MsrB3 acive site C126 is independent of the presence of the resolving cysteines, it was deemed appropriate to employ a double mutant (DM) MsrB3 provided by Bulleid's lab whose resolving C03 and C09 are mutated to alanine

MsrB3 DM sequence:

GPLGGSARDKKNAKVVFSQQELRKRLTPLQYHVTQEKGTESAFEGEYTHHKDPGIYKCVVCG
TPLFKSETKFDSGSGWPSFHDVINSEAITFTDDFSYGMHRVETSCSQCGAHLGHIFDDGPRP

TGKRYCINSAALSFTPADSSGTAEGGSGVASPAQADKAEL

C03A and C09A mutations

For this experiment, a double-mutant version of MsrB3 was employed. Both MsrB3 DM resolving cysteines which correspond to C03 and C09 in the WT protein are mutated to alanines. The Dabsyl Methionine (DABS-Met) and Dabsyl-Methionine Sulfoxide (DABS-MetO) were synthesised by Professor Richard Hartley's lab at the School of Chemistry of the University of Glasgow.

The reaction mixture (200 µl final volume) contained 20 mM Tris–HCl buffer, pH 7.5, 150 mM NaCl, 10 µM MsrB3A DM and either 10 mM DTT for the reducing reaction or 10mM MetO for the oxidising reaction. The mixture was incubated at 37 °C for 30' before adding either 50uM of DabsMet or 50uM of DabsMetO. The samples were incubated at 37 °C for 6h before being loaded onto a C18 column (25 cm Apex ODS 5 µ, Jones Chromatography) equilibrated in 100 mM sodium acetate (pH 6) and 30% v/v acetonitrile. The samples were eluted through a linear gradient from 30% to 70% v/v of acetonitrile. An Akta Micro-

Chromatography controlled by the Unicorn software (v.5.2) was used to monitor the dabsyl derivatives by absorbance at 460nm.

3.12. Preparation of the samples for the LC/MS/MS analysis of the MsrB3-mediated oxidation of His-Myc hSPARC FS-EC

The reaction mixtures contained 20 mM Tris–HCl buffer, pH 7.5, 150 mM NaCl, 10 µM MsrB3A DM and either 10 mM DTT for the reducing reaction or 10mM MetO for the oxidising reaction. After a pre-incubation at 37 °C for 30', the oxidising and reducing reactions were split into triplicates and 10uM of purified His-Myc hSPARC FS-EC, for a total reaction volume of 40µl containing 71.5% $H_2{}^{18}O$. The samples were incubated overnight at 37 °C. The protein was precipitated with ice-cold acetone for 2h at -20°C and sent for MS analysis.

The LC/MS/MS analysis was performed by Sergio Lilla at the CRUCK Scotland Institute Proteomics unit. Sergio kindly provided the description of the methods employed, reported below.

"Peptides resulting from all trypsin digestions were separated by nanoscale C18 reverse-phase liquid chromatography using an EASY-nLC II 1200 (Thermo Scientific) coupled to an Orbitrap Fusion Lumos mass spectrometer (Thermo Scientific). Elution was carried out at a flow rate of 300 nl/min using a binary gradient, into a 50 cm fused silica emitter (New Objective) packed in-house with ReproSil-Pur C18-AQ, 1.9 µm resin (Dr Maisch GmbH), for a total run-time duration of 135 minutes. Packed emitter was kept at 50 °C by means of a column oven (Sonation) integrated into the nanoelectrospray ion source (Thermo Scientific). Eluting peptides were electrosprayed into the mass spectrometer using a nanoelectrospray ion source. An Active Background Ion Reduction Device (ESI Source Solutions) was used to decrease air contaminants signal level. The Orbitrap Fusion Lumos tune version 4.0.4091 and Xcalibur 4.6 (Thermo Scientific) were used for data acquisition. A full scan was acquired at a resolution of 120000 at 200 m/z, over mass range of 350-1500 m/z. HCD fragmentation was triggered for the top 15 most intense ions detected in the full scan. Ions were isolated for fragmentation with a target of 5E4 ions, for a maximum of 175 ms, at a resolution of 15,000 at 200 m/z. Ions that have already been selected for MS2 were dynamically excluded for 10 sec. In order to select for fragmentation peptides

that incorporated ^{18}O water during reaction, the Exclude isotopes option and the MIPS filter (Monoisotopic Precursor Selection) were both disabled.
The MS Raw data were processed with MaxQuant software version 1.6.14.0 and searched with Andromeda search engine, querying SwissProt Homo sapiens (45401 entries) and the sequences of SPARC and MsrB3. First and main searches were performed with precursor mass tolerances of 20 ppm and 4.5 ppm, respectively, and MS/MS tolerance of 20 ppm. The minimum peptide length was set to six amino acids and specificity for trypsin cleavage was required. Cysteine carbamidomethylation was set as fixed modification, whereas N-terminal acetylation and Methionine oxidation light (+15.9949 Da) and heavy (+17.9992 Da) were specified as variable modifications. For peptides modified with oxidised Methionine, a neutral loss of light (- 66.0025 Da) and heavy (- 63.9983 Da) methanesulfenic acid

from peptide product ions was configured in MaxQuant oxidation modifications. The peptide, protein, and site false discovery rate (FDR) was set to 1%. All MaxQuant outputs were analysed with Perseus software version 1.6.2.3."

3.13. Immunofluorescence

Cells grown overnight on 13mm glass coverslips (VWR) coated with Poly-D Lysine (Sigma Aldrich, P6407) were washed in DPBS and fixed in cold 4% w/v paraformaldehyde (Thermo Scientific™ 28906) in DPBS for 15 minutes or ice-cold methanol for 10 minutes. Cells fixed in paraformaldehyde were then permeabilised in 0.2% v/v Triton X-100 in DPBS for 5 minutes. The specimens where blocked with 0.2% w/v BSA in DPBS for 30 minutes prior being incubated face-down on Parafilm with ANTI-FLAG® M2 antibody (Sigma-Aldrich F3165) (in 1/300 dilution in the blocking solution) for 45 minutes for the detection of FLAG-tagged proteins.

After washing the primary antibody with DPBS, specimens were incubated face-down on Parafilm with Goat anti-Mouse IgG Alexa Fluor™ 488 in 1/200 dilution in blocking buffer for 30 minutes. The coverslips were washed in DPBS and then in ddH_2O then mounted on glass coverslides using Vectashield (VectorLabs H-1700-2).

The cells were imaged using A Zeiss Axio Observer A1 inverted microscope equipped with a 40X oil immersionFluor lens. Fluorescence excitation light was generated by the Colibri illumination system with excitation wavelength at 470 nm.

4. RESULTS

A selection of the experimental results acquired during the investigative year of the MRes project are reported here. This section will reference gene knockout (KO), gene knock-in (KI) and stable cell lines. A KO cell line is established by ablating (knocking out) a certain gene. Gene knock-in refers to a genetic engineering method aimed to insert or modify DNA sequences in a specific locus of the genomic DNA (gDNA) of a cell. Stable cell lines are established by isolating a single cell that has stably integrated a construct of interest into its genome following transfection.

4.1. MsrB3 is not fully translocated to the ER and mitochondria, and it is also retained in the cytoplasm.

At the beginning of the project, it was necessary to find an antibody suitable for the detection of endogenous levels of MsrB3 in mammalian cell lysate to study its expression in vivo. MSRB3 Monoclonal Antibody clone OTI2A2 (Invitrogen MA526601) proved to be most efficient, but this antibody appeared to also have affinity for another protein present in cultured cells, as disclosed by WB analysis, producing a non-specific band of ~50 kDa as shown in ***Figure 7***.

4.1.1. KO experiment screening results.

Producing a cell line lacking the expression of MsrB3 was the first objective of the investigation. Human HT1080 cells are widely used in Prof. Bulleid's lab to produce transgenic cell lines. For this reason, the same cell line was selected in this investigation to produce MSRB3 KO cells. This choice will allow a direct comparison of experimental results between this and other HT1080 transgenic lines produced in the same lab, in future research. WB analysis was employed as a first screening method for the KO clones, using an antibody sensitive to endogenous MsrB3 found in cell lysate that was identified in previous research in Bulleid's lab.

Comparison of the WB results of the putative MsrB3 KO clones Total Cell Lysate (TCL) with HT1080 WT TCL disclosed that seven KO clones did not express MsrB3 and one clone, B3, expressed the enzyme but at a lower level compared to the WT (***Figure 7***). This result also showed that the 50kDa band seen in the blots is a

protein that the anti-MsrB3 antibody has non-specific affinity to, since it is expressed by both the HT1080 WT and putative MsrB3 KO clones.

The generation of the putative KO cell lines also revealed that the slower (s) and the faster (f) migrating bands seen in the WT TCL WB analysis (***Figure 7***) both correspond to MsrB3 since neither of these bands are seen for the MsrB3 KO clones. These MsrB3 species needed to be further characterised to understand why there is a difference in their mobility in SDS PAGE.

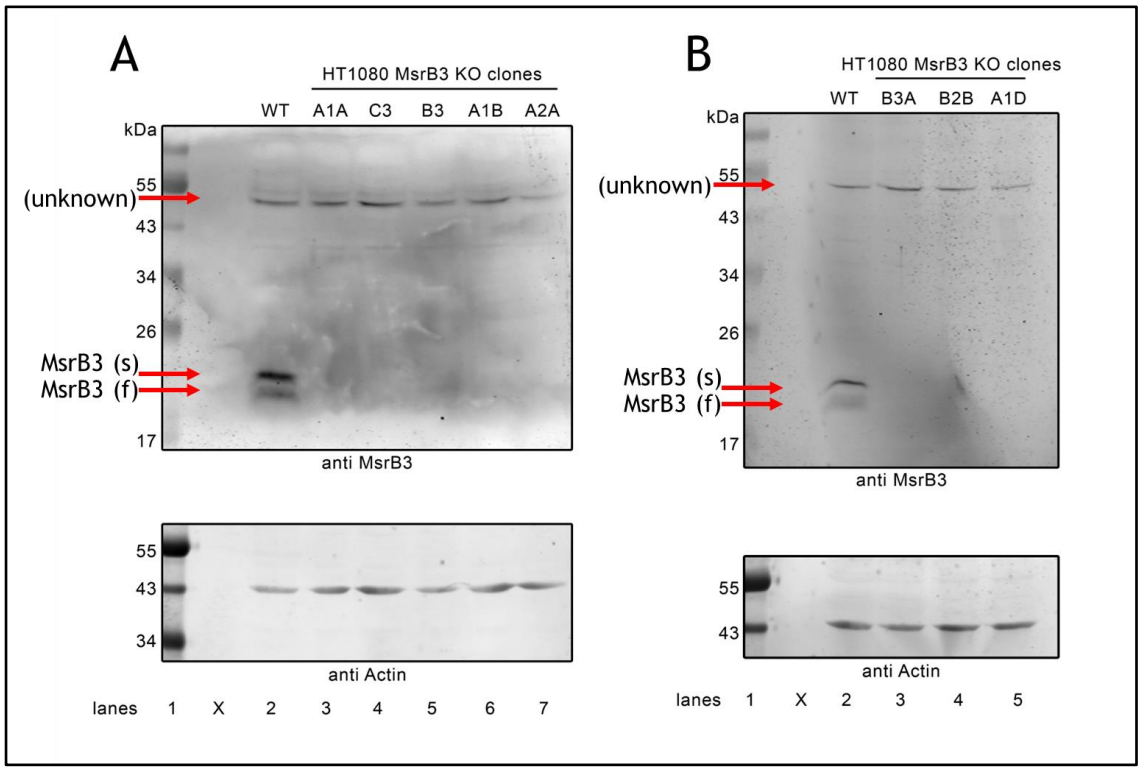

Figure 7: MsrB3 KO screening results*. Single clones originating from the HT1080 WT cells electroporated to knock-out the MSRB3 gene were lysed, and the TCL was analysed by WB to detect the expression of MsrB3. Panel A shows the MsrB3 expression level of HT1080 WT (panel A, lane 2) compared to the levels found in putative HT1080 MsrB3 KO clones A1A, C3, B3, A1B and A2A shown in this order in lanes 3 to 7. Panel B shows the WT MsrB3 expression level (panel B, lane 2) to the MsrB3 KO clones B3A, B2B and A1D reported in lanes 3, 4, and 5, respectively. The arrows indicate the slower (s) and faster(f)-migrating species of MsrB3 and an unidentified ~50kDa product detected non-specifically by the anti-MsrB3 antibody. The blots were incubated with anti-MsrB3 (*MA526601*) and anti-Actin from Sigma (A2103) as a loading control. The protein molecular weight marker (*NEB P7718S*) was loaded in lanes 1. The Molecular Weight is shown in kDa.*

To confirm whether the MSRB3 gene was successfully knocked out in the putative KO clones, the DNA regions flanking the KO site were amplified by nested PCR and sequenced to characterise the mutations introduced. Before sending the samples for sequencing, the PCR products obtained from HT1080 WT and five of the MsrB3 KO clones were analysed by agarose gel electrophoresis. The results shown in **Figure 8** revealed that the PCR products of three of the five KO clones analysed were smaller than the WT amplicon (**Figure 8**, lanes 9, 10 and 13 compared to lane 8), suggesting that they could harbour deletions in the MsrB3 exon that was targeted for knock-out. The nested PCR failed for the remaining two clones analysed, B3 and A1B, so only the WT, clones A1A, C3 and A2A PCR samples were sent for sequencing.

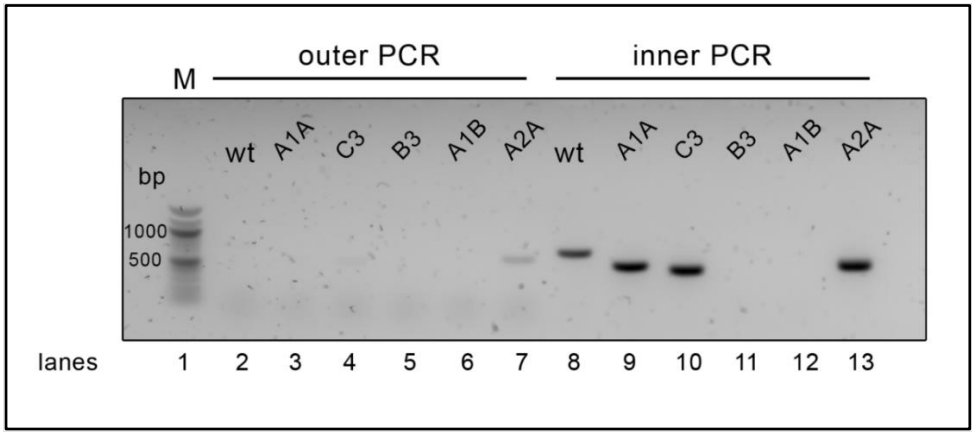

Figure 8: Nested PCR-amplified DNA regions flanking the exon of MSRB3 targeted for KO in WT and MsrB3 KO cells gDNA*. The 100bp DNA ladder from New England Biolabs (N3231S) was loaded in lane 1. The products of the first PCR reaction using the "outer" primers and gDNA template from WT, MsrB3 KO clones A1A, C3, B3, A1B and A2A were loaded, in this order, in lanes 3 to 7. The products of the second PCR reactions performed using the "inner" primers were loaded in lanes 8 to 13. The outer and inner PCR reactions were cycled 30 and 25 times, respectively.*

The sequencing analysis disclosed that all three clones featured a large deletion compared to the WT sequence either preceding or following the PAM recognition sites. The putative KO clones A1A and A2A were found to have deletions following the PAM crRNA site of 185 and 203 bp, respectively, whereas the MsrB3 KO clone C3 featured two tandem deletions of 190 and 180 bp, interspaced by a short-mutated sequence, both preceding the PAM site. The sequencing results for each KO clone are shown in the Appendix figures 1, 2 and 3. The presence of these deletions supported the evidence that the selected clones were indeed MsrB3 knock outs. Clone C3 was chosen for use in the following experiments.

4.2. Cell fractionation results

An earlier study that aimed to investigate the subcellular distribution of different Msrs revealed that the MsrB3A signal sequence and the tetrapeptide KAEL retention signal found at the C-terminus of the human MsrB3 sequence are required for targeting MsrB3 to the ER and its retention there. By contrast, only the signal sequence of MsrB3B is required for its targeting to the mitochondria, although the KAEL signal is present in both MsrB3A and B (Kim and Gladyshev 2004). However, this study gave no indication of the endogenous abundance of MsrB3 in the ER and the mitochondria of human cells, partly because of a lack of antibodies sensitive enough to detect endogenous levels of this reductase in mammalian cells and tissues.

To investigate the nature of the MsrB3 bands described in section 4.1.1 and to determine the distribution of MsrB3 between the mitochondria and the ER, a cell fractionation experiment was performed. The fractionation samples were analysed by WB using the following cell markers:

detection of	**antibody**
Mitochondria	αTOMM40 (Proteintech, 18409-1-AP).
Membrane and ER	αMHCI : HC10 (serum mouse antibody raised against MHC class I).
ER	αPDI (gift from Stephen High).
cytoplasm	αGAPDH (ThermoFisher, 10515025).
Golgi	αGM130 (gift from Martin Lowe).
MsrB3	αMsrB3 (ThermoFisher 15956194).

Table 4: Sub-cellular markers antibodies used in WB.

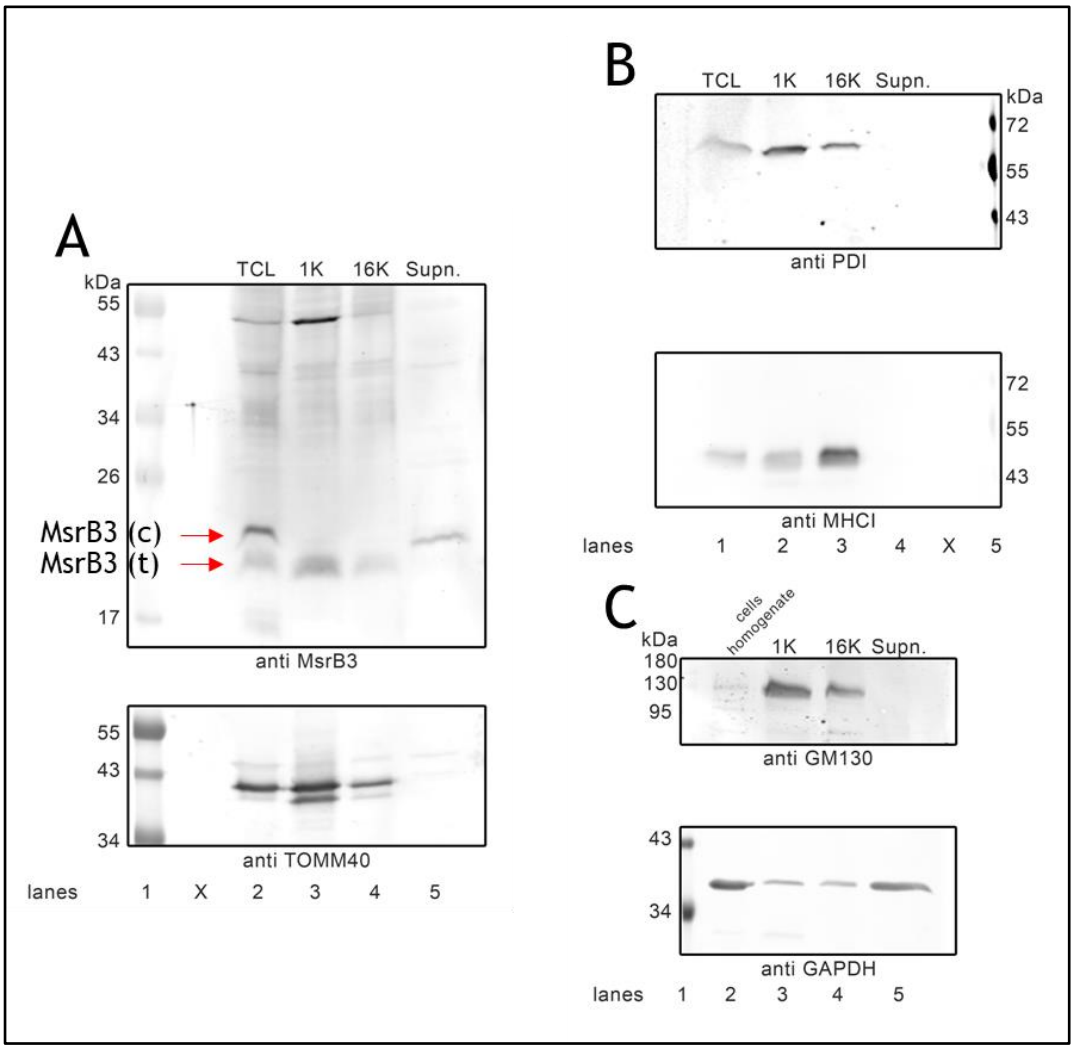

Figure 9: HT1080 cell fractions analysed in by WB to determine the localisation of the endogenous MsrB3 species*. In panels A and B, HT1080 WT Total Cell Lysate (TCL) was used as a control because the cell homogenate was too diluted to produce a signal for some of the cell markers employed. In panel A, the cytosolic (c) and the targeted (t) forms of the endogenous MsrB3 are indicated by separate arrows. Each panel represents the results of individual Western blots.*

In this experiment, the separation of the mitochondria and ER was attempted by sequentially centrifugating the cell homogenate at 1000g (1K pellet) and 16000g (16K pellet). However, the results revealed that this separation was not achieved, as indicated by the presence of all cell markers in the 1K and 16K samples. The TOMM40 mitochondrial marker was most abundant in the 1K pellet but also seen, to a lesser degree, in the 16K pellet (**Figure 9**, panel A, lanes 3 and 4). The PDI and HC10 ER markers were present in the 1K pellet as well as the 16K pellet (**Figure 9**, panel B, lane 2). Furthermore, the GAPDH cytosolic

marker appeared in all fractions (**Figure 9**, panel C) but at different levels. However, the results indicated that the supernatant "Supn." was free of any organelle material as none of the ER and mitochondrial markers were seen for in this sample (**Figure 9**, panels A and B). Only the cytosolic marker, GAPDH, was detected in the Supn.(**Figure 9**, bottom panel C), as in indication that the method used successfully produced a sample containing only cytosolic proteins. Interestingly, MsrB3 was detected in the Supn. sample and exclusively in its slower-migrating from (**Figure 9**, panel A, MsrB3 (c)). On the contrary, only faster migrating MsrB3 species were present in the 1K and 16K fractions (**Figure 9**, panel A). Coincidently, the GAPDH found in these samples was reduced compared to the amounts found in the other samples, while the ER, mitochondria and Golgi markers were abundant. This was an indication that the 1000g and 16000g spins yielded cell fractions enriched with cell organelles proteins, and depleted of the cytosolic protein. As expected, both MsrB3 species were detected in the WT TCL (panel A).

This evidence suggests that the slower migrating species of MsrB3 seen in WB is found exclusively in the cytosol (MsrB3 (c)), while the MsrB3 either targeted to the ER and mitochondria appears to have a lower molecular weight (MsrB3 (t)). It is reported that rat MsrA featuring the N-terminal mitochondrial signal peptide is found in both the cytosol and the mitochondria, with the more slowly folding forms of MsrA being targeted to the former (Kim and Gladyshev 2007). Therefore, it is likely that the cytosolic MsrB3 species seen here originates from the translation of untargeted MsrB3 retaining its signal peptide. This hypothesis, however, requires further investigation.

While these results explained where the slower migrating form of MsrB3 seen in WB analysis localises, it was still unclear what the distribution of the enzyme is between the ER and the mitochondria.

Immunofluorescence experiments using the same anti-MsrB3 monoclonal antibody used in WB had been attempted in Prof Bulleid's lab to visualise MsrB3 in fixed cells, but due to the apparently low endogenous expression of MsrB3 and the non-specific binding of the available antibody to another protein, these attempts were inconclusive.

4.3. A triple FLAG tag helps detect endogenous levels of MsrB3 in Western blot analysis

The fractionation experiment disclosed that the predominant MsrB3 species, which presents itself as the slower migrating band seen in WB, is the cytosolic version of this enzyme. However, more sensitive methods such as immunofluorescence techniques were needed to better determine the sub-cellular distribution of MsrB3 between the ER and mitochondria. Previous attempts carried out in Prof Bulleid's lab revealed that the only antibody sensitive to MsrB3 levels endogenously expressed by mammalian cells (Invitrogen 15956194) in WB wasn't suitable for immunofluorescence microscopy, as its non-specific binding seen in Figure 5 made interpretation of the fluorescence signal ambiguous. The general lack of alternative, cheaper anti-MsrB3 antibodies was also a disadvantage for the investigation. Thus, it was decided to modify the endogenous MsrB3 expressed by the mammalian cells used in this investigation so that the enzyme could be detected by antibodies with a better specificity. It was also desirable to modify MsrB3 to generate a stronger signal in immunofluorescence and WB analysis. Therefore, it was decided to knock-in a triple (x3) FLAG tag at the C terminus of MsrB3, preceding the KAEL retention sequence, in both HeLa and HT1080 cells. The two cell lines were selected for this experiment for different reasons. HT1080 cells are widely used in Prof Bulleid's research group and thus creating mutant cell lines in the HT1080 background would be desirable, allowing the mutant to be compared to other cell lines available in the lab in future experiments. However, the KI procedure had only previously been implemented on HeLa cells, with positive results, so they were also selected to increase the chances of obtaining a MsrB3 - x3 (triple) FLAG-KAEL KI line.

The triple FLAG tag was chosen because anti-FLAG antibodies don't have specificity for any endogenous protein present in mammalian cells, and the presence of a triple epitope would hopefully give rise to a greater signal for MsrB3 in antibody-based assays. The HDR donor described in the methods (section 3.4) was designed to encode a short linker sequence of four tandem glycine residues before the triple tag, to reduce the likelihood of the FLAG tags interfering with the enzyme's structure and function.

Following the gene knock-in (KI) procedure, clones originating from the HT1080 WT cell line were less viable and only expressing WT MsrB3, therefore the results for the KI experiment on HeLa WT cells will be reported. The MsrB3-x3 FLAG-KAEL KI clones were first screened by WB, which revealed that KI clones A2, A3A and A4A were expressing a slower migrating species of MsrB3 (**Figure 10**, panel A, lanes 2, 5 and 6) recognised by the anti-MsrB3 antibody, which was also detected by the anti-FLAG antibody (**Figure 10**, panel B, same lanes). Clones A2 and A3A also expressed the faster migrating species of MsrB3 (**Figure 10**, panel A, lanes 2 and 5) not detected by the anti-FLAG antibody, which was thought to correspond to the WT enzyme. As hoped, the anti-FLAG antibody didn't show specificity for any other target in WB analysis. To condense the names given to the x3FLAG MsrB3 knock-in HeLa clones, these will be referred as "KI" clones in this manuscript.

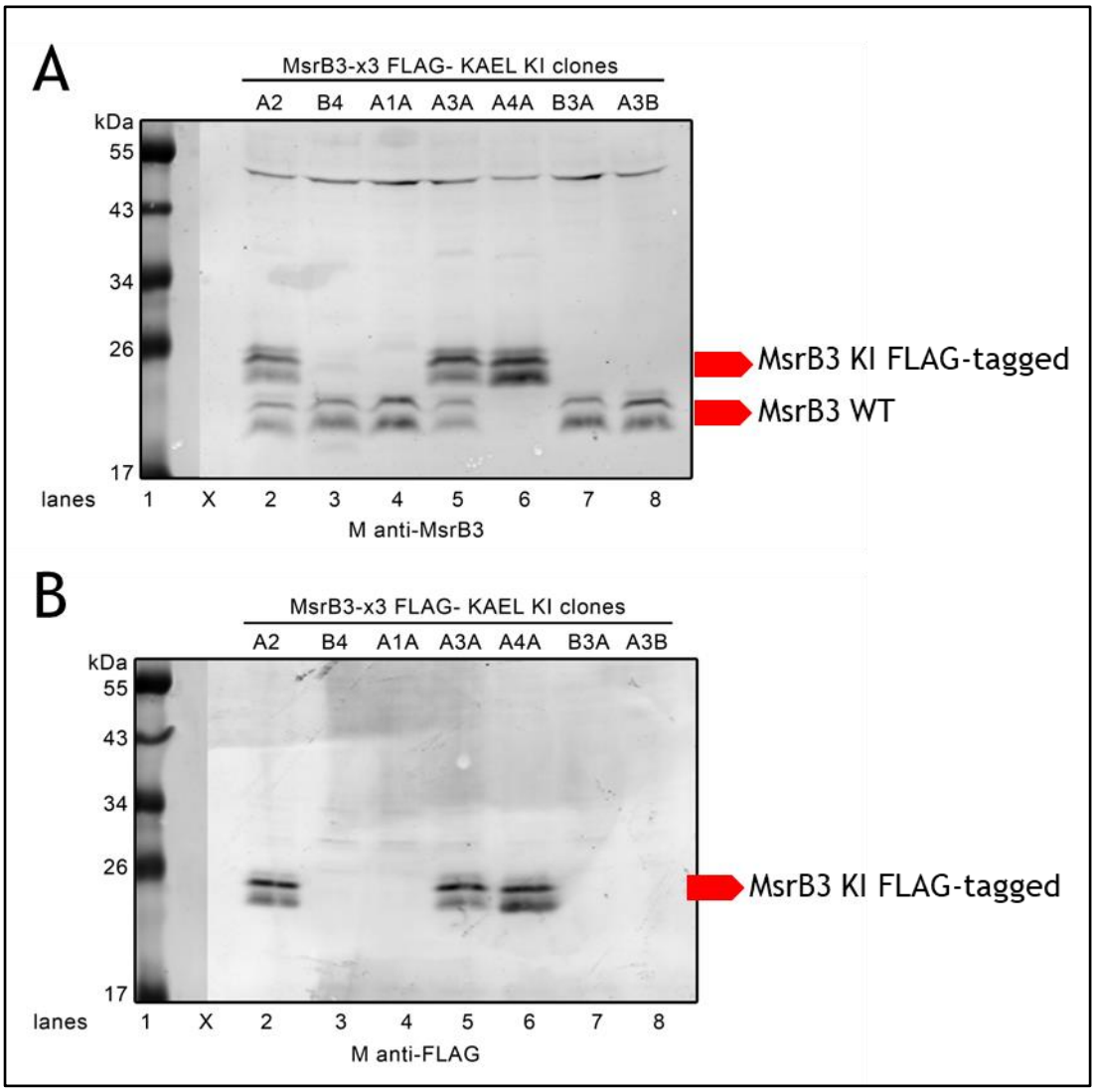

Figure 10: Screening of the MsrB3 x3FLAG-KAEL KI clones by WB. *HeLa cell lines obtained from the KI experiment were lysed and the TCL was examined by WB for the detection of FLAG-tagged MsrB3. One blot was incubated with the anti-MsrB3 antibody (A) and panel B shows the results for a second blot incubated with the anti-FLAG antibody from Sigma (F3165). The results of the KI clones A2, B4, A1A, A3A, A4A, B3A and A3B are reported in both blots, in this order, in lanes 2 to 8. The protein marker is shown in lanes 1.*

Based on these findings, A4A appeared to be a clone exclusively expressing FLAG-tagged endogenous MsrB3, suggesting that the KI procedure introduced the desired mutation on both alleles or that one allele was modified and the second allele encoding WT MSRB3 was knocked-out. KI clones A2 and A3A were believed to be heterozygous for the KI insertion, because both WT and x3-FLAG tagged MsrB3 are expressed by either clone. Sequencing analysis was needed to explore these hypotheses, so HeLa WT and the putative MsrB3-x3FLAG-KI clones gDNA was extracted to amplify the DNA sequence flanking the KI site for sequencing.

The results shown in **Figure 11** proved that the nested PCR reactions worked. Although unambiguous resolution of the PCR samples wasn't achieved, the agarose gel electrophoresis suggested that there was a small size difference between the PCR products obtained from HeLa WT and KI clones A2, A3A and A4A, as the mutants' inner PCR products in lanes 7, 8 and 9 appeared to be slightly longer than the WT amplicon loaded in lane 6 (**Figure 11**).

Clone A4A's PCR product was selected for sequencing because it more likely represented a mutant whose MSRB3 alleles were both mutated by inclusion of the desired triple-FLAG tag.

The sequencing results shown in **Figure 12** revealed that A4A differed from the WT sequence after the PAM site recognised by the gRNA, but the chromatogram shows ambiguous signals from the PAM site onward. The A4A MSRB3 alleles' sequences might differ from that point on, hence producing the mixed sequencing result.

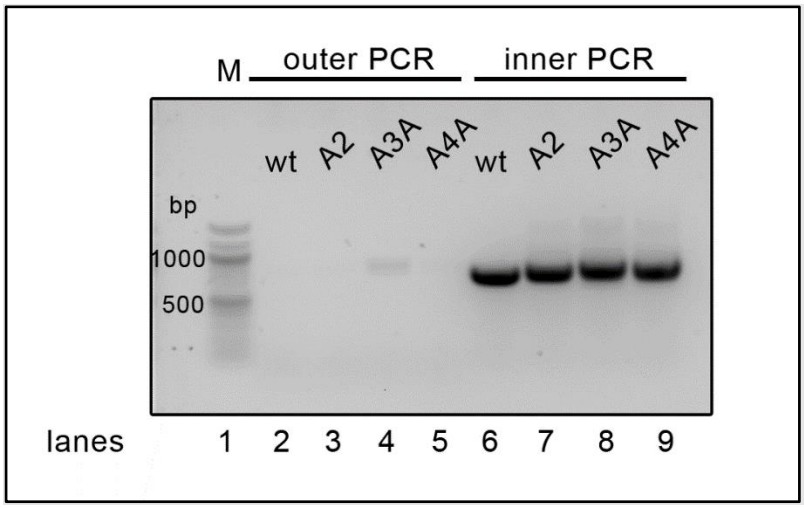

Figure 11 : Gel electrophoresis analysis of the nested PCR-amplified MSRB3 exon targeted for KI in WT and selected KI clones' gDNA. *Genomic DNA from HeLa WT and HeLa KI clones A2, A3A and A4A was used as template for the nested-PCR amplification of the DNA sequence flanking the mutation site at exon 7 of the MSRB3. The products obtained were then analysed by agarose gel electrophoresis. The 100 bp DNA ladder from New England Biolabs (N3231S) was loaded in lane 1. The samples of the first PCR reaction using the "outer" primers and gDNA template from WT, MsrB3 KI clones A2, A3A and A4A were loaded, in this order, in lanes 2 to 5. The products of the second PCR reactions performed using the "inner" primers were loaded in lanes 6 to 9. The outer and inner PCR reactions were set for a x25 cycle.*

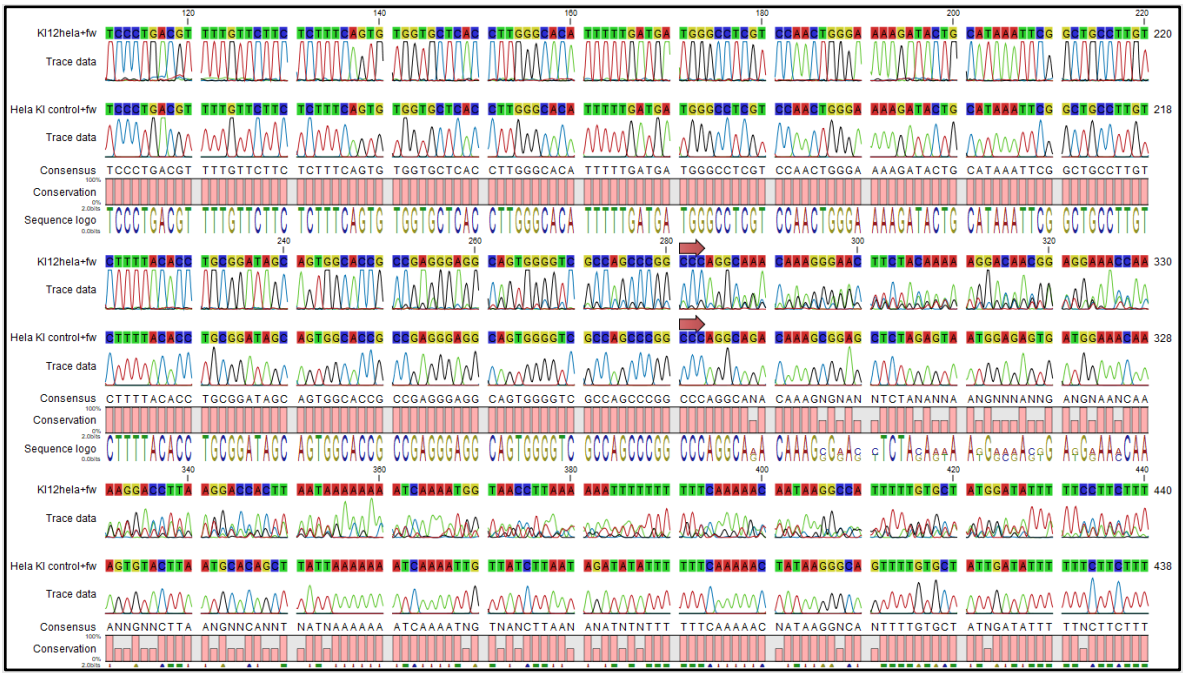

Figure 12: Sequences of the PCR-amplified MSRB3 exon targeted for KI from HeLa WT and HeLa KI clone A4A gDNA*. The sequences of the amplified MSRB3 region targeted in the KI experiment in WT and KI clone A4A gDNA were aligned using CLC Genomics Workbench version 7.5.1. The PAM site of the gRNA employed for this experiment is marked by a red arrow above each sequence. The WT sequence, is referred to as HeLa KI control and the putative KI clone A4A as KI 12 HeLa. The nucleic acid sequences in are represented in the 5' to 3' direction.*

To investigate the mutation generated in the KI clone A4A alleles singularly, the A4A PCR amplicon was cloned into pGEM3Z. Considering that the size of the WT PCR KI amplicon, given by the number of base pairs between the two inner primers, is 695 bp, ~100 ng of the PCR reaction obtained from the KI clone A4A were used in the ligation mix to achieve a 1:4 vector-to-insert ratio. Details on the size and amount of the vector used for the ligation are found in the methods section 3.6.1. The ligation mix should yield pGEM3Z products re-ligated with the PCR amplicons originating from either KI A4A allele. These products are replicated by transformation into XL1-Blue cells, which will generate white colonies in the growth conditions detailed in the methods sections 3.7. Colonies containing re-ligated pGEM3Z with no insert will produce ß-galactosidase, which hydrolyses the X-Gal provided. This condition will turn these colonies blue in colour, making them easy to discriminate. Six white colonies were picked and amplified to miniprep the plasmid DNA.

The analysis of the allele-specific sequences returned two alternative results. Two of the minipreps analysed had the desired x3-FLAG sequence at the designed site, followed by the KAEL retention motif. One example of this is reported in **Figure 13**, "KI 12 clone 4". A third miniprep – "Ki 12 clone 5"- featured the same mutation, as well as a single alanine deletion caused by a missing triplet, 14 amino acids before the KI site.

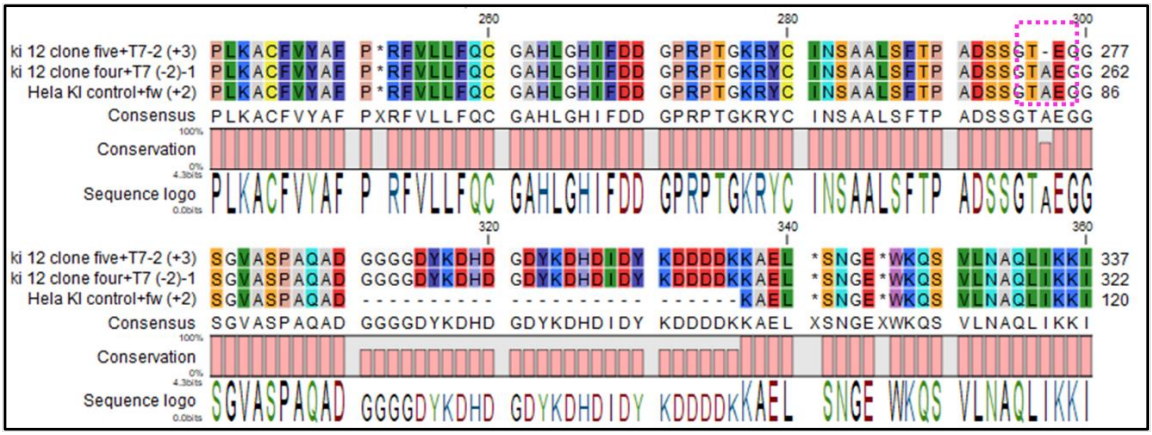

Figure 13: Multiple protein sequence alignment of the regions flanking the MsrB3 KI site in WT DNA and KI clone A4A alleles*. The minipreps obtained from the blunt-end ligation of the KI clone A4A PCR amplicon were sent for sequencing and analysed with CLC Genomics Workbench version 7.5.1. The translation of two minipreps (KI 12 clones five and four) were aligned with the WT sequence (Hela KI control). The dashed magenta box highlights the single aa deletion found in one of the KI A4A alleles represented by the KI 12 clone 5 sequence. This and the alternative allele both feature an insertion between position 311 and 336 compared to the WT sequence which is consistent with the triple-FLAG tag design. The nucleic acid sequences in are represented in the 5' to 3' direction.*

This variation could plausibly explain the ambiguous signal seen in the previous sequencing results of the KI clone A4A, shown in **Figure 12**.

Based on these results, the KI clone A4A alleles appeared to both encode the desired FLAG tag. Because the additional mutation of one allele missing the A residue didn't result in a frameshift, nor the loss of a catalytically active feature of MsrB3, the triple FLAG KI procedure was deemed successful in introducing the desired change in both MSRB3 alleles without disrupting the protein's translation.

This evidence, supported by the WB of KI clone A4A, confirmed that the MSRB3 gene in this cell line encodes the triple-FLAG tag at the desired site in MSRB3. More importantly, the mutant MsrB3 was detected by the anti-FLAG antibody, thus offering an alternative to the anti-MsrB3 antibody. The characterisation of the KI A4A clone encouraged the progression into the next step of this aspect of the investigation, which focused on determining the distribution of MsrB3 within the mammalian cell through IF experiments exploiting the FLAG-tag of the MsrB3 expressed in the KI clone A4A.

In the attempt to find a suitable antibody for IF microscopy, two antibodies were tested on WT and KI A4A cells fixed with methanol. The results for the anti-FLAG Boster Bio M30971 and the Sigma Aldrich F3165 antibodies are shown in ***Figure 14*** and ***Figure 15***, respectively. To ascertain whether either antibody was suitable for IF analysis, specimens from HeLa cells transiently transfected with FLAG-tagged Lipase Maturation Factor 1 (LFMF1) in pcDNA3.1 were included. LMF1 is a membrane bound ER resident protein.

The results in Figure 11 showed that the antibody worked on cells exogenously expressing the FLAG-tagged LMF1, transfected the day before the experiment, proving that the M30971 can bind to FLAG-tagged proteins in cells fixed with methanol. In this specimen (***Figure 14***, top row, left panel), the cells expressing the recombinant LMF1 displayed bright fluorescence upon 470 nm LED excitation at 25% intensity. By comparison, the cells in the same specimen not expressing FLAG-tagged LMF1 were only emitting a dim, near-background fluorescence, proving that the antibody didn't have affinity to non-specific targets.

However, KI A4A cells stained with the same antibody, shown in Figure 11 -middle panels-, didn't display fluorescence above background levels, and there was no visible difference between these and the HeLa WT cells shown in the bottom panels.

Similar observations were made for the results of the same IF procedure carried out using the alternative F3165 antibody. However, this antibody appeared to be less effective in staining FLAG-tagged LMF1-expressing cells (**Figure 15**, top row, left panel) compared to the anti-FLAG M30971, while also producing a greater background fluorescence at the same 470 nm wavelength excitation intensity.

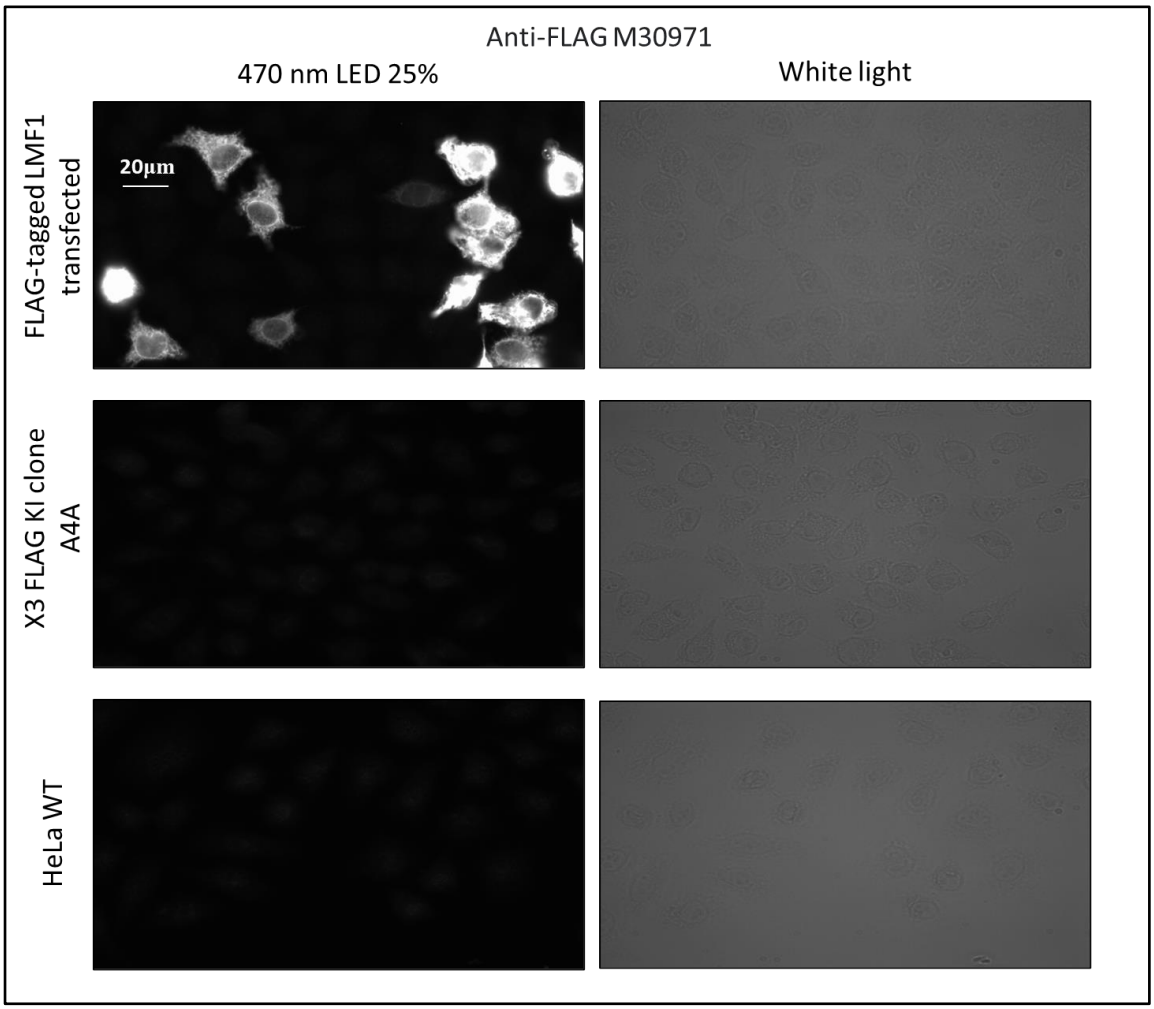

Figure 14: Immunofluorescence microscopy of HeLa WT, HeLa KI clone A4A and HeLa cells exogenously expressing FLAG-tagged LMF1 stained with anti-FLAG Ab M30971. *Mutant HeLa KI A4A cells expressing the x3 FLAG-tagged MsrB3 mutant (x3 FLAG KI clone A4A, middle row) were compared to HeLa WT cells (bottom row) in immunofluorescence analysis. As a control for the efficacy of the primary antibody used, cells transiently expressing FLAG-tagged LMF1 were included (top row). Cells were fixed in methanol and stained with anti-FLAG antibody from Bolster Bio at 1/150 dilution followed by incubation with anti-mouse Alexa Fluor™ 488. The specimens were observed under 470 nm LED excitation at 25% intensity (left column) and white light (right column). The scale bar is 20 µm.*

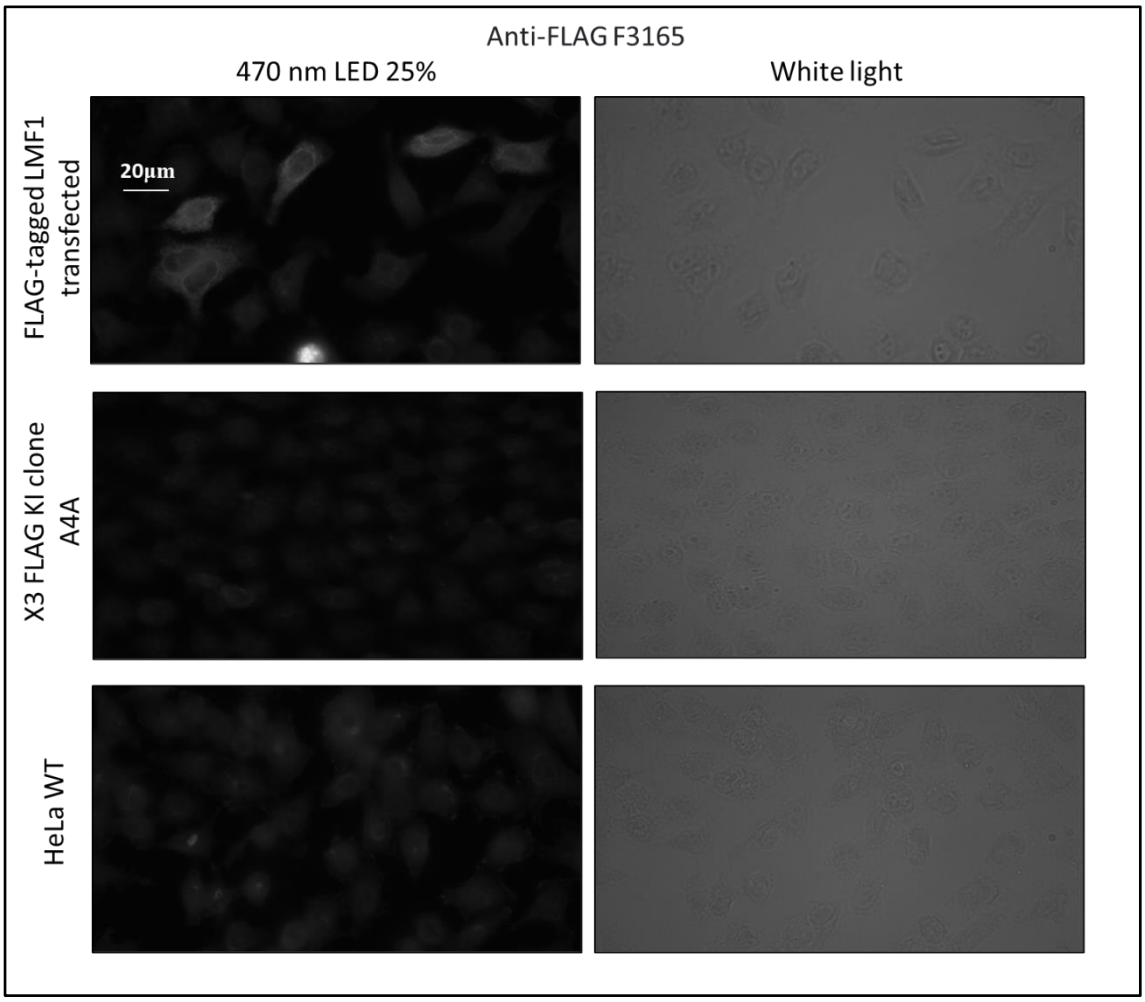

Figure 15: Immunofluorescence microscopy of HeLa WT, HeLa KI clone A4A and HeLa cells exogenously expressing FLAG-tagged LMF1 stained with anti-FLAG Ab F3165. *Mutant HeLa KI cells A4A expressing x3 FLAG MsrB3 were compared to HeLa WT cells in immunofluorescence analysis. To test the suitability of the primary antibody used, cells exogenously over-expressing FLAG-tagged LMF1 (top row) were added to the experiment. The specimens were fixed in methanol and stained with anti-FLAG F3165 (1/150 dilution) followed by incubation with anti-mouse Alexa Fluor™ 488 to allow the visualisation of the anti-FLAG antibody-bound targets. The specimens were observed under the excitation of a 470 nm LED at 25% (left column) and white light (right column). The scale bar is 20 µm.*

To ascertain whether the FLAG-tagged MsrB3 in the A4A KI cells and the FLAG-tagged LMF1 in the transfected cells were correctly expressed, the pools of cells used for the IF experiments above were lysed for WB. The anti-epitope tag primary antibodies used for this analysis were the same as those employed in the IF experiment.

Surprisingly, the WB results disclosed that the F3165 antibody had good affinity to the triple-FLAG tag of the mutant MsrB3 expressed by the KI A4A cells, but it couldn't detect the FLAG-tagged LMF1 as effectively, although the difference in the loading evidenced by the anti-Actin antibody exaggerated this difference (**Figure 16**, panel A). In contrast, the M30971 antibody displayed a strong signal for the FLAG-tagged LMF1, but it wasn't effective in detecting the triple-FLAG tagged MsrB3 as shown in **Figure 16**, panel B. This suggested that the M30971 antibody wasn't suitable for the detection of MsrB3 in the KI A4A cells in IF microscopy due to its low affinity to the triple-FLAG epitope of the mutant MsrB3. F3165 displayed good affinity to the mutant MsrB3 expressed by the KI cells in WB, but not in IF microscopy, so the fixation method used in the latter analysis might have negatively affected the antibody affinity for the triple-FLAG tagged MsrB3.

Therefore, another IF experiment was attempted using this primary antibody, this time by fixing cells in 4% w/v formaldehyde. The F3165 antibody was employed at a greater dilution (1/200) to reduce the background fluorescence produced in the previous experiment as seen in **Figure 15**. The results of this analysis, summarised in **Figure 17**, showed cells with an unusual morphology, characterised by loss of structure of the cell membrane. This phenomenon might be due to the formaldehyde fixation or the permeabilisation with 0.2% v/v Triton X-100 that followed being too damaging to the cells. Even so, FLAG-tagged LMF1 was detected by the antibody in cells exogenously expressing this recombinant protein (**Figure 17**, top-left panel), which showed that the IF method worked for this specimen. There wasn't any difference between the KI A4A cells and the HeLa WT cells, shown in the middle and bottom panels of **Figure 17**, that could suggest that the triple FLAG-tagged MsrB3 in the KI cell line was detected. Because of the time limitations, further attempts to visualise endogenous MsrB3 in mammalian cells by IF microscopy were not made.

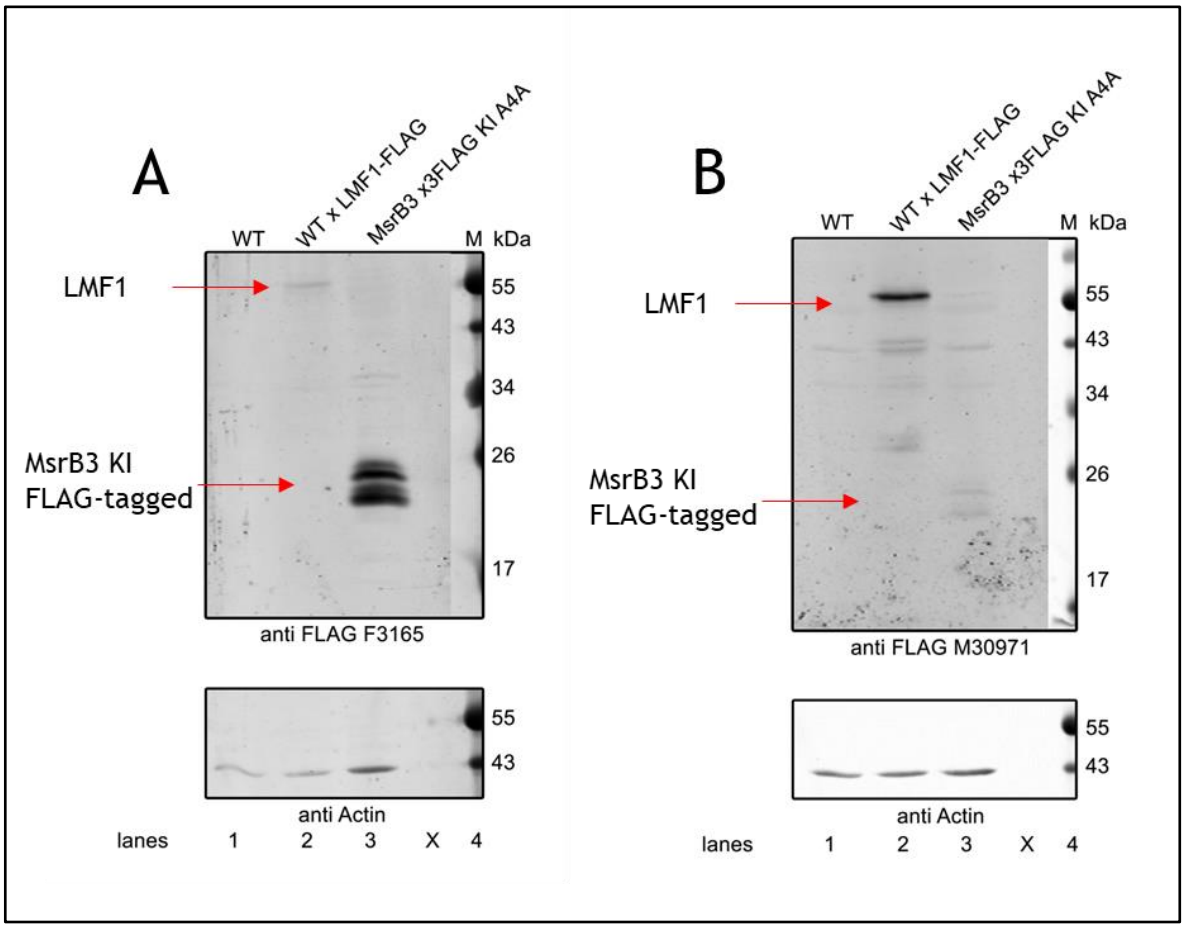

Figure 16: WB control of the cells analysed in IF microscopy.

WB results of the TCL from WT, x3 FLAG MsrB3 KI cells and cells transiently expressing FLAG-tagged MsrB3 are shown in lanes 1, 2 and 3, respectively, of blots A and B. Blot A was incubated with the primary anti-FLAG antibody F3165, blot B with the anti-FLAG M30971 antibody. The results from the Sigma Aldrich anti-Actin (A2103), used as a loading control, are reported in the same lanes below the epitope-tag results. LMF1 and the MsrB3 expressed by the triple-FLAG tagged MsrB3 KI cell line detected by the F3165 and the M30971 antibodies are reported, respectively, in panels A and B. The protein marker is reported in lanes 4.

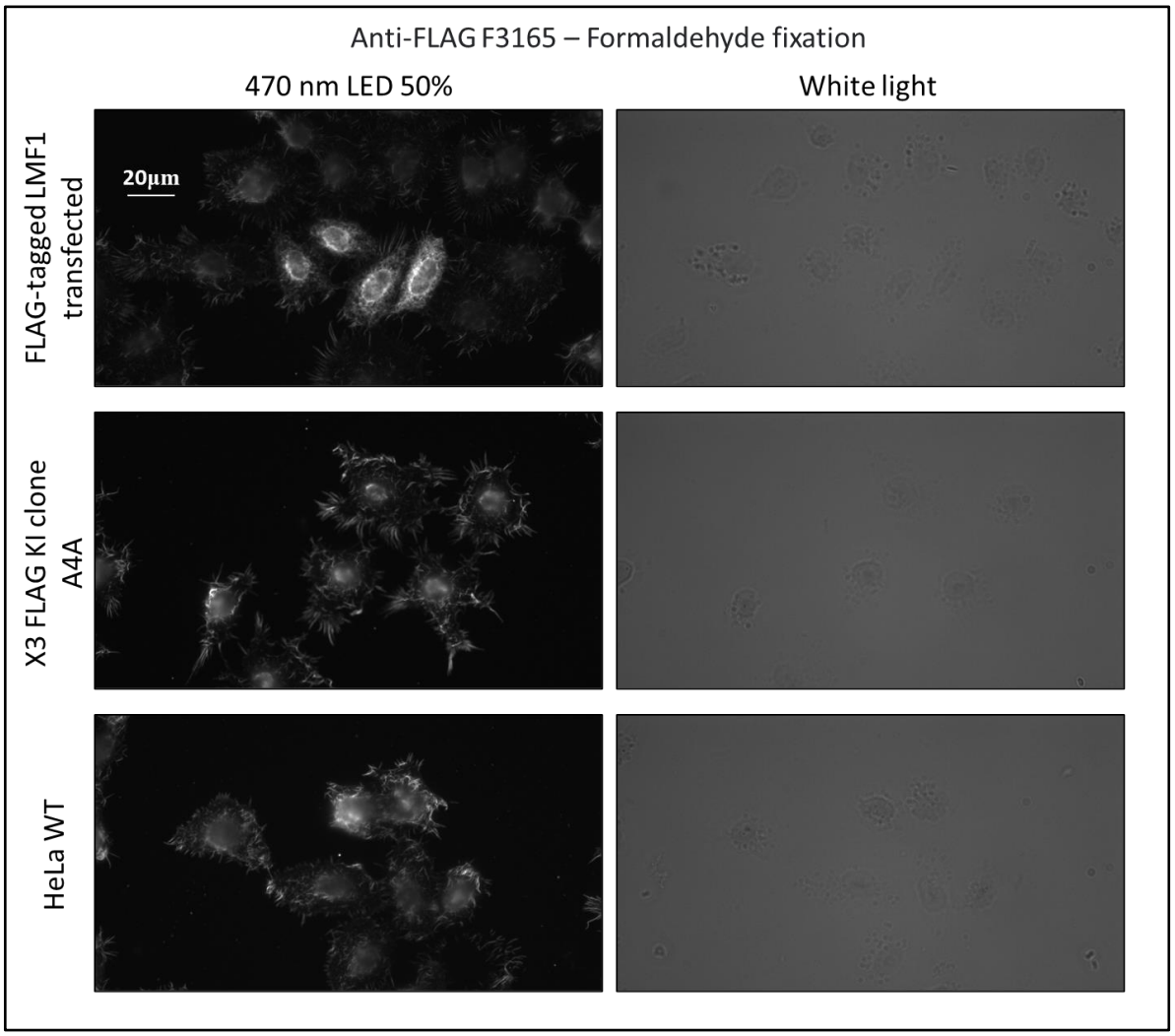

Figure 17: Immunofluorescence microscopy of HeLa WT, HeLa KI clone A4A and HeLa cells exogenously expressing FLAG-tagged LMF1 fixed in 4% v/v formaldehyde. The anti-FLAG antibody from Sigma-Aldrich (F3165) was employed in immunofluorescence analysis of the x3 FLAG-MsrB3 KI clone A4A compared to HeLa WT cells fixed in 4% v/v formaldehyde. HeLa cells were transiently transfected with a FLAG-tagged LMF1 construct and included in the experiment to test the efficacy of the primary antibody, used in a 1/200 dilution. The targets bound to the primary antibody were detected by incubating the specimens with anti-mouse Alexa Fluor™ 488. Cells were imaged under both white light and 470 nm LED light at 50% intensity. The scale bar is 20 µm.

4.4. MsrB3 isn't efficiently targeted to the mitochondria in MsrB3B over-expressing stable cell line.

The antibody-based assays on MsrB3 KO and MsrB3 WT cell lines described so far showed that MsrB3 is present in the cytosol but could not determine its distribution between the mitochondria and ER in HT1080 cells. A cell line endogenously expressing FLAG-tagged MsrB3 represented a promising alternative to visualise MsrB3 in fixed cells while determining its distribution. However, the IF attempts using the gene KI cell line, described in section 4.3, did not allow observation of MsrB3. Although the question regarding the sub-cellular distribution of MsrB3 was still pending, it was also necessary to focus on the other aims of this investigation. One of these objectives consisted of producing stable cell lines overexpressing ER-targeted MsrB3 (MsrB3A) or MsrB3 targeted to the mitochondria (MsrB3B), which could be employed in future investigations to elucidate the activity of MsrB3A and MsrB3B in their respective cell compartments. The HT1080 MsrB3 KO clone C3 cell line was selected as the starting point from which to generate cell lines stably over-expressing MsrB3 targeted to either the ER or the mitochondria, without the background expression of endogenous MsrB3. First, the MsrB3B construct purchased from OriGene and detailed in section 3.9, was cloned into pTetOne so that both MsrB3A and MsrB3B were expressed in the same vector (3.6.2). pTetOne plasmid DNA and MsrB3B cloned into pCMV6 were digested with both EcoRI and AgeI and separated through a 1% w/v agarose gel. The digested vector and insert, shown in **Figure 18**, were extracted to clone Myc-FLAG MsrB3B into doubly cut pTetOne. The ligation product was used to transform competent XL-1 Blue cells for the isolation of the plasmid DNA, and sequencing analysis followed to confirm that the MsrB3B insert was correctly cloned into pTetOne. The sequencing results detailed in **Appendix figure 4** were obtained using a pTetOne vector forward primer purchased from Sigma Aldrich provided by Prof Bulleid's group (5'-GCTGCAGAGATCTGG -3').

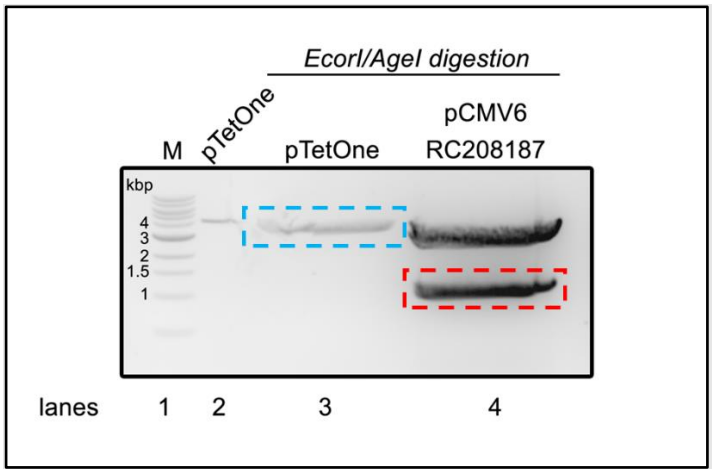

Figure 18: EcoRI and AgeI digested pTetOne and MsrB3B in pCMV6 (RC208187). *The dashed blue and red boxes indicate the gel areas selected to extract the EcoRI/AgeI digested pTetOne and Myc-FLAG MsrB3B insert, respectively. Uncut pTetOne was loaded in lane 2 to compare it with the digested vector.*

To generate cells with stably integrated highly inducible genes expressing either MsrB3 species, MsrB3 KO cells were co-transfected with 0.2ug of pPUR plasmid and 2ug of the mitochondrial or ER targeted MSRB3 pTetOne constructs described in section 3.9. The pPUR empty vector was added to the transfection mix to select successfully transfected cells by supplementing the growth media with Puromycin.

The Puromycin-resistant cell pools obtained from the transfection were used to grow single clones by limiting dilution, and they were separately tested in WB for the inducible expression of V5-tagged MsrB3A and Myc-FLAG-tagged MsrB3B. This preliminary analysis, aimed to ascertain if the transfections worked, was important in determining if at least some of the puromycin-resistant cells were also correctly expressing the recombinant MsrB3 species.

The results proved that the transfected cells were expressing V5-tagged MsrB3A and FLAG-tagged MsrB3B after an overnight induction with 1ug/ml doxycycline hyclate (**Figure 19**, lanes 4 and 5, respectively).

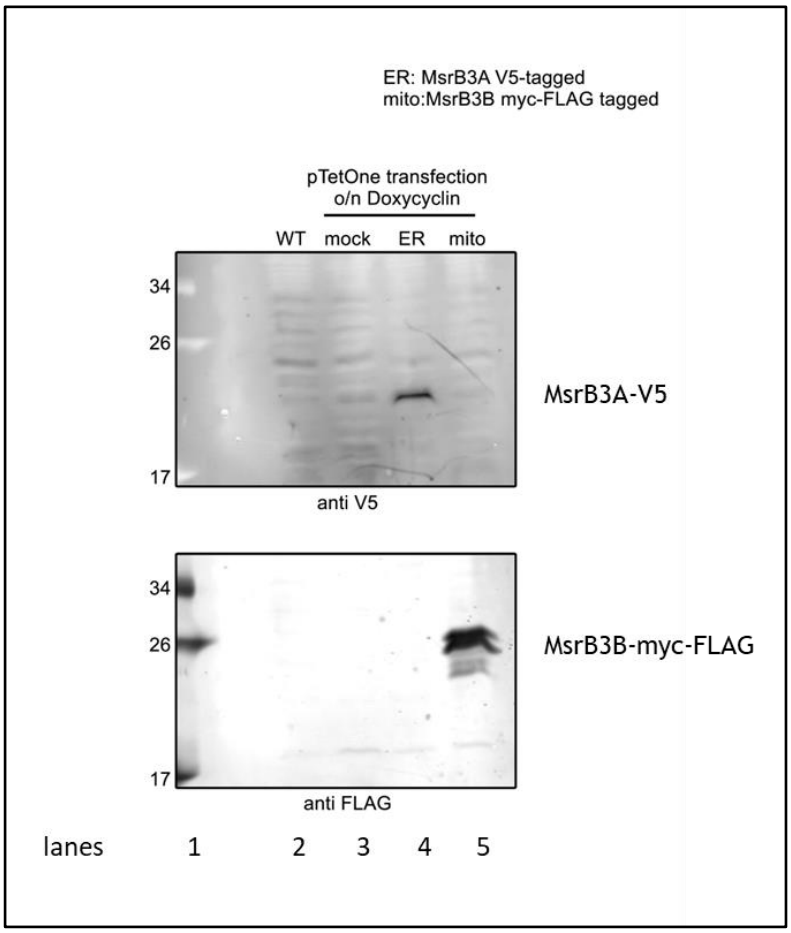

Figure 19: Analysis of the pools of cells expressing V5-tagged MsrB3A or FLAG-tagged MsrB3B*. MsrB3 KO cells were transfected with MsrB3A or MsrB3B constructs cloned into pTetOne. When the cells growing in puromycin selection were confluent, 1ug/ml doxycycline was added to the cell media to induce the exogenous expression of recombinant MsrB3A and MsrB3B, respectively detected in the cell lysate with V5-Tag (D3H8Q) from Cell Signalling (#13202) and anti-FLAG from Sigma Aldrich (F3165) antibodies in WB. HT1080 WT (lane 2) and MsrB3 KO mock-transfected cell lysate (lane 3) were included as controls. The protein marker was loaded in lane 1.*

Single clones originating from the pools of transfected cells were picked and tested for the expression of either MsrB3A or MsrB3B using the induction method just described. None of the clones tested expressed V5-tagged MsrB3A after induction, but three among the selected clones could express FLAG-tagged MsrB3B (the construct, reported in section 3.9, encodes a Myc tag too but an anti-FLAG antibody was used in WB to detect MsrB3B to make the analysis simpler). One stable cell line over-expressing FLAG-tagged MsrB3B, identified as

clone 7, was selected for the following experiments on mitochondria targeting of MsrB3B.

A time course analysis of the FLAG-tagged MSrB3B expressed by the selected clone under doxycycline induction (0.2ug/ml) showed that 2h induction is enough for the cell line to express detectable levels of MsrB3B under these conditions (**Figure 20**, lane 3). In WB, MsrB3B appeared to be expressed in the form of multiple bands with different mobility, already seen in the preliminary analysis displayed in **Figure 19** (bottom blot). These bands could be grouped into a main, slow-migrating species 'MsrB3B (s)' and a faster-migrating species 'MsrB3B(f)'. The latter seemed to accumulate until the 4h induction mark (**Figure 20**, lane 4) and didn't display any noticeable variation in the successive time points (**Figure 20**, lanes 5 and 6).

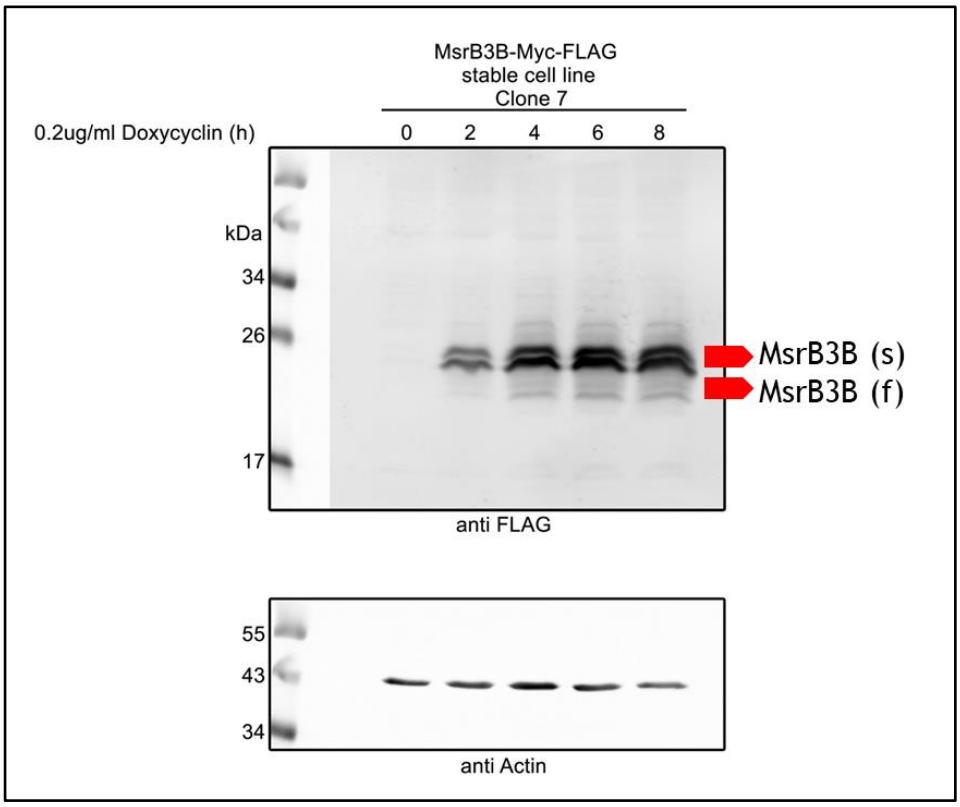

Figure 20: Time course of doxycycline-induced expression of FLAG-tagged MsrB3B in MsrB3B stable cell line clone 7. *Cells stably expressing Myc-FLAG tagged MsrB3B under the Tet-On system, derived from the MsrB3 KO HT1080 line, were induced for the expression of recombinant MsrB3B by adding 0.2ug/ml Doxycycline to the cell media for 0, 2, 4, 6 and 8h. The cell lysate was analysed in WB using anti-FLAG (Sigma Aldrich F3165) for the expression of the recombinant MsrB3B and anti-Actin (Sigma Aldrich A2103) as a loading control. The protein molecular weight marker (NEB P7718S) was loaded in lane 1. The Molecular Weight is shown in kDa.*

To discover which of the MsrB3B bands correspond to the form of the enzyme found in the mitochondria, a fractionation experiment was performed on the MsrB3B stable cell line after a 4h doxycycline induction. The concentration of doxycycline was reduced to 0.01ug/ml to try to induce MsrB3B expression at a level more similar to wild type levels and a separate pool of cells had carbonyl cyanide m-chlorophenylhydrazone (CCCP) added at 15 μM. CCCP is an oxidative phosphorylation uncoupler, which disrupts the mitochondrial membrane potential that is required for the translocation of newly synthesised proteins into the mitochondria (Miyazono, Hirashima et al. 2018).

CCCP was used in this experiment to prevent the translocation of any MsrB3B to the mitochondria in the treated cells, thus allowing us to determine which of the MsrB3B bands seen in WB correspond to the enzyme found in the mitochondria of the untreated cells. Untreated and CCCP treated cells were fractionated separately on the same day after receiving the same doxycycline induction treatment. A closer study of fractionation procedures aimed to isolate mitochondria from mammalian cells and tissue suggested that a low-speed spin (performed at 1000g for the results in 4.2) is usually carried out to clear the homogenate from cell debris, unbroken cells, and cells nuclei. The supernatant in then spun at a greater relative centrifugal force (10000-15000 g, with some variations between different protocols) to isolate the crude mitochondria (Fernández-Vizarra, Ferrín et al. 2010, Liao, Bergamini et al. 2020). For the purpose of the experiments carried out at this stage of the investigation, there was no need to try separating the ER from the mitochondrial fraction of the cells, because no MsrB3B should be targeted to or retained in the ER. It was assumed that untargeted MsrB3B, if any, would be found in the cytosol, so the fractionation procedure was designed to separate the cytosolic fraction from the other cell fractions.

To do this, the cell homogenate was spun at 1000 g to obtain the 1K pellet, and the supernatant was spun at 21’000g (21K) to pellet all the other cell fractions which could be retained in the supernatant from the 1K spin, including the remaining mitochondria. Lastly, the protein present in the supernatant (Supn.) was precipitated as described in section 3.3 to obtain the cytosolic fraction. The samples were analysed by WB for the abundance of FLAG-tagged MsrB3B, which was compared to the expression levels of a mitochondrial marker protein,

TOMM40, and a cytosolic marker, GAPDH. Total cell lysate (TCL) and cell homogenate obtained from the same cells used in this experiment were also analysed.

Unfortunately, the faster migrating MsrB3B bands weren't present in the TCL and cell homogenate, regardless of the CCCP treatment (**Figure 21**, panel A1, lanes 2 to 4), and therefore this MsrB3B species seen in previous evidence (**Figure 20**, MsrB3B(f)) wasn't present in the fractionation samples. While the expression of the mitochondrial and cytosolic proteins was equivalent between the same fractions obtained from all the samples (+ and – CCCP treated cells), less MsrB3 was detected in the fractions of cells treated with CCCP (panel A1 lanes 3, 5, 7 and panel B1 lane 5, **Figure 21**), compared to the same samples obtained from untreated cells (respectively: A1 lanes 2, 4 and 6, B1 lane 4 in **Figure 21**). TOMM40 was mostly detected in the mitochondrial fractions (1K) and, to a lesser level, in the ER fraction (21K), and only faint bands corresponding to GAPDH were detected in the same samples (panel A2,lanes 6-7, panel B2, lanes 2-3, **Figure 21**). The proportions of TOMM40 and GAPDH seen in the 1K and 21K samples were reversed in the supernatant (Spn., the cytosolic fractions) from + and – CCCP cells. TOMM40 was detected in very faint bands in the cytosolic fractions, while GAPDH present in much higher quantities compared to the 1K and 21K fractions (B2, lanes 4-5). The ratios of TOMM40 and GAPDH detected in the fractions suggested that most of the mitochondria were pelleted in the 1K and 21K samples, which were separated from the cytosolic protein mainly found in the Spn. samples. Coincidently, low levels of FLAG-tagged MsrB3B were observed in the 1K samples and it was almost undetectable in the in 21K samples as seen in panel A1 (1K, lanes 6-7) and B1 (21K, lanes 2-3) of **Figure 21**, but the slower-migrating MsrB3B, seen in the TCL and cell homogenate, was precipitated together with the cytosolic protein in the Spn. samples (**Figure 21**, panel B1, lanes 4-5).

This finding showed that the slower migrating MsrB3B, which is the main species expressed by the stable cell line used in this experiment, was associated with the GAPDH cell marker and not TOMM40. From this evidence, it was deduced that most – if not all - of the slow-migrating MsrB3B seen in WB is untargeted MsrB3B in the cytosol.

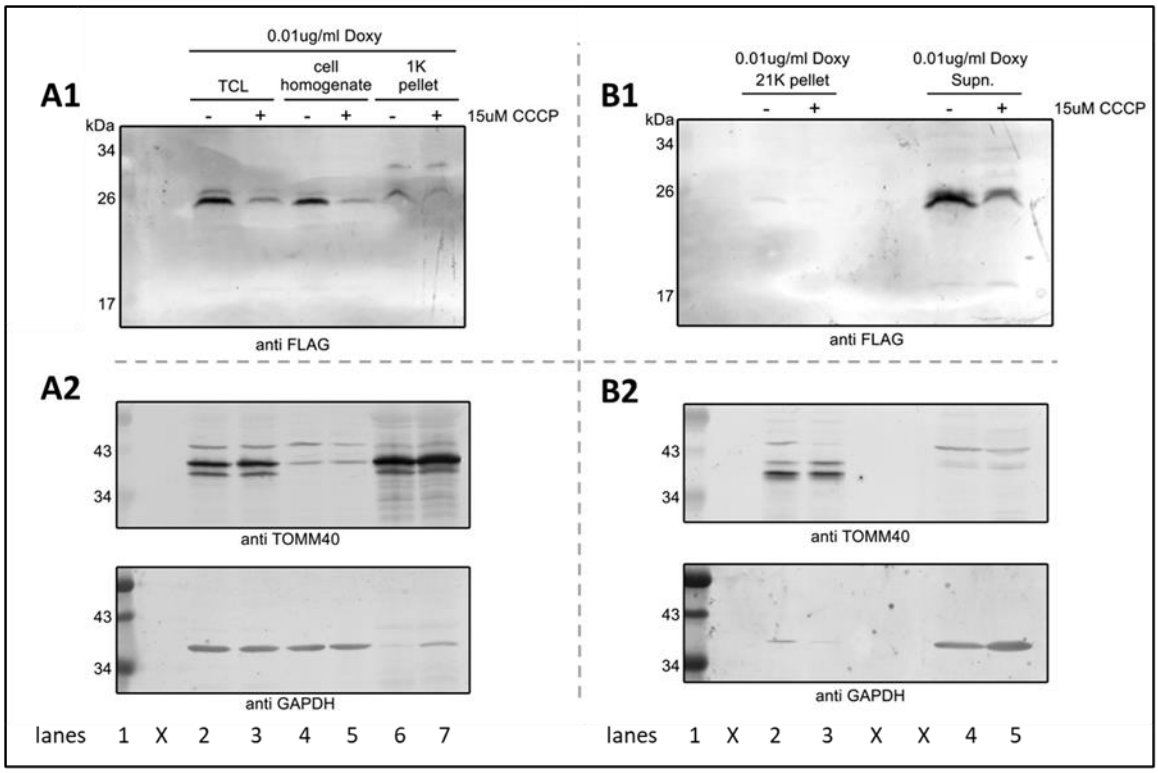

Figure 21: WB of the fractionation samples derived from Myc-FLAG MsrB3B clone 7 cells under different treatments. *FLAG-tagged MsrB3B expression in MsrB3B stable cell line (clone 7) was induced for 4h by adding 0.01ug/ml doxycycline to the cell media, with and without CCCP treatment (15uM). Cells were homogenised to obtain the nuclear (1K), mitochondrial/ER (21K) and cytosolic (Supn.) cell fractions. Total cell lysate (TCL), cells homogenate and the fractionation samples were analysed in WB for the expression of FLAG-tagged MsrB3B; TOMM40 and GAPDH detected with Sigma Aldrich F3165 anti-FLAG antibody; Thermofisher anti-GAPDH (10515025) and Proteintech anti-TOMM40 (18409-1-AP). Panels A1 and A2 show the FLAG-tagged MsrB3B and cell markers, respectively, detected in the TCL, cell homogenate and 1K pellet of + and – CCCP cells. Panel B1 shows the FLAG-tagged MsrB3B detected in the 21K pellet and cytosolic fraction (Supn.) The dashed lines separate the blots obtained from different SDS-PAGE gels.*

4.5. MsrB3 DM acts as a stereospecific methionine reductase and oxidase.

As outlined in the introduction of this manuscript in more detail, MsrB3 was found to have a dual function as a reductase and oxidase in previous *in vitro* experiments. According to what was postulated by Cao and colleagues, MsrB3 active site thiol -C126- becomes sulfenylated upon reduction of Methionine-R Sulfoxide. The S-sulfenylation of C126 can be reversed by the resolving cysteine residues C03 and C09, which will form a disulphide bond in the recycling of C126, allowing for an additional substrate reduction. In the presence of thioredoxin, a reducing agent, any sulfenylated active site thiol and disulphide bonds between C03 and C09 are reduced, thus recycling MsrB3 for its reductase activity (Cao, Mitchell et al. 2018). When MsrB3 is fully oxidised, the sulfenylated active site C126 can reduce itself by oxidising methionine into methionine-R-O (Cao, Mitchell et al. 2018). These previous observations were made in in vitro assays on MsrB3 activity using the synthetic probes derived from dabsyl methionine (4-dimethylaminoazobenzene-4'-sulfonyl-methionine). The oxidised derivatives of dabsyl methionine (DABS Met), like MetO in protein, exist in the form of the two enantiomers dabsyl-Met-(R or S)-O. Developed in 1994 (Minetti, Balduini et al. 1994), DABS Met and DABS MetO have shed light on the stereospecific activity of MsrA and MsrB on Met-S-O and Met-R-O. These substrates provide an easy assay in RP-HPLC for the activity of MsrB3, as the retention volume of DABS-Met is greater than that of DABS-MetO. Moreover, by eluting samples with a linear gradient between 30% and 70% v/v acetonitrile, the S-Sulfox and R-sulfox epimers from DABS-MetO can also be separated. Prof Richard Hartley's lab kindly provided DABS Met and oxidised derivatives (**Figure 22**) for this part of the investigation focussing on MsrB3 candidate target SPARC Met245. The synthetic probes were needed to ascertain whether the MsrB3 mutant used had oxidase activity before experimenting with the client substrate.

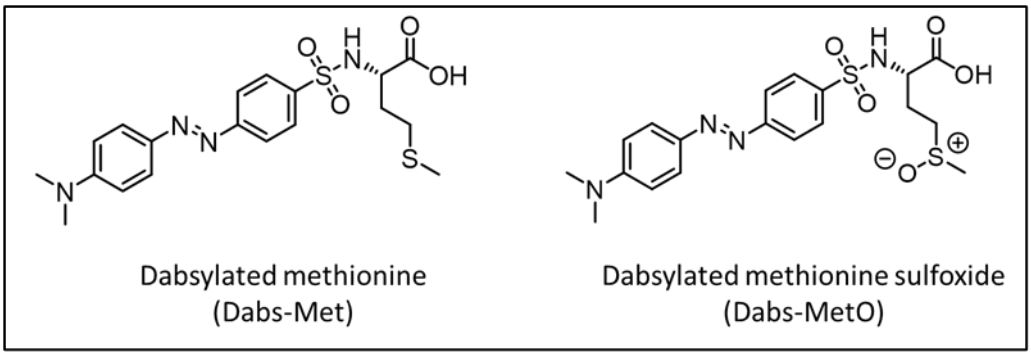

Figure 22: Schematic representation of DABS Met and DABS MetO*. Courtesy of Professor Richard Hartley's lab, School of Chemistry, University of Glasgow.*

The C03A C09A MsrB3 Double Mutant (MsrB3 DM), described in chapter 3.11, was selected for this part of the investigation to study the oxidase activity of this enzyme without the effects of the MsrB3 WT self-recycling activity (**Figure 4**): in the absence of the C03 and C09 residues, the sulfenic acid of C126 in the fully oxidised MsrB3 DM wouldn't be reduced by the resolving cysteine, thus promoting its oxidising behaviour. In reducing conditions, MsrB3 DM still acts as a reductase and its active site thiol is recycled by the addition of DTT. The MsrB3 DM was incubated with either DTT or MetO to fully reduce or oxidise the active site C126 before adding DABS-Met or DABS-MetO to the mixture (methods section 3.11).

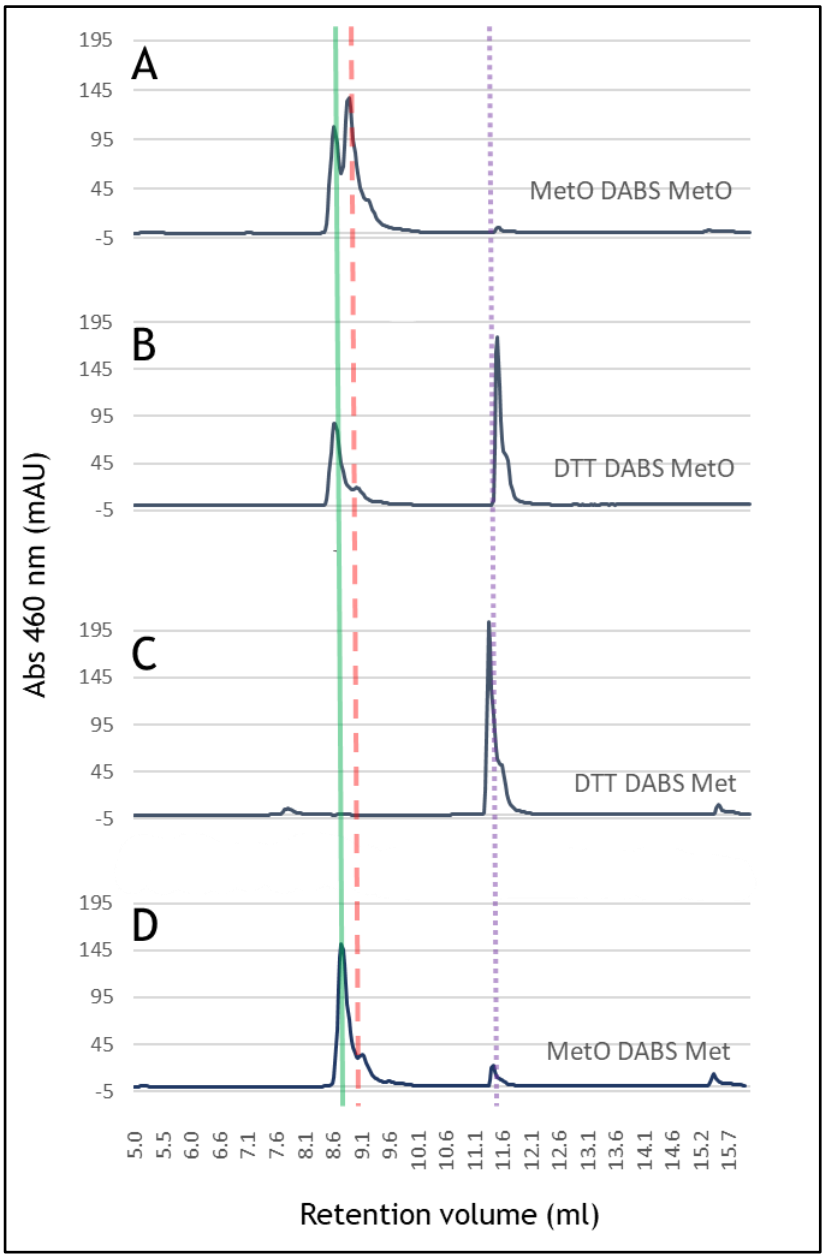

Figure 23: HPLC analysis of DABS Met and DABS MetO incubated with MsrB3 DM in reducing and oxidising conditions. *The activity of MsrB3 DM was assayed in reducing conditions with the addition of DTT (B and C) and in oxidising conditions with MetO (A and D) by RP-HPLC analysis. The substrates provided were either a mixture of Dabsylated methionine R- and S- sulfoxide ("DABS MetO", panel A and B) or fully reduced Dabsylated Methionine ("DABS Met", C and D) in both conditions. The vertical green line and the dashed vertical red line indicate, respectively, where DABS-S-Sulfox and the DABS-R-Sulfox are eluted. The reduced DabsMet elute is indicated by the dotted vertical purple line.*

The HPLC analysis of DABS MetO incubated with MsrB3 DM in reducing conditions showed that DABS Met was generated, (**Figure 23**, panel B, purple line). As expected, DABS Met was not detected in the sample produced with MsrB3 DM reacting with DABS MetO in oxidising conditions (**Figure 23**, panel A, purple line). DABS Met-S-O, which can be reduced by MsrA due to its stereospecificity (Cao, Mitchell et al. 2018), was present in both these assays shown in panels A and B in comparable amounts, but the DABS-R-O was only found in the control generated with DABS MetO and MsrB3 DM in oxidising conditions (**Figure 23**, panel A). Thus, in reducing conditions only the R-epimer of Dabs MetO is reduced to DABS Met by MsrB3 DM.

The results reported in **Figure 23**, panel D, indicate that DABS-Met-R-O was generated when DABS Met was incubated with MsrB3 DM in oxidising conditions. The R epimer of DABS-MetO wasn't present in either the control sample with DABS Met in reducing conditions (**Figure 23**, panel C) nor in the additional controls performed without the enzyme (suggesting that the DABS-Met was converted to Dabs-R-MetO by the oxidised MsrB3 DM enzymatic activity.

These findings supported the dual reductase/oxidase behaviour of MsrB3 DM provided by Prof Bulleid's lab. This result confirmed that MsrB3 DM was a good model for the identification of MsrB3 candidate methionine substrates in protein, thus shifting the focus away from its activity assayed with synthetic substrates. As explained in the introduction, Prof Bulleid's lab group had previously pinpointed Met245 of human SPARC as a candidate target of MsrB3-mediated oxidation. Therefore, MsrB3 DM was deemed suitable for the following experiment aimed to investigate the putative oxidase activity of MsrB3 on Met245 of hSPARC follistatin-like (FS) and an EF-hand calcium-binding (EC) domain.

4.6. His-myc hSPARC FS-EC purification

His-myc hSPARC FS-EC was purified from the transfected HEK cells' media by Ni^{2+} affinity chromatography and the elution samples were analysed along with samples of the cell media taken before and after adding it to the column, by SDS/PAGE and WB.

The SDS PAGE analysis (**Figure 24**, panel A) of the His-myc hSPARC FS-EC purification showed that some elution fractions yielded a single product of about

40 kDa (**Figure 24** panel A, indicated by the arrows) which was demonstrated to be the His-myc tagged recombinant protein by WB analysis (**Figure 24**, panel B). The selected eluates were then concentrated to obtain the purified His-Myc-hSPARC FS-EC protein for subsequent MS experiment analysis.

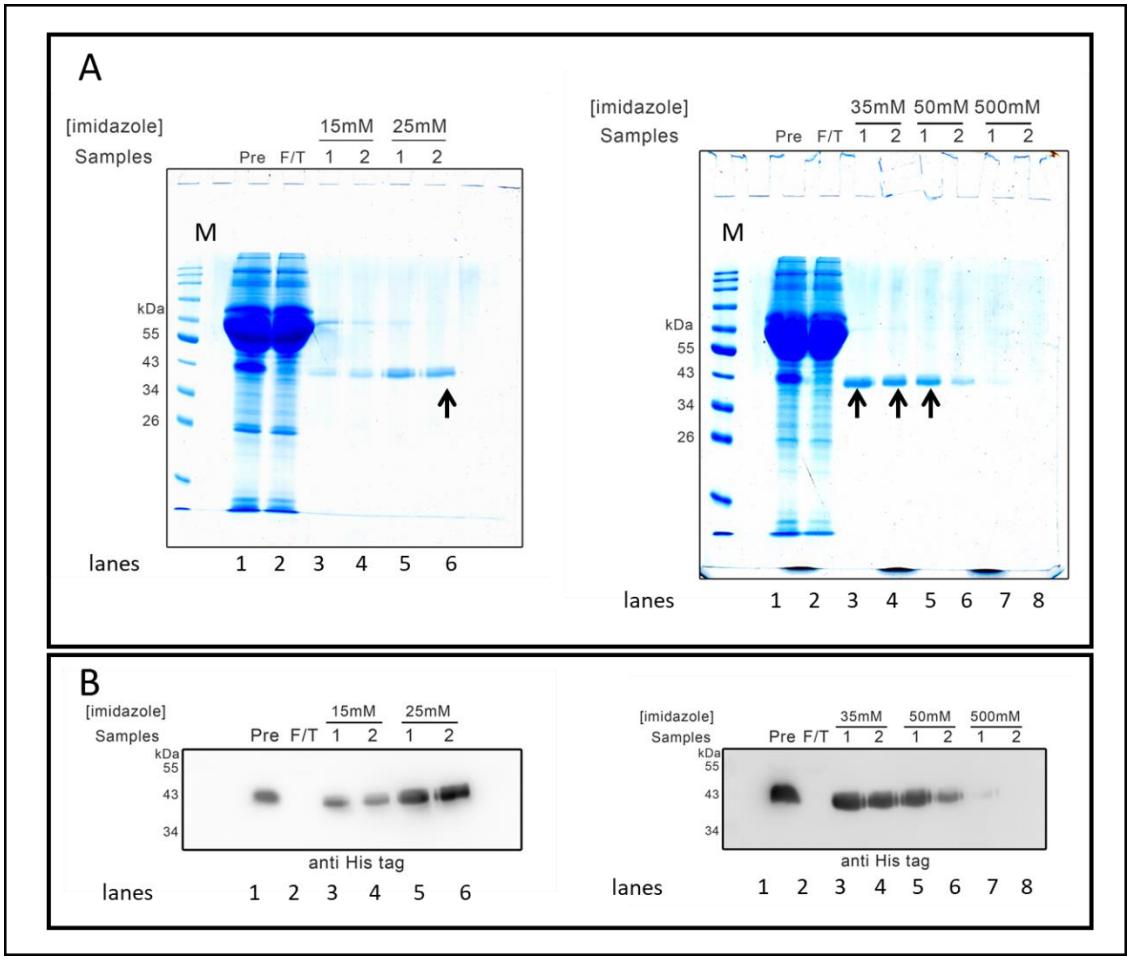

Figure 24: His-Myc hSPARC purification results. *Panel A shows the SDS/PAGE analysis, of Histidine-tag purification of His-Myc hSPARC FS-EC domains from cultured cell media of HEK T cells transfected with pCEP-PU hSPARC-FS-EC. The eluates were obtained by adding half column volumes of buffer with an increasing imidazole concentration (15mM, 25mM, 35mM, 50mM and 500mM imidazole). The samples were eluted twice at each imidazole concentration. The cell media before purification (Pre) and the flow-through (F/T) were also analysed. Panel B: WB results of the elutes from the His-myc hSPARC FS-EC purification. The blots were incubated with an anti-His antibody for the detection of the recombinant protein.*

4.7. LC-MS-MS results analysis

The MS analysis reported in this section was carried out by Dr Sergio Lilla, CRUK Scotland Institute.

Analysing the redox status of specific methionine residues in proteins can be technically difficult as protein redox changes can arise from several factors. Experimental procedures and exposure of the protein samples to oxygen can lead to oxidation of methionine residues that can obscure the true picture. Interpreting MsrB3's oxidoreductase activity on DABS-Met derivatives in the RP-HPLC analysis was relatively straightforward: exposure of the substrates to ROS during and after the experiment could be controlled and the products' redox state was assayed directly by HPLC analysis (**Appendix figure 6**). Therefore, any changes in the chromatogram profiles of the synthetic DABS Met substrates incubated with MsrB3 DM, as seen in **Figure 23**, could be confidently attributed to the enzyme's redox activity.

In the following experiment, the MsrB3-mediated methionine oxidation of the recombinant hSPARC was assessed. The candidate target, transiently expressed in mammalian cells, could have accumulated redox changes during expression. Moreover, sample processing for MS analysis can also result in methionine oxidation in proteins. To avoid confusion between this stochastic oxidation and MsrB3-induced oxidation, the samples containing SPARC were incubated with oxidised or reduced MsrB3 DM were prepared in 71.5% $H_2{}^{18}O$. If water is the oxygen donor in MsrB3 catalysed reaction, any enzymatically oxidised methionine in the candidate target should be detected as Met-^{18}O in proportion to the heavy water content. Since the primary occurring oxygen isotope is ^{16}O, any heavy-oxygen MetO detected by the MS analysis could be attributed exclusively to the MsrB3 activity, as Met-^{18}O cannot be generated from the background stochastic oxidation. Peptides featuring an oxidised Met residue will follow a standard isotopomer distribution seen in MS/MS analysis. However, if any methionine is oxidised with heavy oxygen, the combined isotopomer distribution will be differently weighted due to the +2 mass difference compared to the the Met-^{16}O peptide. An example of the typical pattern indicating an ^{18}O oxidised peptide is reported in **Figure 25**. Dr Lilla investigated these patterns in

determining if any methionine in the recombinant SPARC was found in the form of Met-^{18}O.

In chapter 3.12, details of the sample preparation for MS analysis are reported. His-myc hSPARC bFS-EC incubated with fully reduced MsrB3 DM in DTT was provided as a control to measure the samples' oxidation arising from their production and processing for MS analysis.

The LC-MS-MS analysis disclosed that the hSPARC peptide containing M245 was not oxidised with heavy oxygen in any of the samples and that the extent of oxidation of MetO245 did not differ substantially between the reducing and oxidising samples (**Appendix figure 5**). However, it was found that MetO32 and MetO38 of the recombinant hSPARC tag peptide were oxidised with heavy and light oxygen in proportion to the $H_2{}^{18}O$/ $H_2{}^{16}O$ ratio in the oxidising MsrB3 DM samples. Interestingly, while both of these residues are found in the same peptide fragment of hSPARC, Met38 was more oxidised than Met32 in all samples prepared with MsrB3 DM in oxidising conditions. This observation is illustrated in the diagram found in **Figure 26**. Although the data presented for the oxidation of the tag peptide Met38 in the oxidising reactions hadn't been corrected for the overlap between the +2 isotope of Met^{16}O38 and Met^{18}O38 peptides (the total MetO is reported instead), it still denotes that the encountered Met38 was comparatively much more oxidised than Met32 in the same samples. The true proportions of heavy and light oxygen MetO38 are reported in the bottom-right table in **Figure 25**.

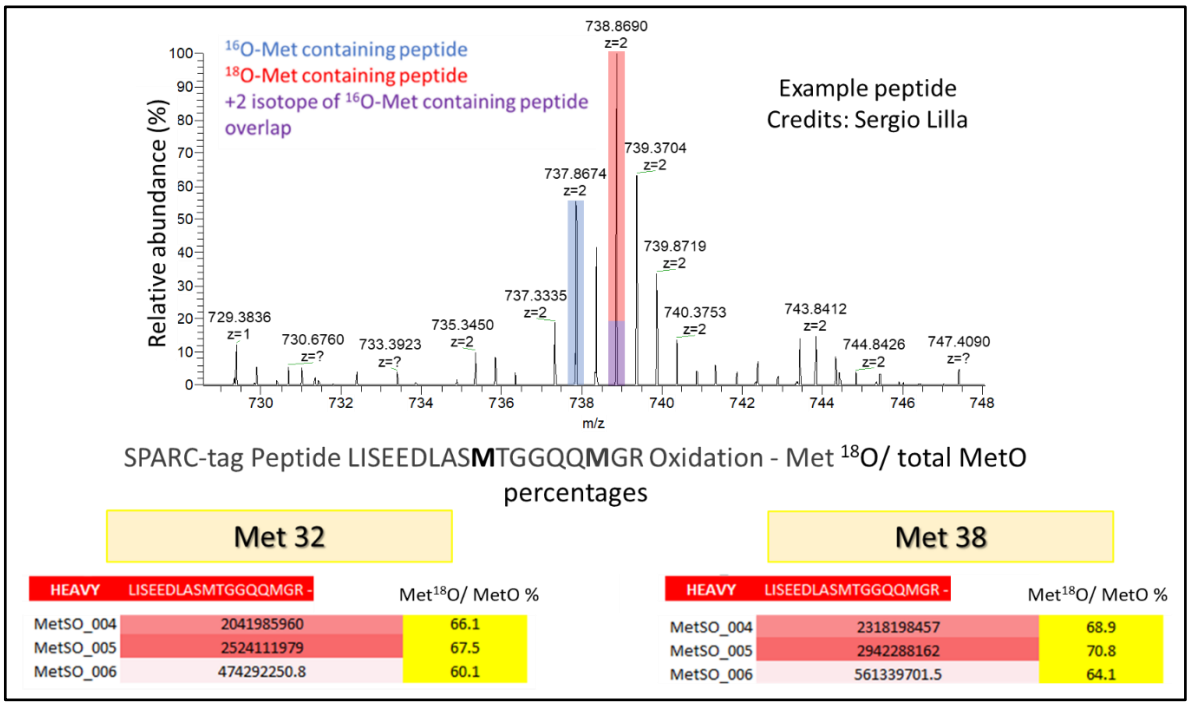

Figure 25: Heavy Oxygen percentage of MetO32 and MetO38 of the recombinant hSPARC Myc tag. *Above, an example of the altered isotopomer distribution of peptides partly oxidised with ^{18}O is shown. The percentages of heavy or light oxygen MetO32 and MetO38 in the SPARC-tag peptide (LISEEDLASMTGGQQMGR) found in the oxidising samples triplicates (MetSO_004,005 and 006) are reported at the bottom of the diagram. Diagrams & data courtesy of Sergio Lilla.*

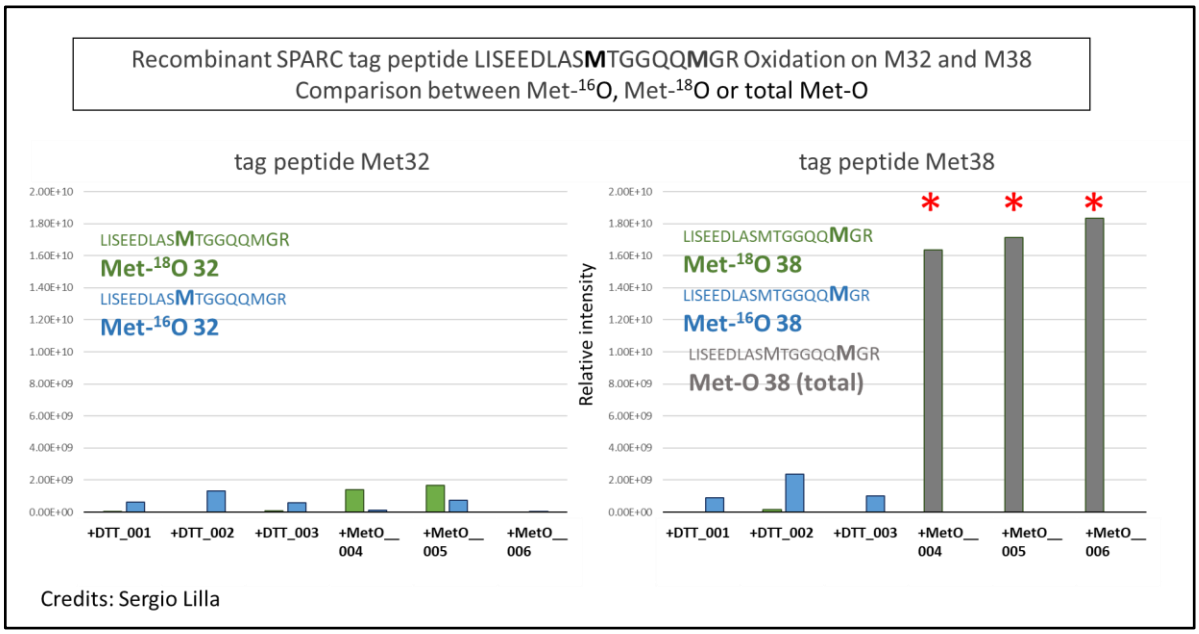

Figure 26: Oxidation of the recombinant SPARC tag at M32 and M38. *The graphs report the abundance of Met-^{16}O and Met-^{18}O for either M32 or M38 found in the recombinant hSPARC tag peptide LISEEDLASMTGGQQMGR. The results are shown for each replicate of the reducing (+DTT_001-003) and oxidising (MetO_004-006) reactions samples. The red asterisks indicate that for the M38 oxidised samples the Met-^{16}O38 peptide isotope and Met-^{18}O38 peptide data are not deconvoluted, therefore the total Met-O38 is reported instead. The relative abundance of MetO is measured in ion count. Data courtesy of Sergio Lilla.*

5. DISCUSSION

The various, but interlinked aspects of MsrB3 investigated during this project will be discussed separately. The implications of untranslocated MsrB3 in the human cell cytosol, evidenced by the results of this study, will be addressed first. Then, the significance of the MS findings will be discussed. Lastly, additional suggestions for future research pertaining to the activity of MsrB3 *in vivo* will be offered.

5.1. MsrB3B as the candidate precursor of untranslocated MsrB3

Here, it was reported that MsrB3 is also found in the cytosol and not only in the mitochondria and the ER of mammalian cells, as reported in the literature, and a commercial antibody for detecting endogenous levels of MsrB3 expressed by mammalian cells was identified. In light of the results described here, it is proposed that cytosolic MsrB3 could result from the incomplete targeting of MsrB3 retaining its signal sequence. This would explain why this MsrB3 species runs slower in SDS PAGE analysis than the targeted enzyme as seen in **Figure 9**. To complement this theory, the fractionation experiment designed to characterise the localisation of the mitochondrial MsrB3 (MsrB3B) in the over-expressing cell line proved that the prevalent species of MsrB3B seen in WB is, in fact, found in the cytosol (Chapter 4.4). This suggests that the endogenous cytosolic MsrB3 expressed in mammalian cells could originate from the incomplete targeting of MsrB3B retaining its signal peptide. Although further analysis is required to confirm this, the following evidence from research literature supports the hypothesis that the translation of endogenous MsrB3B could generate the untranslocated MsrB3.

Mitochondrial proteins like MsrB3B rely on cytosolic ribosomes for the synthesis of their precursors and chaperones to mediate protein translocation to the mitochondria (Avendaño-Monsalve, Ponce-Rojas et al. 2020). By contrast, MsrB3A translation, like other ER resident proteins, depends on ribosomes that become ER-bound by recognition of their signal peptide, and their translocation to the endoplasmic reticulum occurs co-translationally (Nicchitta 2002).

The comparison between mitochondria and ER protein translation highlights the relatively less efficient targeting of mitochondrial proteins, which can give rise to cytosolic intermediates as seen for mammalian MsrA (Kim and Gladyshev

2006). It is worth noting that the information about the differential targeting of mammalian MsrA featuring a mitochondrial signal sequence comes from studies mostly focused on rat and mouse MsrA, which differ from hMsrA in their signal sequences (Vougier, Mary et al. 2003, Hunnicut, Liu et al. 2015).

5.1.1. Future experiments

To explain the presence of a significant proportion of MsrB3 in the cytosol, it would be reasonable to study the translation of MsrB3B as its likely precursor. To support this hypothesis, it would be necessary to confirm whether the ER MsrB3 (MsrB3A) splice variant is fully targeted to the ER. This observation would have been easier if a stable cell line over-expressing MsrB3A had been obtained to characterise MsrB3A sub-cellular sorting. However, the initial attempt to establish a cell line over-expressing V5-tagged MsrB3A was not fruitful and the time limitations precluded further attempts. For future experiments, it would be beneficial to re-attempt the generation of cells selectively over-expressing MsrB3A and determine what proportion of this MsrB3 splice variant, if any, is found in the cytosol through a fractionation experiment. As seen in this investigation, fractionating cells by following the protocol detailed in Chapter 3.3 effectively isolates the cell cytosol for WB analysis. While this feature of the fractionation protocol gave solid evidence that A: the slow-migrating endogenous MsrB3 is found in the cytosol and B: the predominant form of recombinant MsrB3B is also expressed in the cytosol, this procedure is less effective in separating the mitochondria from the ER. For this reason, this investigation could not answer how endogenous MsrB3 is distributed between the ER and mitochondria. Therefore, even the evidence pertaining to the localisation of recombinant MsrB3A and MsrB3B in cells over-expressing these variants (either stably or transiently) should be confirmed by both IF analysis and fractionation. Fractionating the over-expressing cells would determine the amount of MsrB3A and MsrB3B is found in the cytosol, and IF can reveal their distribution in the cells' organelles. Labelling of the recombinant MsrB3 species in immunofluorescence can be performed by employing antibodies against the epitope tags specific to the over-expressed V5-tagged MsrB3A and Myc-FLAG MsrB3B, overcoming the need for an anti-MsrB3 antibody. Although the IF experiments attempted to detect endogenous FLAG-tagged MsrB3 in KI cells using the anti-epitope antibodies failed, the immunolabeling of over-expressed

MsrB3 variants in this type of analysis should be promoted by the abundance of the recombinant proteins in the cells. However, it is important to consider that different expression level can affect the targeting of a protein.

The results produced by the suggested experiments above, together with the findings gathered in this investigation, would constitute evidence to debate the previous indication of MsrB3B being fully targeted to the mitochondria, provided by Kim and Gladyshev (2003). This original study was performed on recombinant MsrB3B-GFP fusion protein transiently expressed in mammalian cells, but it is unclear whether the GFP could contribute to the difference in the targeting of MsrB3B. It is also possible that the expression level of the recombinant MsrB3B in this investigation and the research paper just mentioned could have influenced the targeting of MsrB3B.

In the study on the dual targeting of mitochondria MsrA mentioned earlier, the cytosolic MsrA was partly purified and characterised by MS analysis. This type of analysis confirmed that the slower-migrating, cytosolic MsrA seen in WB featured the mitochondrial signal sequence (Vougier, Mary et al. 2003), confirming that the cytosolic MsrA variant arises from untargeted mitochondrial isoform.

In light of this previous investigation on MsrA, it would be interesting to also analyse the endogenous MsrB3 species seen in WB to characterise the slower migrating form, which might retain a signal peptide, by MS analysis. Performing an IP to isolate endogenous MsrB3 from WT cell lysate was beyond the scope of this MRes investigation, but this approach could produce satisfactory amounts of the endogenous protein forms for MS. As an alternative, the MsrB3-x3 FLAG-KAEL KI cell line could be employed to purify the mutant FLAG-tagged MsrB3 to characterise the slower-migrating MsrB3 species. Using the KI cell line would offer alternative antibodies for the purification of endogenous MsrB3. Furthermore, the triple tag expressed by either MSRB3 alleles in this cell line would provide increased affinity to anti-epitope antibodies in both IP and affinity-purification methods.

These suggestions could be employed to investigate the nature of cytosolic MsrB3, and the targeting of MsrB3A and MsrB3B in over-expressing cells. However, ultimately determining what proportion of endogenous MsrB3 is found in the ER and the mitochondria is important for understanding the role of MsrB3

within the mammalian cell. In this investigation, the IF experiments that attempted to study the endogenous MsrB3 distribution did not produce the desired outcome, and the fractionation techniques employed for the same objective did not efficiently separate the ER from the mitochondria localised MsrB3. Other fractionation protocols should be considered for future experiments to achieve a better separation between the cell organelles. In general, it can be challenging to achieve a clear separation of the ER and mitochondria, but fine-tuning the sequential centrifugation steps and adopting different homogenisation methods in fractionation can improve their separation. Homogenising cells can damage the mitochondria, leading to contamination of the other cell fractions with mitochondrial protein (Djafarzadeh and Jakob 2017)

The literature suggests using a Dounce homogeniser for the extraction of mitochondria and ER from cultured cells. Because this device moderately shears cells, it is widely used for the isolation of intact mitochondria (Djafarzadeh and Jakob 2017, Leiro, Ventura et al. 2023).

Other sources recommend purifying ER and mitochondria fractions from other cellular components in centrifugation using sucrose gradients (Williamson, Wong et al. 2015). A summary of the suggested experiments focused on determining the organelle-localisation of MsrB3 in mammalian cells is shown in **Figure 27**.

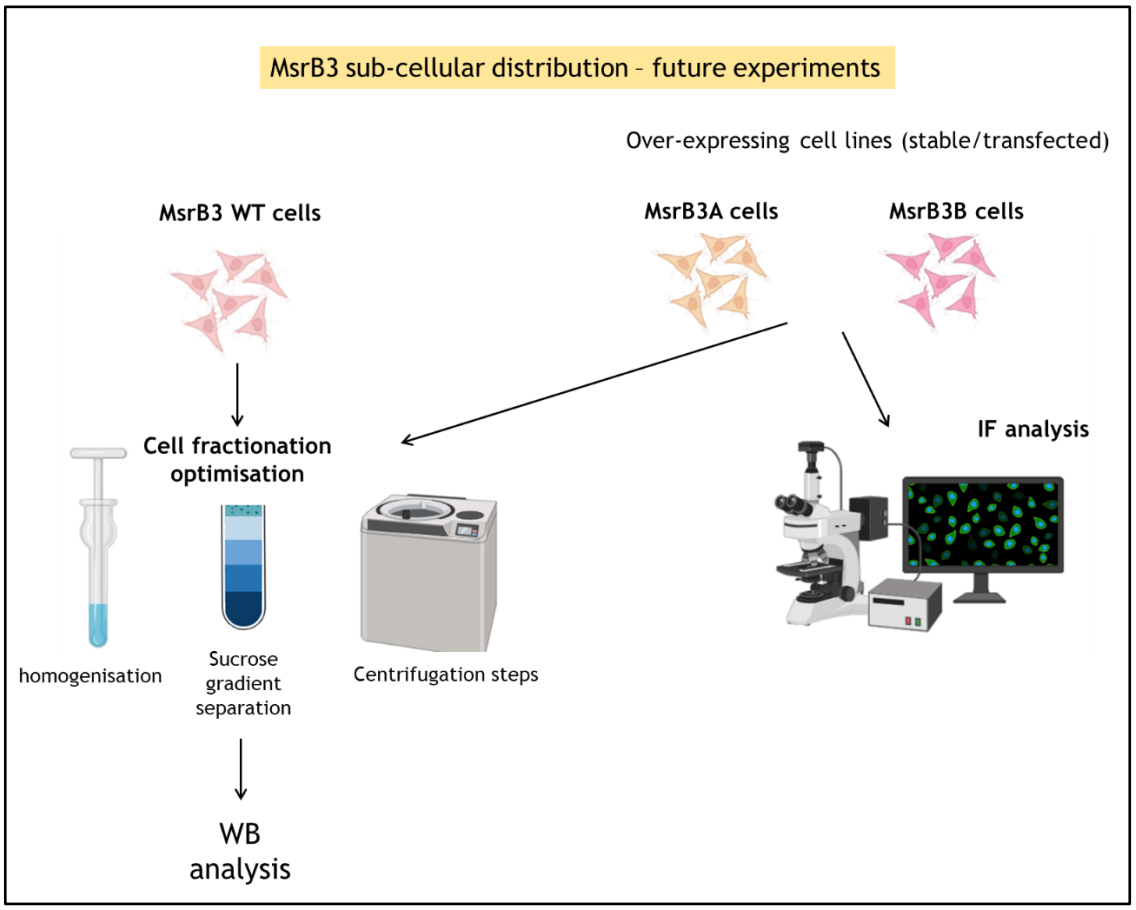

Figure 27: Proposed experiments to elucidate MsrB3 sub-cellular distribution. *Different steps of cell fractionation methodologies can be optimised and combined to determine the distribution of endogenous MsrB3 between the ER and mitochondria. For cell lines selectively over-expressing MsrB3A and MsrB3B, IF techniques can also be employed for the same goal. The untranslocated MsrB3 present in the cytoplasm was investigated in this project using a standard fractionation protocol (see chapter 4.2 and 4.4).*

5.1.2. Significance

Why is it important to understand the distribution of MsrB3 in the mammalian cell? In the introduction, examples of research detailing the ROS-protective properties of MsrB3 and its impact on cancer prognosis are reported. Determining the proportion of the enzyme's sub-cellular distribution will give insights into the MsrB3-mediated modifications of methionine in the proteome, which are closely interlinked with the associations made with cancer and neurodegenerative diseases. When using rodents as model organisms to study the role of MsrB3 in humans and other animals, it is important to consider that they might only express ER-localised MsrB3 (Kim and Gladyshev 2004, Kim 2013). In

general, clarifying MsrB3 distribution in the cell will help determine whether the reductase activity is responsible for regulating redox processes in the endoplasmic reticulum, mitochondria, or both. Other methionine reductases are found in the cytosol (**Figure 2**), including another MsrB (MsrB1), so the function of MsrB3 in the cytosol is likely redundant. However, proving that cytosolic, untranslocated MsrB3 arises from the translation of MsrB3B can provide insights into the "demand" of the reductase in the mitochondria. If MsrB3B is minimally targeted to the mitochondria, in which other Msrs are found (**Figure 2**), it is possible that MsrB3 enzymatic activity primarily impacts the redox processes in the ER. In addition, the presence of MsrB3 should be accounted for in the past and future research focusing on the activity of MsrA and MsrB1 in the cytosol, which are thought to be the only methionine reductases to reside in this cell compartment in mammals. This is because untranslocated MsrB3 activity might overlap with the enzymatic function of MsrA and MsrB1.

Therefore, the sub-cellular distribution of endogenous MsrB3 should be further studied to better guide future research focused on this and other methionine reductases.

5.2. MsrB3 can oxidise methionine in protein

The comparison of the LC-MS-MS analysis of His-Myc-hSPARC incubated with MsrB3 DM in oxidising and reducing conditions returned evidence of the oxidoreductase activity of MsrB3. First of all, the presence of MetO32 and MetO38 in the same recombinant SPARC Myc tag peptide in the oxidising samples, but not in the reducing replicates, suggested that this modification was enzymatically driven and that the oxygen donor in MsrB3 activity is indeed water. Although the candidate Met245 wasn't oxidised by MsrB3 as hypothesised, its consistent baseline oxidation in all the replicates (**Appendix figure 5**) underlines that stochastic oxidation did not contribute significantly to the measured redox state of methionine residues in the recombinant substrate in any reaction. These observations constitute additional evidence that MsrB3 can act as an oxidase, a behaviour that had already been documented but only from experiments carried out with DABS-Met, a synthetic substrate. Furthermore, the MS analysis provided empirical proof that H_2O is the source or destination of oxygen in MsrB3's oxidoreductase activity, as it is for MsrA. Another interesting

aspect of these findings is that MrsB3 DM showed a preference for oxidising the Myc tag peptide Met38 over Met32.

Not only was SPARC Met245 not found to be oxidised with ^{18}O, but the results clearly exclude the possibility that MsrB3 can oxidise this candidate target in the purified substrate because it was found as unmodified (not oxidised) in all the oxidising reactions as seen in **Appendix figure 5**. If Met245 was found exclusively in the form of Met^{16}O due to stochastic oxidation before the incubation with oxidised MsrB3 DM, then it could be speculated that the enzymatic oxidation of the candidate target was prevented due to the absence of unmodified Met245.

5.2.1. Future experiments

Previous research has demonstrated that SPARC affinity to collagen is modulated by extracellular proteolytic modifications. This was first evidenced by a 15-fold increased binding affinity to collagen IV of mouse tissue-derived SPARC compared to recombinant hSPARC (Maurer, Hohenadl et al. 1995).

A follow-up study revealed that the tissue-derived SPARC was cleaved at the 197-198 peptide bond of the EC domain αC. This modification could be replicated in recombinant hSPARC by matrix metalloproteinases, and was accompanied by increased affinity to collagen (Sasaki, Göhring et al. 1997). It was then speculated that the αC of the EC domain of SPARC partly masks the collagen binding epitope and its proteolysis enhances collagen binding activity (Sasaki, Miosge et al. 1999).

The proteolytic cleavage of SPARC was replicated in a study employing recombinant SPARC FS-EC domains lacking the EC αC sequence highlighted in orange in **Figure 6**. This mutant SPARC also showed a 10-fold increase in collagen affinity, mirroring the observations made on protease-cleaved SPARC in the studies referenced above, and it was suggested to be a good model for subsequent studies on SPARC as it might exist in tissues. Indeed, non-cleaved SPARC still has affinity to collagen, but the hindrance by the unmodified EC αC might require a conformational change of the latter to allow substrate binding (Sasaki, Hohenester et al. 1998).

Therefore, even the crystal structure of SPARC EC domain bound to collagen was resolved using purified recombinand hSPARC EC domain lacking the αC helix (Hohenester, Sasaki et al. 2008).

For this reason, it would be sensible to investigate the interactions of other proteins with either cleaved SPARC or with the recombinant protein lacking the EC αC helix (ΔαC). This also applies to future efforts pertaining to MsrB3 and its candidate target, SPARC M245. Because the presence of the αC hinders the binding of SPARC to collagen, it is likely that the same helix precluded any MsrB3-redox modification of Met245 of the fully-folded hSPARC FS-EC employed in this investigation. Modifying the EC αC isn't a suggestion based on the presumption the MsrB3 could interact with endogenously cleaved Ostenectin Met245 *in vivo*, since the cleavage of SPARC likely occurs outside of the ER in the ECM where MsrB3 is not found. However, as SPARC is processed in the ER - where MsrB3 is expressed – like other secreted proteins (Sicari, Igbaria et al. 2019), it will be found in this cell compartment precursors to its fully-folded conformation in which its collagen-binding epitope may be more exposed to modifications. Therefore, it would be useful to study the oxidase activity of MsrB3 on a SPARC mutant in which the EC αC is ablated, to provide a model of SPARC more similar to its ER, partly-folded conformation. Alternatively, recombinant SPARC can be treated with denaturing agents to replicate its unfolded state in the ER, before assessing whether MsrB3 can induce any changes on Met245. If hSPARC EC ΔαC Met245 is oxidised by MsrB3, then it would be worthwhile analysing the effects of this modification on its collagen-binding affinity.

More importantly, for future experiments assessing the oxidoreductase activity of MsrB3, the Myc tag of the recombinant hSPARC FS-EC (or of other candidate targets) should be omitted or cleaved, since MsrB3 DM showed activity towards the two methionines in this tag. Thanks to an Enterokinase site encoded by the construct used in this investigation 3.9), the epitope tags of hSPARC FS-EC variants derived from the same construct can be easily cleaved using commercially available Enterokinase.

5.2.2. Significance

Although the results of the LC-MS-MS analysis were unexpected, they provided valuable insights into MsrB3 oxidoreductase activity. To our knowledge, the results in section 4.7 represent the first evidence of MsrB3 oxidising methionine in protein. This is a development from previous research on MsrB3, which had focused on assaying its oxidoreductase activity using synthetic probes only. Moreover, the higher affinity of MsrB3 for M38 over M32 in the recombinant hSPARC peptide tag suggests that MsrB3 substrate interactions depend on the sequence the target methionine is found in. These sequences could be closely analysed in future research to help identifying the yet-unknown MsrB3 targets in mammalian cells.

Recently, the mitochondrial protein Ndufaf2 has been identified as a candidate MsrB3 binding partner, and it was shown that the *E. coli* MsrB can reduce its methionine (Park, Trujillo-Hernandez et al. 2023).

This is a captivating finding and the first evidence of an *in vivo* MsrB3 binding protein. However, to this date, there is no evidence of a substrate that can be regulated by MsrB3 oxidoreductase activity. Thus, investigating hSPARC M245 as a candidate target of MsrB3 was extremely interesting as M245 is crucial for SPARC affinity to collagens: as discussed in the introduction, site-directed mutagenesis of SPARC Met245 into alanine, which is also nonpolar, greatly decreased its binding affinity. Thus, oxidative modifications of the same methionine in SPARC would have similar, if not greater, effects on its collagen binding activity. So, if MsrB3 can modify Met245 of SPARC during its maturation, this would likely position MsrB3 as a regulator of SPARC activity. For these reasons, it is relevant to continue characterising the possible interactions between MsrB3 and SPARC – considering the modifications of the matricellular protein suggested earlier. It is worth noting that in this project the focus was shifted to MsrB3 oxidase modifications of a target substrate, rather than its reductase activity. In part this is because heavy water could be exploited to "mark" any enzymatically generated MetO, which made the detection of MsrB3-derived oxidation easier. But in principle, analysing the oxidase activity of MsrB3 on methionine in protein can simultaneously disclose candidate targets of MsrB3 reducing activity. It is also important to stress that these considerations don't

just apply to the candidate target Met245 of Osteonectin (SPARC) studied in this project, but to any client target of MsrB3 in future research.

5.3. Analysis of MsrB3 activity in the mammalian cell

As demonstrated in previous literature and in this investigation, MsrB3 can act both as a reductase and oxidase *in vitro*. It is known that MsrB3 is important for redox-stress response in tissue and living organisms, but its oxidoreductase activity *in vivo* has never been analysed. These observations are possible for MsrA, thanks to the development of a fluorescent chemical S-Sulfox substrate, whose emission changes give a readout of the reductase activity *in vivo* (Makukhin, Tretyachenko et al. 2016)

However, to this day no such probe for MsrBs has been developed. This has driven our collaboration with Professor Richard Hartley's lab at the School of Chemistry, University of Glasgow, who are focusing on developing a chemical substrate whose absorbance or emission properties can measure MsrB3 activity in living cells. This is an ongoing effort, and establishing stable cell lines over-expressing MsrB3A or MsrB3B selectively is part of the mutual goal between Bulleid's and Hartley's lab. We believe that, due to the low expression level of MsrB3 in WT cells, cell lines over-expressing the reductase either in the ER or the mitochondria could provide a better model for experiments involving any newly developed MsrB3 synthetic substrate. Thus, developing a stable cell line over-expressing the ER targeted MsrB3 (MsrB3A) is not only relevant to confirm its distribution within the mammalian cell, but it is also important for future investigations focusing on MsrB3 activity. Therefore, more attempts should be made to establish an MsrB3A over expressing cell line for later research.

Recently, a new technique for the analysis of methionine redox state in the cell was proposed. This methodology, called methionine oxidation by blocking (MobB), consists of labelling any reduced methionine in endogenous protein in tissues by perfusion with $H_2{}^{18}O_2$. The heavy-oxygen hydrogen peroxide oxidises any reduced methionine into Met-^{18}O, thus differentiating them from the already oxidised methionine in the proteome which are detected as Met-^{16}O in LC-MS-MS analysis (Bettinger, Simon et al. 2022).

In principle, MobB could also be applied to cultured cells to analyse the redox state of the methionine in the cell proteome. Although this method does not

allow the measurement of MsrB3 oxidoreductase activity in real-time, it could still be employed to identify methionine in the proteome that is more or less oxidised in correlation with the cells' MsrB3 expression levels. A rationale is set out in **Figure 28**. These comparisons could be validated by applying MobB to MsrB3 KO, WT and MsrB3 over-expressing cells. To strengthen any possible correlation between changes in methionine redox state in the proteome and of MsrB3 levels, it would be practical to use stable cell lines with an inducible system for the expression of MsrB3 that can be modulated for the application of the methodology just described. This way, it would be easier to identify any correlation of methionine redox state in the proteome with either the level or duration of MsrB3 expression in the cell.

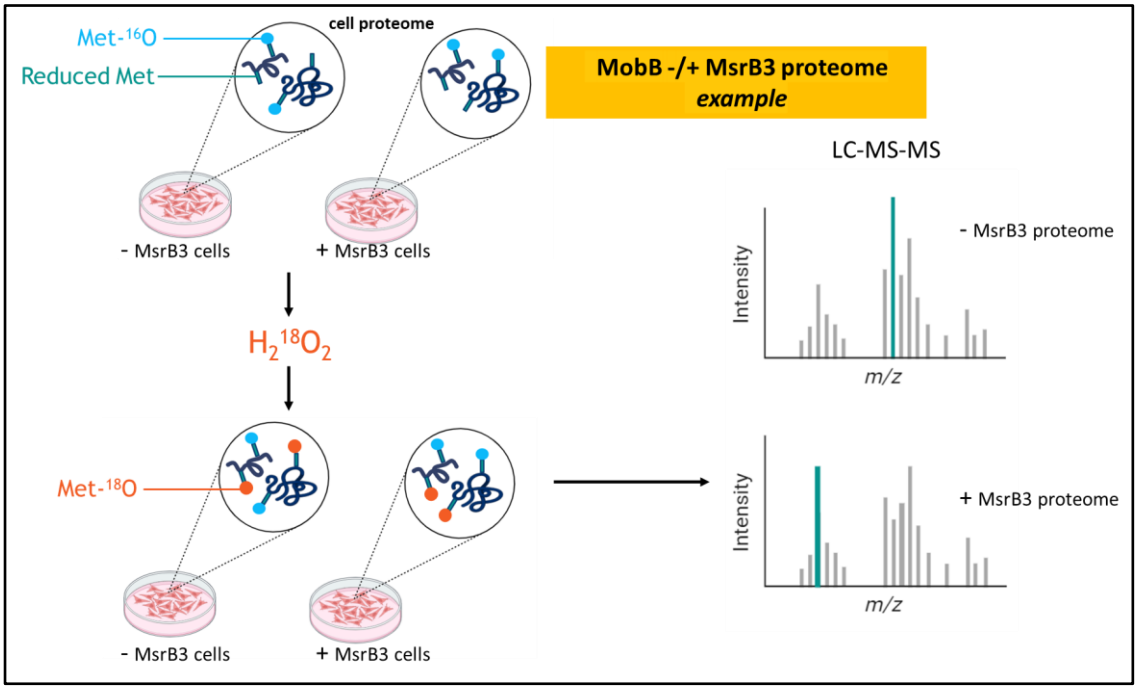

Figure 28: Rationale of the proposed MobB application to study MsrB3 activity.

6. CONCLUDING REMARKS

This investigation provided valuable insights into MsrB3 activity by detecting its oxidase activity on methionine in a model protein and determining that untranslocated MsrB3 is found in the mammalian cell cytosol. Either finding represents an advancement from previous studies, in which MsrB3 localisation was thought to be restricted solely to the ER and mitochondria and its activity had only been assayed with synthetic substrates. Moreover, it is proposed that MsrB3 might have sequence-specific preferences for its oxidoreductase activity, evidenced by the fact that the enzyme oxidised M38 more than M32 in the Myc-tag of the recombinant hSPARC-FS-EC.

Time limitations and technical difficulties prevented identifying the precursor of untranslocated MsrB3, and the question regarding MsrB3 distribution between the mitochondria and ER remains unanswered. The original aims of this project were also focused on investigating a candidate MsrB3 substrate and producing cell lines for studying the *in vivo* oxidoreductase activity. Neither of these aims were wholly satisfied, but they originated useful observations to inspire future research on MsrB3.

7. REFERENCES

Adams, S. L., L. Benayoun, K. Tilton, O. R. Chavez, J. J. Himali, J. K. Blusztajn, S. Seshadri and I. Delalle (2017). "Methionine sulfoxide reductase-B3 (MsrB3) protein associates with synaptic vesicles and its expression changes in the hippocampi of Alzheimer's disease patients." Journal of Alzheimer's Disease **60**(1): 43-56.

Ahmed, Z. M., R. Yousaf, B. C. Lee, S. N. Khan, S. Lee, K. Lee, T. Husnain, A. U. Rehman, S. Bonneux and M. Ansar (2011). "Functional null mutations of MSRB3 encoding methionine sulfoxide reductase are associated with human deafness DFNB74." The American Journal of Human Genetics **88**(1): 19-29.

Antoine, M., A. Gand, S. Boschi-Muller and G. Branlant (2006). "Characterization of the amino acids from Neisseria meningitidis MsrA involved in the chemical catalysis of the methionine sulfoxide reduction step." Journal of Biological Chemistry **281**(51): 39062-39070.

Avendaño-Monsalve, M. C., J. C. Ponce-Rojas and S. Funes (2020). "From cytosol to mitochondria: the beginning of a protein journey." Biological Chemistry **401**(6-7): 645-661.

Azim Jr, H. A., S. Singhal, M. Ignatiadis, C. Desmedt, D. Fumagalli, I. Veys, D. Larsimont, M. Piccart, S. Michiels and C. Sotiriou (2013). "Association between SPARC mRNA expression, prognosis and response to neoadjuvant chemotherapy in early breast cancer: a pooled in-silico analysis." PloS one **8**(4): e62451.

Bettinger, J. and S. Ghaemmaghami (2020). "Methionine oxidation within the prion protein." Prion **14**(1): 193-205.

Bettinger, J. Q., M. Simon, A. Korotkov, K. A. Welle, J. R. Hryhorenko, A. Seluanov, V. Gorbunova and S. Ghaemmaghami (2022). "Accurate proteomewide measurement of methionine oxidation in aging mouse brains." Journal of Proteome Research **21**(6): 1495-1509.

Bettinger, J. Q., K. A. Welle, J. R. Hryhorenko and S. Ghaemmaghami (2019). "Quantitative analysis of in vivo methionine oxidation of the human proteome." Journal of proteome research **19**(2): 624-633.

Boschi-Muller, S., A. Gand and G. Branlant (2008). "The methionine sulfoxide reductases: catalysis and substrate specificities." Archives of biochemistry and biophysics **474**(2): 266-273.

Brekken, R. A. and E. H. Sage (2000). "SPARC, a matricellular protein: at the crossroads of cell–matrix." Matrix Biology **19**(7): 569-580.
Brown, D. R., B. Schmidt and H. A. Kretzschmar (1997). "Effects of oxidative stress on prion protein expression in PC12 cells." International journal of developmental neuroscience **15**(8): 961-972.
Brown, D. R., B. Schmidt and H. A. Kretzschmar (1998). "Effects of copper on survival of prion protein knockout neurons and glia." Journal of neurochemistry **70**(4): 1686-1693.
Cao, Z., L. Mitchell, O. Hsia, M. Scarpa, S. T. Caldwell, A. D. Alfred, A. Gennaris, J.-F. Collet, R. C. Hartley and N. J. Bulleid (2018). "Methionine sulfoxide reductase B3 requires resolving cysteine residues for full activity and can act as a stereospecific methionine oxidase." Biochemical Journal **475**(4): 827-838.
Ceinos, R. M., E. Torres-Nuñez, R. Chamorro, B. Novoa, A. Figueras, N. M. Ruane and J. Rotllant (2013). "Critical role of the matricellular protein SPARC in mediating erythroid progenitor cell development in zebrafish." Cells Tissues Organs **197**(3): 196-208.
Chandran, S. and D. Binninger (2023). "Role of Oxidative Stress, Methionine Oxidation and Methionine Sulfoxide Reductases (MSR) in Alzheimer's Disease." Antioxidants **13**(1): 21.
Chao, C.-C., Y.-S. Ma and E. R. Stadtman (1997). "Modification of protein surface hydrophobicity and methionine oxidation by oxidative systems." Proceedings of the National Academy of Sciences **94**(7): 2969-2974.
Chen, J., D. Shi, X. Liu, S. Fang, J. Zhang and Y. Zhao (2012). "Targeting SPARC by lentivirus-mediated RNA interference inhibits cervical cancer cell growth and metastasis." BMC cancer **12**(1): 1-15.
Djafarzadeh, S. and S. M. Jakob (2017). "Isolation of intact mitochondria from skeletal muscle by differential centrifugation for high-resolution respirometry measurements." JoVE (Journal of Visualized Experiments)(121): e55251.
Dong, J., C. S. Atwood, V. E. Anderson, S. L. Siedlak, M. A. Smith, G. Perry and P. R. Carey (2003). "Metal binding and oxidation of amyloid-ß within isolated senile plaque cores: Raman microscopic evidence." Biochemistry **42**(10): 2768-2773.
Feng, J. and L. Tang (2014). "SPARC in tumor pathophysiology and as a potential therapeutic target." Current Pharmaceutical Design **20**(39): 6182-6190.

Fernández-Vizarra, E., G. Ferrín, A. Pérez-Martos, P. Fernández-Silva, M. Zeviani and J. A. Enríquez (2010). "Isolation of mitochondria for biogenetical studies: An update." Mitochondrion **10**(3): 253-262.
Fitzgerald, M. C. and J. E. Schwarzbauer (1998). "Importance of the basement membrane protein SPARC for viability and fertility in Caenorhabditis elegans." Current Biology **8**(23): 1285-1288.
Gao, Z.-w., C. Liu, L. Yang, T. He, X.-n. Wu, H.-z. Zhang and K. Dong (2021). "SPARC overexpression promotes liver cancer cell proliferation and tumor growth." Frontiers in molecular biosciences **8**: 775743.
Gilmour, D. T., G. J. Lyon, M. B. Carlton, J. R. Sanes, J. M. Cunningham, J. R. Anderson, B. L. Hogan, M. J. Evans and W. H. Colledge (1998). "Mice deficient for the secreted glycoprotein SPARC/osteonectin/BM40 develop normally but show severe age-onset cataract formation and disruption of the lens." The EMBO journal **17**(7): 1860-1870.
Glaser, C. B., G. Yamin, V. N. Uversky and A. L. Fink (2005). "Methionine oxidation, α-synuclein and Parkinson's disease." Biochimica et Biophysica Acta (BBA)-Proteins and Proteomics **1703**(2): 157-169.
Hohenester, E., P. Maurer, C. Hohenadl, R. Timpl, J. N. Jansonius and J. Engel (1996). "Structure of a novel extracellular Ca2+-binding module in BM-40." Nature structural biology **3**(1): 67-73.
Hohenester, E., T. Sasaki, C. Giudici, R. W. Farndale and H. P. Bächinger (2008). "Structural basis of sequence-specific collagen recognition by SPARC." Proceedings of the National Academy of Sciences **105**(47): 18273-18277.
Hsu, Y. R., L. O. Narhi, C. Spahr, K. E. Langley and H. S. Lu (1996). "In vitro methionine oxidation of escherichia coli-derived human stem cell factor: Effects on the molecular structure, biological activity, and dimerization." Protein science **5**(6): 1165-1173.
Hunnicut, J., Y. Liu, A. Richardson and A. B. Salmon (2015). "MsrA overexpression targeted to the mitochondria, but not cytosol, preserves insulin sensitivity in diet-induced obese mice." PLoS One **10**(10): e0139844.
Janssen-Heininger, Y. M., B. T. Mossman, N. H. Heintz, H. J. Forman, B. Kalyanaraman, T. Finkel, J. S. Stamler, S. G. Rhee and A. van der Vliet (2008). "Redox-based regulation of signal transduction: principles, pitfalls, and promises." Free Radical Biology and Medicine **45**(1): 1-17.

Kim, G., S. J. Weiss and R. L. Levine (2014). "Methionine oxidation and reduction in proteins." Biochimica et Biophysica Acta (BBA)-General Subjects **1840**(2): 901-905.
Kim, H.-Y. (2013). "The methionine sulfoxide reduction system: selenium utilization and methionine sulfoxide reductase enzymes and their functions." Antioxidants & redox signaling **19**(9): 958-969.
Kim, H.-Y. and V. N. Gladyshev (2004). "Characterization of mouse endoplasmic reticulum methionine-R-sulfoxide reductase." Biochemical and Biophysical Research Communications **320**(4): 1277-1283.
Kim, H.-Y. and V. N. Gladyshev (2004). "Methionine sulfoxide reduction in mammals: characterization of methionine-R-sulfoxide reductases." Molecular biology of the cell **15**(3): 1055-1064.
Kim, H.-Y. and V. N. Gladyshev (2006). "Alternative first exon splicing regulates subcellular distribution of methionine sulfoxide reductases." BMC molecular biology **7**: 1-6.
Kim, H.-Y. and V. N. Gladyshev (2007). "Methionine sulfoxide reductases: selenoprotein forms and roles in antioxidant protein repair in mammals." Biochemical Journal **407**(3): 321-329.
Kwak, G.-H. and H.-Y. Kim (2017). "MsrB3 deficiency induces cancer cell apoptosis through p53-independent and ER stress-dependent pathways." Archives of Biochemistry and Biophysics **621**: 1-5.
Kwak, G.-H., T.-H. Kim and H.-Y. Kim (2017). "Down-regulation of MsrB3 induces cancer cell apoptosis through reactive oxygen species production and intrinsic mitochondrial pathway activation." Biochemical and biophysical research communications **483**(1): 468-474.
Kwak, G.-H., D.-H. Lim, J. Y. Han, Y. S. Lee and H.-Y. Kim (2012). "Methionine sulfoxide reductase B3 protects from endoplasmic reticulum stress in Drosophila and in mammalian cells." Biochemical and biophysical research communications **420**(1): 130-135.
Kwon, T.-J., H.-J. Cho, U.-K. Kim, E. Lee, S.-K. Oh, J. Bok, Y. C. Bae, J.-K. Yi, J. W. Lee and Z.-Y. Ryoo (2014). "Methionine sulfoxide reductase B3 deficiency causes hearing loss due to stereocilia degeneration and apoptotic cell death in cochlear hair cells." Human Molecular Genetics **23**(6): 1591-1601.

Lai, L., J. Sun, S. Tarafdar, C. Liu, E. Murphy, G. Kim and R. L. Levine (2019). "Loss of methionine sulfoxide reductases increases resistance to oxidative stress." Free Radical Biology and Medicine **145**: 374-384.
Lane, T. F. and E. H. Sage (1994). "The biology of SPARC, a protein that modulates cell-matrix interactions." The FASEB Journal **8**(2): 163-173.
Lee, S. H., S. Lee, J. Du, K. Jain, M. Ding, A. J. Kadado, G. Atteya, Z. Jaji, T. Tyagi and W. h. Kim (2019). "Mitochondrial MsrB2 serves as a switch and transducer for mitophagy." EMBO molecular medicine **11**(8): e10409.
Leiro, M., R. Ventura, N. Rojo-Querol and M. I. Hernández-Alvarez (2023). "Endoplasmic Reticulum Isolation: An Optimized Approach into Cells and Mouse Liver Fractionation." Bio-protocol **13**(17).
Levine, R. L., L. Mosoni, B. S. Berlett and E. R. Stadtman (1996). "Methionine residues as endogenous antioxidants in proteins." Proceedings of the National Academy of Sciences **93**(26): 15036-15040.
Liao, P.-C., C. Bergamini, R. Fato, L. A. Pon and F. Pallotti (2020). Isolation of mitochondria from cells and tissues. Methods in cell biology, Elsevier. **155:** 3-31.
Lim, D.-H., J. Y. Han, J.-R. Kim, Y. S. Lee and H.-Y. Kim (2012). "Methionine sulfoxide reductase B in the endoplasmic reticulum is critical for stress resistance and aging in Drosophila." Biochemical and biophysical research communications **419**(1): 20-26.
Lim, J. C., Z. You, G. Kim and R. L. Levine (2011). "Methionine sulfoxide reductase A is a stereospecific methionine oxidase." Proceedings of the National Academy of Sciences **108**(26): 10472-10477.
Ma, X., J. Wang, M. Zhao, H. Huang and J. Wu (2019). "Increased expression of methionine sulfoxide reductases B3 is associated with poor prognosis in gastric cancer." Oncology Letters **18**(1): 465-471.
Makukhin, N., V. Tretyachenko, J. Moskovitz and J. Míšek (2016). "A ratiometric fluorescent probe for imaging of the activity of methionine sulfoxide reductase A in cells." Angewandte Chemie International Edition **55**(41): 12727-12730.
Mann, M. and O. N. Jensen (2003). "Proteomic analysis of post-translational modifications." Nature biotechnology **21**(3): 255-261.
Martinek, N., R. Zou, M. Berg, J. Sodek and M. Ringuette (2002). "Evolutionary conservation and association of SPARC with the basal lamina in Drosophila." Development genes and evolution **212**: 124-133.

Mason, I. J., D. Murphy, M. Münke, U. Francke, R. Elliott and B. Hogan (1986). "Developmental and transformation-sensitive expression of the Sparc gene on mouse chromosome 11." The EMBO journal **5**(8): 1831-1837.
Maurer, P., C. Hohenadl, E. Hohenester, W. Göhring, R. Timpl and J. Engel (1995). "The C-terminal portion of BM-40 (SPARC/osteonectin) is an autonomously folding and crystallisable domain that binds calcium and collagen IV." Journal of molecular biology **253**(2): 347-357.
Minetti, G., C. Balduini and A. Brovelli (1994). "Reduction of DABS-L-methionine-dl-sulfoxide by protein methionine sulfoxide reductase from polymorphonuclear leukocytes: stereospecificity towards the l-sulfoxide." The Italian journal of biochemistry **43**(6): 273-283.
Miyazono, Y., S. Hirashima, N. Ishihara, J. Kusukawa, K.-i. Nakamura and K. Ohta (2018). "Uncoupled mitochondria quickly shorten along their long axis to form indented spheroids, instead of rings, in a fission-independent manner." Scientific reports **8**(1): 350.
Morel, A.-P., C. Ginestier, R. M. Pommier, O. Cabaud, E. Ruiz, J. Wicinski, M. Devouassoux-Shisheboran, V. Combaret, P. Finetti and C. Chassot (2017). "A stemness-related ZEB1–MSRB3 axis governs cellular pliancy and breast cancer genome stability." Nature medicine **23**(5): 568-578.
Nicchitta, C. V. (2002). "A platform for compartmentalized protein synthesis: protein translation and translocation in the ER." Current opinion in cell biology **14**(4): 412-416.
Park, S., J. A. Trujillo-Hernandez and R. L. Levine (2023). "Ndufaf2, a protein in mitochondrial complex I, interacts in vivo with methionine sulfoxide reductases." Redox Report **28**(1): 2168635.
Purcell, L., J. Gruia-Gray, S. Scanga and M. Ringuette (1993). "Developmental anomalies of Xenopus embryos following microinjection of SPARC antibodies." Journal of Experimental Zoology **265**(2): 153-164.
Radzinski, M., T. Oppenheim, N. Metanis and D. Reichmann (2021). "The cys sense: thiol redox switches mediate life cycles of cellular proteins." Biomolecules **11**(3): 469.
Ramazi, S. and J. Zahiri (2021). "Post-translational modifications in proteins: resources, tools and prediction methods." Database **2021**.

Ramezani, F. (2023). "miR-331-3p, miR-338-3p, hsa-let-7b-3p, and HSF2 regulate MSRB3 expression and ROS-mediated apoptosis in cervical cancer; insights from bioinformatics study." Journal of Epigenetics.

Ranaivoson, F. M., M. Antoine, B. Kauffmann, S. Boschi-Muller, A. Aubry, G. Branlant and F. Favier (2008). "A structural analysis of the catalytic mechanism of methionine sulfoxide reductase A from Neisseria meningitidis." Journal of molecular biology **377**(1): 268-280.

Reed, M. and E. Sage (1996). "SPARC and the extracellular matrix: implications for cancer and wound repair." Attempts to Understand Metastasis Formation I: Metastasis-Related Molecules: 81-94.

Rosset, E. M. and A. D. Bradshaw (2016). "SPARC/osteonectin in mineralized tissue." Matrix Biology **52**: 78-87.

Rotllant, J., D. Liu, Y.-L. Yan, J. H. Postlethwait, M. Westerfield and S.-J. Du (2008). "Sparc (Osteonectin) functions in morphogenesis of the pharyngeal skeleton and inner ear." Matrix Biology **27**(6): 561-572.

Sage, H., R. B. Vernon, S. E. Funk, E. A. Everitt and J. Angello (1989). "SPARC, a secreted protein associated with cellular proliferation, inhibits cell spreading in vitro and exhibits Ca+ 2-dependent binding to the extracellular matrix." The Journal of cell biology **109**(1): 341-356.

Sasaki, T., W. Göhring, K. Mann, P. Maurer, E. Hohenester, V. Knäuper, G. Murphy and R. Timpl (1997). "Limited cleavage of extracellular matrix protein BM-40 by matrix metalloproteinases increases its affinity for collagens." Journal of Biological Chemistry **272**(14): 9237-9243.

Sasaki, T., E. Hohenester, W. Göhring and R. Timpl (1998). "Crystal structure and mapping by site-directed mutagenesis of the collagen-binding epitope of an activated form of BM-40/SPARC/osteonectin." The EMBO journal **17**(6): 1625-1634.

Sasaki, T., N. Miosge and R. Timpl (1999). "Immunochemical and tissue analysis of protease generated neoepitopes of BM-40 (osteonectin, SPARC) which are correlated to a higher affinity binding to collagens." Matrix Biology **18**(5): 499-508.

Schwarzbauer, J. E. and C. S. Spencer (1993). "The Caenorhabditis elegans homologue of the extracellular calcium binding protein SPARC/osteonectin affects nematode body morphology and mobility." Molecular biology of the cell **4**(9): 941-952.

Shi, D., K. Jiang, Y. Fu, R. Fang, X. Liu and J. Chen (2016). "Overexpression of SPARC correlates with poor prognosis in patients with cervical carcinoma and regulates cancer cell epithelial-mesenchymal transition." Oncology letters **11**(5): 3251-3258.
Sicari, D., A. Igbaria and E. Chevet (2019). "Control of protein homeostasis in the early secretory pathway: current status and challenges." Cells **8**(11): 1347.
Stefanis, L. (2012). "α-Synuclein in Parkinson's disease." Cold Spring Harbor perspectives in medicine **2**(2): a009399.
Strandjord, T. P., D. K. Madtes, D. J. Weiss and E. H. Sage (1999). "Collagen accumulation is decreased in SPARC-null mice with bleomycin-induced pulmonary fibrosis." American Journal of Physiology-Lung Cellular and Molecular Physiology **277**(3): L628-L635.
Tai, I. T. and M. J. Tang (2008). "SPARC in cancer biology: its role in cancer progression and potential for therapy." Drug Resistance Updates **11**(6): 231-246.
Tarafdar, S., G. Kim and R. L. Levine (2019). "Drosophila methionine sulfoxide reductase A (MSRA) lacks methionine oxidase activity." Free Radical Biology and Medicine **131**: 154-161.
Tarrago, L., A. Kaya, H.-Y. Kim, B. Manta, B.-C. Lee and V. N. Gladyshev (2022). "The selenoprotein methionine sulfoxide reductase B1 (MSRB1)." Free Radical Biology and Medicine.
Termine, J. D., H. K. Kleinman, S. W. Whitson, K. M. Conn, M. L. McGarvey and G. R. Martin (1981). "Osteonectin, a bone-specific protein linking mineral to collagen." Cell **26**(1): 99-105.
Trombetta, J. M., A. D. Bradshaw and R. H. Johnson (2010). "SPARC/osteonectin functions to maintain homeostasis of the collagenous extracellular matrix in the periodontal ligament." Journal of Histochemistry & Cytochemistry **58**(10): 871-879.
Varadarajan, S., J. Kanski, M. Aksenova, C. Lauderback and D. A. Butterfield (2001). "Different mechanisms of oxidative stress and neurotoxicity for Alzheimer‘s Aß (1− 42) and Aß (25− 35)." Journal of the American Chemical Society **123**(24): 5625-5631.
Vougier, S., J. Mary and B. Friguet (2003). "Subcellular localization of methionine sulphoxide reductase A (MsrA): evidence for mitochondrial and cytosolic isoforms in rat liver cells." Biochemical Journal **373**(2): 531-537.

Walsh, C. (2006). Posttranslational modification of proteins: expanding nature's inventory, Roberts and Company Publishers.
Williamson, C. D., D. S. Wong, P. Bozidis, A. Zhang and A. M. Colberg-Poley (2015). "Isolation of endoplasmic reticulum, mitochondria, and mitochondria-associated membrane and detergent resistant membrane fractions from transfected cells and from human cytomegalovirus-infected primary fibroblasts." Current protocols in cell biology **68**(1): 3.27. 21-23.27. 33.
Wong, B.-S., H. Wang, D. R. Brown and I. M. Jones (1999). "Selective oxidation of methionine residues in prion proteins." Biochemical and biophysical research communications **259**(2): 352-355.
Xu, H., N. Raynal, S. Stathopoulos, J. Myllyharju, R. W. Farndale and B. Leitinger (2011). "Collagen binding specificity of the discoidin domain receptors: binding sites on collagens II and III and molecular determinants for collagen IV recognition by DDR1." Matrix Biology **30**(1): 16-26.
Younan, N. D., R. C. Nadal, P. Davies, D. R. Brown and J. H. Viles (2012). "Methionine oxidation perturbs the structural core of the prion protein and suggests a generic misfolding pathway." Journal of Biological Chemistry **287**(34): 28263-28275.
Zhu, A., P. Yuan, F. Du, R. Hong, X. Ding, X. Shi, Y. Fan, J. Wang, Y. Luo and F. Ma (2016). "SPARC overexpression in primary tumors correlates with disease recurrence and overall survival in patients with triple negative breast cancer." Oncotarget **7**(47): 76628.

8. APPENDIX

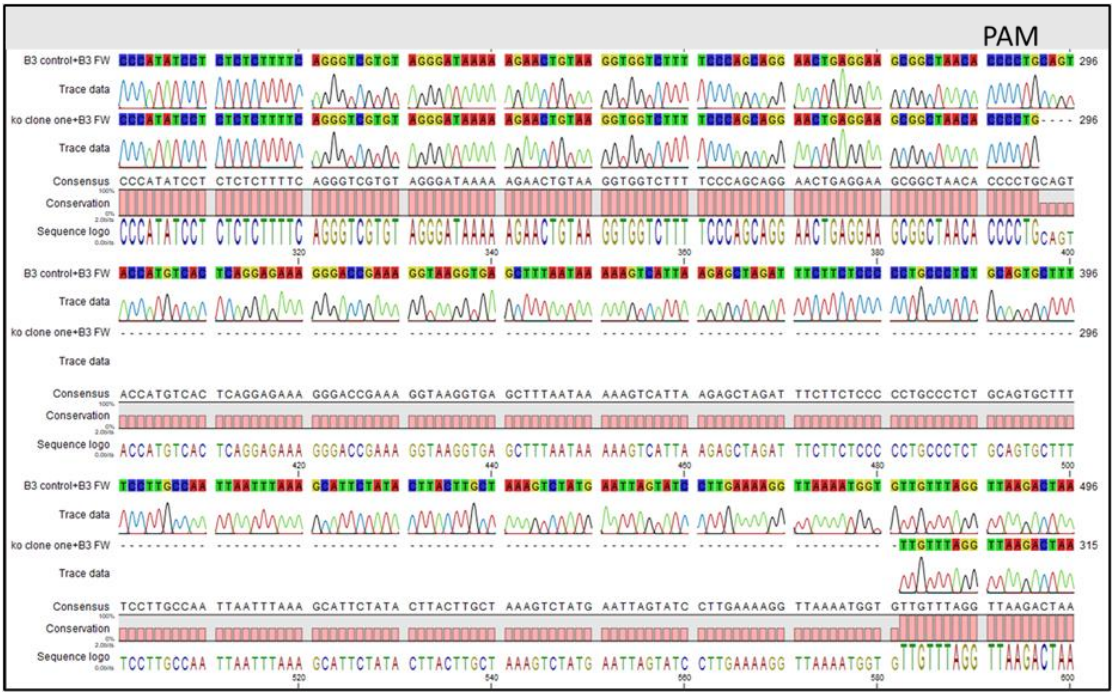

Appendix figure 1: MsrB3 KO clone A1A aligned with MsrB3 WT. *The sequences correspond to the amplified region of the MSRB3 exon following the signal-sequence. The nucleic acid sequences in are represented in the 5' to 3' direction.*

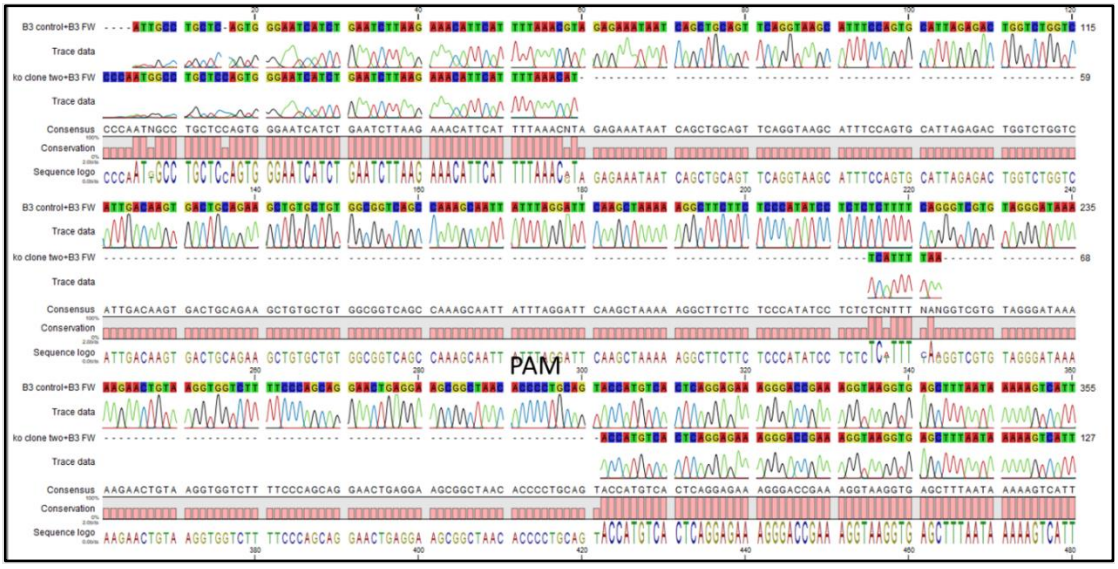

Appendix figure 2: MsrB3 KO clone C3 aligned with MsrB3 WT. *The sequences correspond to the amplified region of the MSRB3 exon following the signal-sequence. The nucleic acid sequences in are represented in the 5' to 3' direction.*

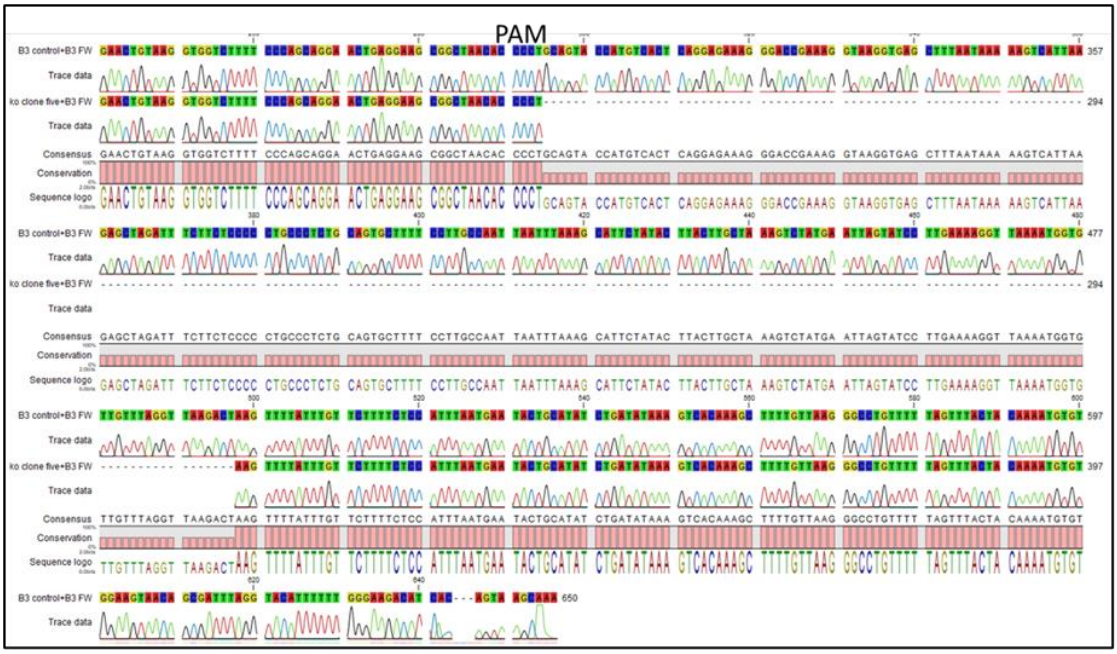

Appendix figure 3: MsrB3 KO clone A2A aligned with MsrB3 WT. *The sequences correspond to the amplified region of the MSRB3 exon following the signal-sequence. The nucleic acid sequences in are represented in the 5' to 3' direction.*

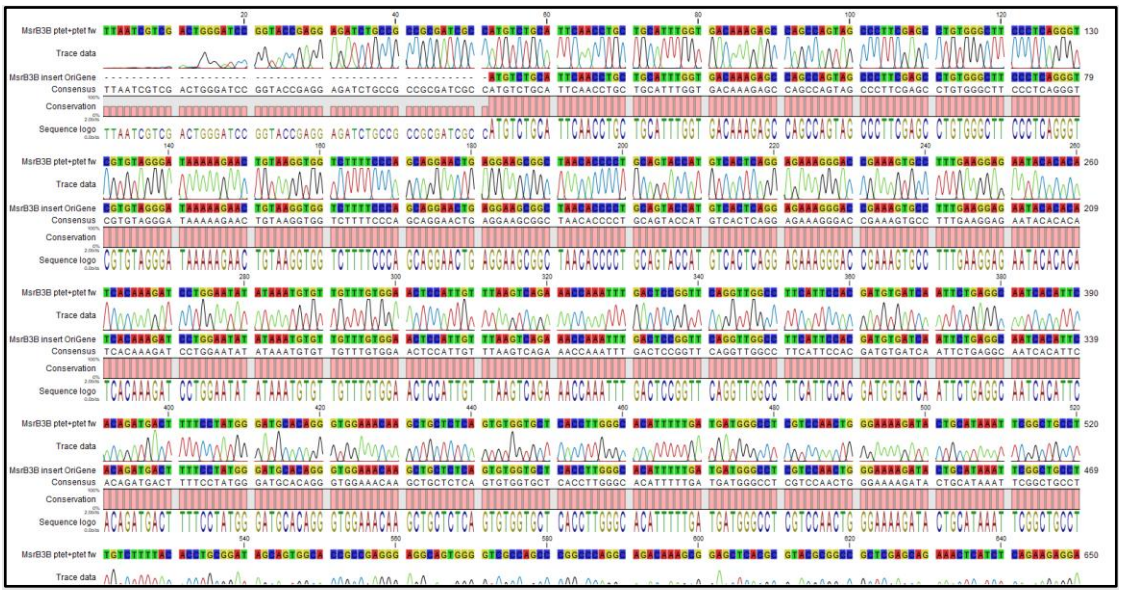

Appendix figure 4: Myc-FLAG MsrB3B cloned in pTetOne aligned with the original insert from OriGene.

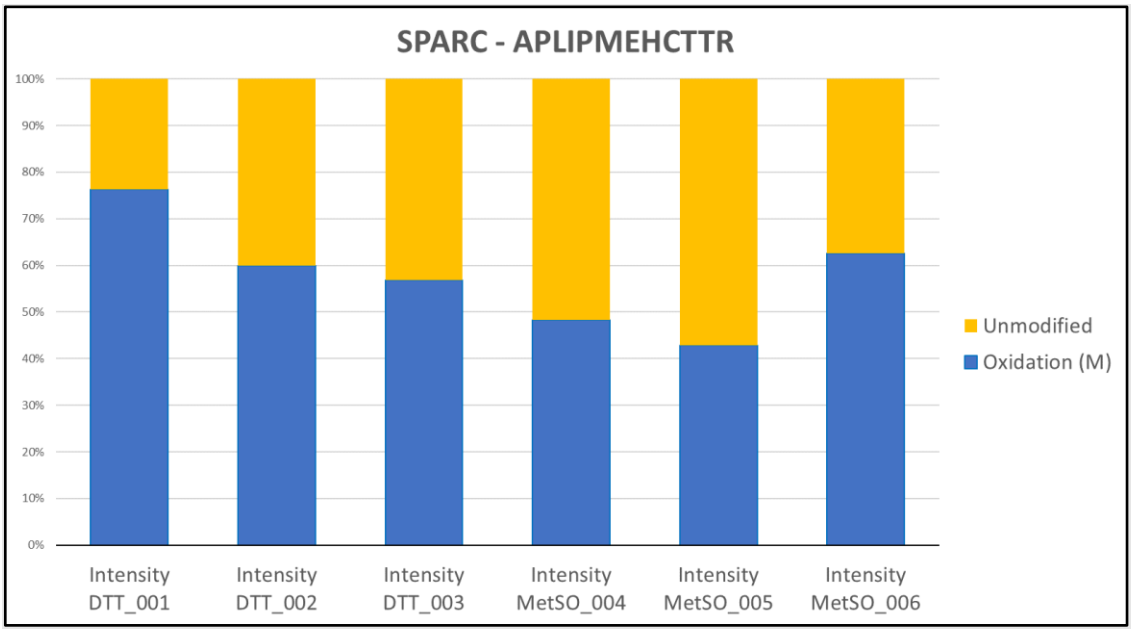

Appendix figure 5: Oxidation of recombinant SPARC Met245.*The relative abundance detected in MS-MS analysis of oxidised and unmodified Met245 of the recombinant hSPARC peptide APLIPMEHCTTR is reported. DTT-001 to DTT_003 indicate the results of the samples generated in reducing conditions, while MetSO_004 to MetSO_006 report the data from the samples created in oxidising conditions. Credits: Sergio Lilla.*

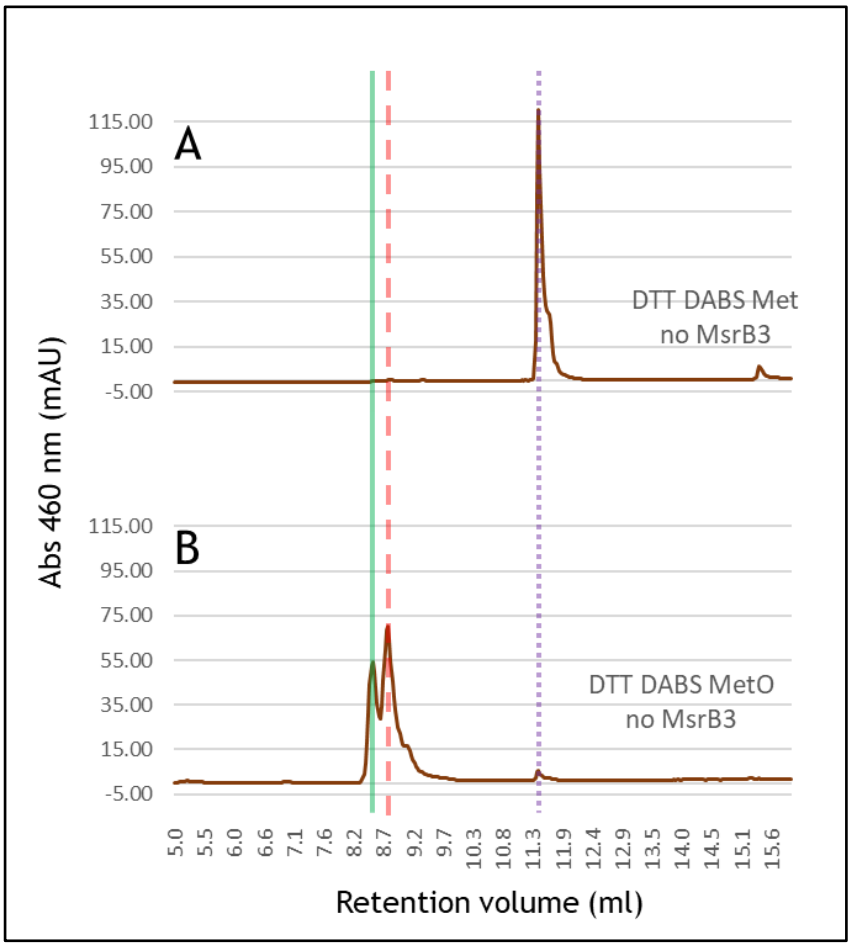

Appendix figure 6: DABS Met and oxidised derivatives controls in HPLC analysis.